Master's thesis

NTNU
Norwegian University of Science and Technology
Faculty of Natural Sciences
Department of Chemistry

Robin Verkerk

Elucidated structures from traditional Nigerian medicinal plants

Master's thesis in Science with Teacher Education
Supervisor: Nebojsa Simic
June 2022

NTNU
Norwegian University of
Science and Technology

Robin Verkerk

Elucidated structures from traditional Nigerian medicinal plants

Master's thesis in Science with Teacher Education
Supervisor: Nebojsa Simic
June 2022

Norwegian University of Science and Technology
Faculty of Natural Sciences
Department of Chemistry

NTNU
Norwegian University of
Science and Technology

Abstract

This thesis aims to elucidate the structures of compounds extracted from *Laportea aestuans, Colocasia esculenta, Xylopia aethiopica* and *Raphiostylis beninensis*, traditional Nigerian medicinal plants. The motivation for this study is assisting in the pursuit of discovering naturally occurring compounds with medicinal application, particularly with respect to possible cytotoxic compounds. With the aid of NMR spectroscopy, IR spectroscopy, and mass spectroscopy, four structures were identified along with a possible fifth that was not fully confirmed, but corresponds extremely well to previously reported spectra. The elucidated compounds were:

(E)-3-methyl-5-((1R,2S,4aS,8aR)-1,2,4a,5-tetramethyl-7-oxo-1,2,3,4,4a,7,8,8a-octahydronaphthalen-1-yl)pent-2-enoic acid

4,4a,6b,8a,11,11,12b,14a-octamethylicosahydropicen-3(2H)-one

4,4a,6b,8a,11,11,12b,14a-octamethyldocosahydropicen-3-ol

4,4,6a,6b,8a,11,11,14b-octamethyl-1,2,3,4,4a,5,6,6a,6b,7,8,8a,9,10,11,12,12a,14,14a,14b-icosahydropicen-3-ol

Kaur-16-en-18-oic acid.

Acknowledgements

This master thesis was carried out at the Department of Chemistry at the Norwegian University of Science and Technology (NTNU) as part of NTNU's MLREAL (Science with Teacher Education) study program. The experiments were performed at the NMR laboratory, MS laboratory, and IR instrument room.

First and foremost, I want to thank my supervisor, Nebojsa Simic, for his guidance, advice, and bountiful patience in face of my procrastination. A special thanks is also extended to Samuel A. Oguntimehin, whose work on extracting and isolating cytotoxic compounds from medicinal plants facilitated this thesis. I'm also grateful for his help elaborating on the extraction methods and origins of the samples in what has been a most pleasurable correspondence. I'd also like to extend my sincere thanks to Torun M. Melø and Susana V. Gonzales for their invaluable help with running specialized NMR experiments and obtaining MS data, respectively. It is no exaggeration to say that without them, structure elucidation of many of the compounds in this thesis would not have been possible.

Speaking of people without whom I would not have been able to finish this thesis, I want to thank my family for their emotional as well as financial support throughout these 5 years. Last but not least, a big and heartfelt thanks to Jenny, for always being there whenever I needed an ear to talk to or a shoulder to rest on.

The greatest teacher, failure is.
- Yoda

Content

Appendix D: Reported NMR spectra

Abbreviations

APCI	Atmospheric Pressure Chemical Ionization
ASAP-MS	Atmospheric Solids Analysis Probe Mass Spectroscopy
COSY	Correlated Spectroscopy
FTIR	Fourier transform Infrared spectroscopy
HMBC	Heteronuclear Multiple Bond Correlation
HSQC	Heteronuclear Single Quantum Coherence
NOAH	NMR by Ordered Acquisition using ^{1}H Detection
NOESY	Nuclear Overhauser Effect Spectroscopy
PANACAEA	Protons and Nitrogen and Carbon *Et Alia*
PANSY	Parallel Acquisition NMR Spectroscopy

Introduction

Cancer is one of the leading causes of death around the world, matched only by cardiovascular disease [3, 4]. While often discussed in the vernacular as a single disease occurring in different areas of the body, cancers can differ wildly from case to case with respect to their malignance, location and spreading. While anyone can develop cancer, certain factors increase this risk. For instance, exposure to carcinogens increase the risk of developing cancer significantly; see no further than to the drastic overrepresentation of smokers among lung cancer patients. While the dangers of smoking are well known by the public today, there are other sources of carcinogens not so easily avoided, like air pollution [5].

By its very nature, each cancer case is unique as cancer, simply put, is the mutation and uncontrolled proliferation of cells in our bodies. While similarities between cases can and do occur, there is never a guarantee that any given treatment will be effective against any given type of cancer. Indeed, one of the reasons cancer has become more treatable over the years is a large arsenal of potential treatments, as well as better methods of early detection. In order to better be able to combat cancer, there exists a perpetual drive to find cytotoxic compounds in nature that might be extracted or be synthesized. Cytotoxic compounds in plants are widely reported and present an extremely promising avenue toward new cancer drugs [6].

Many such plants are used in traditional medicine all over the world, and numerous claims are made about traditional medicinal practice's ability to treat or cure many illnesses. While many traditional treatments lack substantiation in science, the use of medicinal herbs and plants is a more verifiable branch in assessing the efficacy of these This thesis in particular concerns itself with cytotoxic plants used in traditional medicine in Nigeria. Over the course of the last decades, several studies have been compiled that support the claim that many plants used in Nigerian traditional medicine do, in fact, display cytotoxic effects of varying degree [7, 8]. Extracts from four such plants, *L. aestuans, C. esculenta, X. aethiopica* and *R. beninensis*, were found to have cytotoxic effect in an ongoing, separate study, and the goal of this thesis is to elucidate the structures of these fractions.

Theoretical background

Laportea aestuans

L. aestuans is an annual herb belonging to the Laportea genus of the Urticaceae family, and is widespread in tropical zones in Asia and Africa, though native to West India [9, 10]. Its leaves are edible when cooked, and indeed are consumed as a vegetable.

Figure 2.1: *L. aestuans*, picture obtained from West African Plants – A Photo Guide [2].

L. aestuans has a variety of medicinal properties, such as antidiabetic [11], and plants of the *Laportea* genus at large have previously been showed to be a source of antioxidants [12] and antibacterial compounds [13]. Notably, extracts from *L. aestuans* have been shown to display cytotoxic effects, and the plant is a source of tannins and saponins [10], compounds increasingly known for their propensity for cytotoxic activity in a variety of cancer cell lines [14-17].

Colocasia esculenta

C. esculenta is a tropical tuber belonging to the *Araceae* family, of the *Colocasia* genus, originating from South-east Asia [18]. It is, however, also prevalent in many places over the world, and is particularly abundant all over Africa, where it is grown as a crop, given its preference for tropical and subtropical regions with heavy rainfall. Its corms are a rich source of carbohydrates, and traditionally is used in local cuisine in a manner similar to the potato [19, 20].

Figure 2.2: *C. esculenta.* Picture obtained from West African Plants – A Photo Guide [2].

In addition to being a rich source of carbohydrates, various extracts from *C. esculenta* have demonstrated medicinal effects [21]. Notably, *C. esculenta* extracts were reported to have antimetastatic effects against multiple cell lines of breast and prostate cancer [22]. Cytotoxic effect against bone cancer as well as antimicrobial activity have also been demonstrated, and bioactive compounds like flavonoids and steroids have been isolated from its extracts [23].

Xylopia aethiopica

X. aethiopica is an angiosperm belonging to the *Annonaceae* family and the xylopia genus [24]. It thrives in most tropical regions where rainforests are present and is commonly found throughout west Africa, occurring naturally in multiple countries, such as Nigeria, Ghana and Ethiopia – only to name a few - as well as being grown as a crop [25, 26]. Most plants belonging to the xylopia genus are trees or shrubs, and *X. aethiopica* is no different, being an evergreen tree. Its fruit have a long history with use in traditional cuisine and medicine, and various compounds extracted from the plant have demonstrated bioactivity with wide potential medicinal use [25].

Figure 2.3: *X. aethiopica.* Picture obtained from West African Plants – A Photo Guide [2].

Among a host of documented bioactive compounds extracted from *X. aethiopica*, numerous studies have been compiled on the cytotoxic properties of extracts from various parts of *X. aethiopica*. For example, a study performed on an extract from the dried fruits of *X. aethiopica* demonstrated antiproliferative effect in human colon cancer and leukaemia cell lines, with the active compound being identified as ent-15-oxokaur-16-en-19-oic acid [27]. Similar effects have also been demonstrated against breast cancer and cervical cancer cells, where essential oils extracted from the fruits of *X. aethiopica* were found to inhibit cell proliferation and induce apoptosis [28, 29]. The presence of multiple possible cytotoxic classes of compounds like saponins, flavonoids, and tannins have also been demonstrated [30].

Rhaphiostylis beninensis

R. beninensis is an evergreen shrub belonging to the *Raphiostylis* genus of the *Metteniusaceae*. While research on this specimen is not as bountiful as the aforementioned plants, a multitude of medicinal effects have been demonstrated, such as cytotoxicity, antibacterial activity, hepatoprotective activity, and antihaemolytic properties [31-34].

Figure 2.4: *R. beninensis.* Picture obtained from East African Plants – A Photo Guide [1].

Characterization of plant extracts

While the abundant number of bioactive compounds in nature are a potential source for a veritably limitless supply of natural drugs for all manner of ailments, they are notoriously difficult to extract, isolate, and characterize. In this respect the abundance of compounds is both a blessing and a curse; plants rarely contain say, *one* flavonoid that is easily separated from all others. Rather, one almost exclusively and invariably obtains a mixture of compounds that are chemically similar derivatives of a common precursor. Since these behave very similar and sometimes near-identical both chemically and physically, separating these is a herculean task in its own right. The extraction and isolation of potential bioactive compounds from plants is a rigorous process requiring multi-step approaches that often include drying, pulverising, washing/filtering and defatting followed by extraction and chromatographic purification [35]. After (hopefully) pure fractions have been obtained, biochemical characterization and structure elucidation can begin.

Accurate characterization of bioactive compounds is of paramount importance, since relatively minor changes in a chemical structure could radically change the compounds bioactivity. An added difficulty then is found in those cases where purification has failed to completely separate compounds, muddying the proverbial waters. A variety of techniques are then required to determine what the fractions main compound actually is. ^{1}H and ^{13}C NMR are powerful tools to this end, but are susceptible to yield complicated and misleading spectra if multiple compounds of comparable concentrations are present. To help clear up any duplicitous results, MS is often helpful to determine the molecular formula of the main compound, and resulting fragmentations can be helpful to determine structural fragments.

NMR

NMR is probably the single most important method of structure elucidation for small organic compounds. Over the course of the last decades, numerous types of experiments have been developed to help elucidate all sorts of organic compounds. While entire books could – and have – been written on the technical and practical workings of the NMR experiment, a brief and superficial summary of the basic principle is as follows:

Samples to be analysed must be dissolved in a deuterated solvent (as to not have the solvent interfere with the spectra) and the sample is suspended in a strong magnetic field, B_0. Specific elements have an intrinsic nuclear spin, which behaves magnetically. Thus, when they are subjected to the magnetic field, each atom's unique spin has a specific orientation in the magnetic field. An electromagnetic pulse of appropriate frequency then simultaneously excites all chosen nuclei in the sample molecule. Nuclear spins are perturbed from their equilibrium states, and subsequently return to it again after the pulse – this is more commonly referred to as the recovery. This signal is generated and acquired as a so-called free induction decay (FID). The FID is subjected to a mathematical operation known as the Fourier transformation and finally a readable spectrum is obtained [36]. There are two main classes of NMR experiments often used in small organic structure elucidation; 1D experiments, which concern one frequency axis, and 2D experiments, which show correlations between two frequency axes.

The most common 1D experiments used to elucidate smaller organic compounds are ^{1}H proton and ^{13}C experiments, detecting hydrogen atoms and ^{13}C isotopes present in the sample, respectively. These spectra give useful information about groups of atoms of each element present and their chemical environment. Since organic compounds are primarily comprised of hydrogen and carbon, information about these 2 elements alone is usually sufficient for complete structure elucidation. In addition, there are a few common 2D experiments which, when used in conjunction with the 1D experiments mentioned above, yield all the information necessary for arriving on a chemical structure for small organic compounds.

COSY

COSY experiments reveal correlation between nearby protons, mainly ^{2}J(H,H) and ^{3}J(H,H) correlations – though ^{4}J(H,H) are not unheard of. Both the f1 and f2 axes are thus proton spectra, and correlations are visibly in the spectrum as cross-peaks. One notable difficulty with interpreting COSY spectra regards to obtaining clear evidence of coupling between protons with similar shifts. These signals result in cross peaks near the spectrum diagonal. This part of the spectrum is often dominated by signals caused by diastereotopic protons and their coupling that always appear in the spectrum as prominent cross-peaks. These "trivial" peaks can obscure ^{3}J(H,H) and ^{4}J(H,H) peaks close to the diagonal, making it potentially difficult to ascertain couplings between protons with similar chemical shifts. This problem is somewhat reduced with the COSY45 experiment, which reduces diagonal peak intensity [36].

HSQC

Whereas COSY reveals multiple bond correlations between protons, disregarding carbon altogether, HSQC only shows single bond correlations between two different nuclei. On the ^{1}H-^{13}C HSQC spectra, the protons lie along the f2 axis, while the carbons occupy the f1 axis. Protons and carbons that are connected by a single bond are visible in the spectrum, marked by

their cross-peaks. Traditional HSQC only shows that there exists a bond correlation between given protons and carbons, but little else. To obtain information about the degree of substitution, information from HSQC would have to be cross-referenced with the 1D ^{1}H spectrum and specialized ^{13}C experiments, like the DEPT-90 or DEPT-135 experiments [36, 37]. Edited HSQC offers an elegant solution to this problem. In an edited HSQC experiments, cross-peaks corresponding to CH_2 or CH/CH_3 groups have opposite phases, making them readily distinguishable [38]. CH and CH_3 can usually be distinguished by their chemical shift and peak intensity.

HMBC

HMBC is the complementary counterpart of HSQC. HMBC's purpose is to show ^{2}J(C,H)-, ^{3}J(C,H), and occasionally ^{4}J(C,H) correlations, while ^{1}J(C,H) correlations are supressed [36].

NOESY

In addition to the aforementioned 2D experiments, the NOESY experiment is useful in determining stereochemistry. Rather than showing close-bond correlations, i.e. structural proximity, NOESY gives insight to proton's proximity in space. This typically includes some protons in structural proximity as shown in COSY, but in addition to these potentially many more cross-peaks are obtained, painting a good picture of the spatial surroundings of given protons. For example, a NOESY correlation can reveal whether a given set of protons are in *Z* or *E* orientation, or whether protons in cyclic structures occupy an axial or equatorial orientation

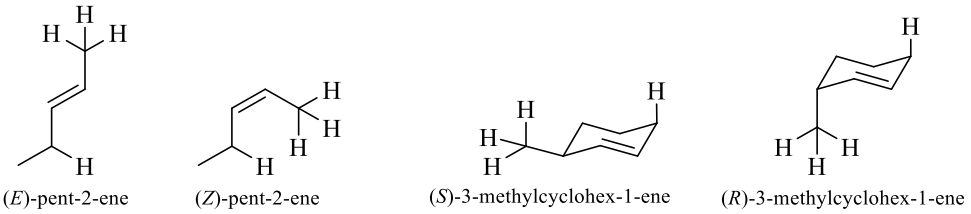

Figure 2.5: Stereochemistry determines whether protons are spatially close enough to show signals in NOESY spectra, which typically can show couplings up to ca. 4-5 Ã. One can expect NOESY signals from (Z)-pent-2-ene and (S)-3-methylcyclohex-1-ene, but the corresponding signals would likely be missing in (E)-pent-2-ene and (R)-3-methylcyclohex-1-ene (somewhat dependent on the particular experiment).

NOAH

The experiments discussed so far are a huge boon to anyone even passingly involved with structure elucidation, and their importance can hardly be overstated. However, they come with one significant drawback, namely time. Running even one set of these experiments can take from several hours up to the better part of a day, which means high cost of analysis in terms of long instrument time and the reduced availability of the instrument for use by others. Apart from the personal convenience of having satisfactory spectra available quickly, the coming shortage of helium makes NOAH-experiments a more sustainable method of running NMR experiments.

Traditionally every experiment in a set has to be run separately – this means for every experiment there is a corresponding pulse sequence, which takes time. Advances in available hardware have given rise to more sophisticated methods of data collection, for example the

PANACAEA, PANSY and later fast-PANACAEA experiments [39, 40], which utilize multiple receivers tuned to different nuclei to perform multiple experiments at once in parallel. This still requires added instrumentation and handling, and is not commonly seen, however. Other approaches, like the COCONOSY [41] experiment, "nests" two experiments – COSY and NOESY in this case – and allows one to effectively perform two experiments "for the price of one", or at least very close to it.

The drive for cheaper, more available, and more efficient ways to perform NMR experiments, eventually culminated into the present day set of NOAH supersequences [42]. The essence of the NOAH sequences consists of utilizing but one single recovery for multiple nested experiments, borrowing the principle behind the COCONOSY experiment, and considerably lowering the amount of time required to conduct a set of experiments. This approach is also available with regular NMR instrumentation and software, as opposed to the PANSY and PANACAEA methods. Particularly for small organic molecules, where only 3-5 experiments at most are needed for a full elucidation, this is a powerful tool indeed. Today many variants of NOAH experiments exist, like NOAH-3 and NOAH-5 [42, 43] experiments. What particular experiments are nested is also increasingly customizable according to the need at hand.

IR

Infrared spectroscopy is a useful tool to identify functional groups in a structure. The general principle behind it is a molecule's absorption of radiation in the infrared spectrum and convert it to either energy of molecular rotation or molecular vibration. This results in absorption bands, often expressed as transmittance, i.e., the ratio of radiant power on the sample vs that of the radiant power incident on the sample. Hence, 100% transmittance of radiation of a given frequency means that no radiation has been absorbed by the compound. While absorption bands give useful information about structural groups present in the sample, the absence of transmittance can be just as useful to determine what groups are *not* present [37].

There are two kinds of molecular vibration of particular importance in identifying groups in organic compounds, namely *stretching* and *bending* vibrations. Stretching vibrations consist of rhythmical contractions and expansions along the bond axis, while bending vibrations consist of changes in the bond angle. Some different kinds of bending and stretching vibrations are displayed in Figure 2.6.

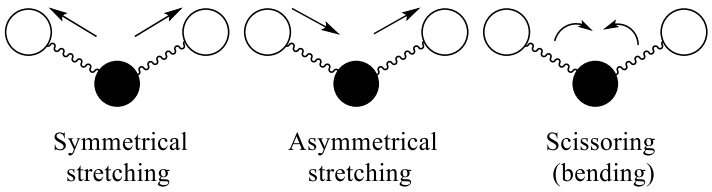

Figure 2.6: Some of the possible modes of vibration in a AX_2 group. For symmetrical stretching, both A-X bonds extend and contract in phase, whereas asymmetrical stretching is characterized by out-of-phase stretching. Scissoring is a type of bending vibration in which the bond angle is reduced, mimicking a "scissor-like" movement.

The particular wavenumber a group converts into a given vibration is highly dependent on the elements involved in the group, the bond length, and angle. Thus, many common chemical groups (such as hydroxyl and carbonyl) have very characteristic transmittance bands.

MS

Mass spectroscopy fills a lot of the gaps left by NMR on the road to structure elucidation, and thus is an important complement to it. Mass spectroscopy's most important function in elucidation of small organic compounds is probably the identification of the molecular weight of the sample. Since organic molecules are primarily comprised of carbon and hydrogen, which are ideally known quantities from NMR, knowledge of the molecular weight allows one to determine what other atoms (like oxygen, nitrogen, or sulphur) might be present based on the remaining weight. The basic workings of the MS experiment is displayed schematically in Figure 2.7. Following injection, usually in a suitable solvent, the sample is evaporated and ionized in vacuum, producing either a positive or negative ion, depending on the ionization method. The ion is detected by its mass-over-charge ration, or *m/z* ratio, where *m* is the molecular mass and *z* is the charge of the ion. The ions are then accelerated and shot past a magnet, which curves them away from their original trajectory, and the ions are registered upon impact with the detector on the far side of the magnet. The change of trajectory is directly correlated to the m/z ratio, and thus the molecular mass. This curvature is compared to that of a known standard, and the m/z ratio of the sample is calculated.

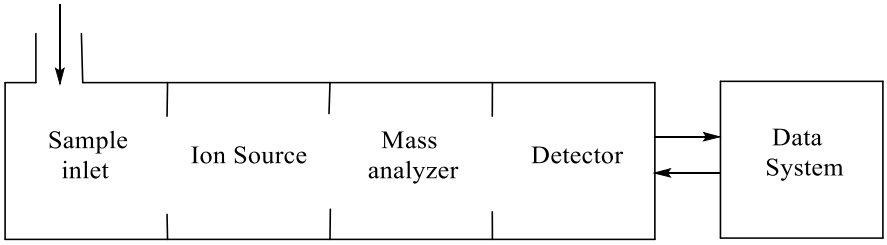

Figure 2.7: A simplified schematic overview of the MS apparatus. The sample is injected into the inlet at atmospheric pressure or vacuum and is then transferred to the ion source, in vacuum. The ionized sample is then transported to the mass analyzer, and upon impact with the detector the system interfaces with a computer system which produces the spectrum.

The information MS conveys about a sample is dependent on the ionization mode used in the experiment. There are two main kinds of ionization, so-called *soft* ionization and *hard* ionization. Soft ionization methods, like electrospray ionization (ESI), produce a molecular ion, which is typically the highest peak in a MS spectrum. Hard ionization, like electron impact (EI) ionization, is generally too powerful to conserve the molecular ion; in the process of ionization, the sample is broken down into smaller, more stable fragments. These fragments, provided they have a charge, are detectable and produce their own peaks in the spectrum. Additionally, there are different ionization methods for different kinds of compounds. For instance there are ion sources better suited for polar compounds, like ESI, or non-polar, like APCI.

By inspecting the m/z ratio of prominent peaks and the m/z difference between adjacent peaks, one can obtain information about stable parts of the molecule which can help with elucidation. For instance, aromatic structures readily produce a fragment with m/z = 77. Over the course of the years many MS spectra for numerous compounds have been compiled into libraries, and in some cases MS spectra alone can be used to identify structures by fragmentation similarity. MS can be used as a standalone spectrometer, or coupled to for instance gas chromatography as a detector.

Materials and methods

All compounds studied were previously extracted and isolated in Nigeria and later prepared for NMR analysis after transport to Norway for identification. While the extraction and isolation of the compounds is outside the scope of this thesis and will not be extensively discussed, they are summarised in brief below.

Extraction and isolation of *L. aestuans*

Fresh aerial parts of *L. aestuans* were coarsely pulverized and weighed. The plant material weighing 25.5 kg was exhaustively extracted with methanol-water 80:20 (v/v). The extract was filtered through Whatman filter paper No. 1 and was evaporated under reduced pressure at 50^{o}C. Crystalline substances were observed in the concentrated extract and were therefore filtered and washed with methanol. The solubility test showed that the crystals were soluble in water but sparingly soluble in methanol. The crystals were dried and coded as Sa-01.

Extraction and isolation of *C. esculenta*

Healthy *Colocasia esculenta* leaves were dried and pulverized into powder. Powdered material was extracted with ethanol by maceration to obtain an ethanol extract. Liquid-liquid fractionation was done with n-hexane, ethyl acetate, and n-butanol. The ethyl acetate was further fractionated with VLC with varying ratios of DCM, EtOAc and methanol. The DCM-EtOAc (50:50) fraction was further purified on silica gel column with successive ratios of n-hexane, DCM, EtOAc, and MeOH. Compounds Sa-02, Sa-03 and Sa-04 were obtained from the column.

Extraction and isolation of *X. aethiopica*

Xylopia aethiopica was obtained from an ethnobotanical survey conducted in Ife North Local Government Area of Osun State, Nigeria. The collection of the bark was done at the botanical garden of the University of Ibadan, Nigeria. It was identified at the herbarium section of the Forestry Research Institute of Nigeria, where a voucher specimen was deposited with voucher number FHI108978. *Xylopia* extract was obtained by macerating 5 kg of pulverized bark with methanol for 72 hours, the extraction procedure was repeated thrice. the concentration of the extract in vacuo yielded 362 g of extract. About 200 g of the extract was adsorbed in silica and eluted gradient with n-hexane, DCM, ethyl acetate, and methanol to yield n-hexane, DCM, ethyl acetate, and Methanol fractions respectively.

The n-hexane fraction was eluted on a silica column, using a gradient mixture of n-hexane and ethyl acetate. A total of 51 fractions were collected and pooled based on their TLC profile into twelve fractions ($XABH_{1\text{-}12}$). Sa-06 and Sa-07 were obtained from PTLC purification of $XABH_2$ while Sa-08 and Sa-09 were obtained from PTLC purification of $XABH_5$.
The DCM fraction was purified by eluting it on a silica column, using a gradient mixture of n-hexane and ethyl acetate. A total of 79 fractions were collected and pooled based on their TLC profile into eleven fractions ($XABH_{1\text{-}11}$). Crystals were noticeable in fraction $XABH_4$ and were therefore purified by washing with n-hexane/ ethyl acetate 8:2 to yield a white grainy substance (Sa-05) which is soluble in both DCM and methanol. Upon dissolution, the grainy nature was lost when dry.

Extraction and isolation of *R. beninensis*

Leaves of *Rhaphiostylis beninensis* were identified at the Department of Botany, University of Ibadan. It was dried under shade and pulverized into powdery form. About 2 kg of the plant material was extracted with methanol at room temperature and concentrated *in vacuo*. Liquid-liquid partitioning was done on the extracted which was portioned into DCM, ethyl acetate, and methanol. The DCM fraction was eluted on a silica column using a gradient mixture of n-hexane and ethyl acetate. A total of 173 fractions were collected. Compounds Sa - 10, Sa – 11, Sa – 12, and Sa -13 were obtained from the washing of fractions 40, 111, 146, and 152 respectively first with n-hexane and then with methanol.

NMR

Samples were previously prepared for NMR analysis prior to the start of this work. The tubes were stored at 3,8℃ over the course of ca. 2 years and most of the samples had lost some or all solvent to evaporation over this time. the vials were refilled with solvent up to a minimum of 3 cm and mixed with a vortexer to solvation.

NMR experiments on were performed with two (see Table 3.1 for an overview of what samples were analyzed with what instrument): The first instrument was a Bruker 600MHz Avance NEO outfitted with a 5mm iProbe and Topspin 4.1.4 IconNMR 5.2.4 software. The second was a Bruker 600MHz Avance III HD outfitted with a 5mm cryogenic CP-TCI z-gradient iProbe and Topspin 3.5pl6 IconNMR 5.0.6 software. The primary instrument used was the 600MHz neo, and the 600MHz with cryoprobe was used for particular dilute samples, or if the first instrument was otherwise occupied. All experiments were run at 298 *K* and results were processed with MestReNova x64 software.

Table 3.1: Summarized in the table are the samples received, the solvent used for their NMR analysis, and the instrument it was performed with.

Sample	Origin	Solvent	Instrument	Comments
Sa-1	*L. aestuans*	N/A		Sample destroyed in transit
Sa-2	*C. esculenta*	$CDCl_3$	600MHz neo	
Sa-3	*C. esculenta*	$CDCl_3$	600MHz cryo	
Sa-4	*C. esculenta*	$CDCl_3$	600MHz cryo	
Sa-5	*X. aethiopica*	$CDCl_3$	600MHz neo	
Sa-6	*X. aethiopica*	$CDCl_3$	600MHz neo	
Sa-7	*X. aethiopica*	$CDCl_3$	600MHz neo	
Sa-8	*X. aethiopica*	$CDCl_3$	600MHz neo	
Sa-9	*X. aethiopica*	$CDCl_3$	600MHz neo	
Sa-10	*R. beninensis*	$CDCl_3$	600MHz neo	
Sa-11	*R. beninensis*	$CDCl_3$	600MHz cryo	
Sa-12	*R. beninensis*	$CDCl_3$	600MHz neo	
Sa-13	*R. beninensis*	$CDCl_3$	600MHz neo	

IR

After NMR analysis, a few drops of the samples were used for FTIR analysis. Being solved in $CDCl_3$ in already appropriate concentrations, IR samples required no preparation and could be analysed as-was. IR analysis was performed with a Bruker ALPHA FTIR spectrometer equipped with a platinum ATR, and the results were processed with Bruker SCOPUS 7.5 software.

MS

The remaining sample was dried and submitted to MS analysis upon completion of NMR and IR experiments. Sample 5 transferred to a roundbottom flask and dried with a Smart EvaporatorC1 from BioChromate with a gentle N_2 flow. The dried sample was transparent and had a waxy consistency, of which 1,3 mg was submitted for elemental composition analysis. The remaining samples were transferred to sample vials and left to dry overnight under a gentle N_2 flow.

Due to their lower purity all other remaining samples were submitted for GC-MS analysis. Analysis of samples was performed with an Agilent 7890A gas chromatograph with a GC Pal autosampler (CTC Analytics, Zwingen, CH) coupled to an Agilent 5975 single quadrupole mass spectrometer. Separation of target compounds was performed on a Thermo Scientific™ TraceGOLD™ TG-5MS GC Column (5% diphenyl/95% dimethyl polysiloxane, 30 m x 0.25 mm inner diameter x 0.5 µm film thickness), keeping the carrier gas flow (helium) at 1 mL min−1 , and the transfer line and the injection port temperatures at 280 ◦C. The temperature program was set as follows: starting at 60◦C for 2 min, followed by a temperature increase at a rate of 15◦C min−1 to 280◦C and held for 1 min, then temperature increase by 50◦C min−1 to 300◦C, and held for 3 min. The overall analysis time for one sample with the selected temperature program was 22 min. Injection volume was 1 µL in splitless mode and the solvent delay was set to 3 min. The mass detector was operated in full scan mode (mz50-500) using electron impact ionization (EI) set at 70 eV.

However, Sa-2, Sa-6, and Sa-9 did not show appreciable results in GC-MS, and were instead analyzed with negative and positive mode MS. Accurate mass determination in positive and negative mode was performed on a "Synapt G2-S" Q-TOF instrument from Water TM. Samples were ionized by the use of ASAP probe (APCI) or ESI probe. No chromatographic separation was used previous to the mass analysis. Calculated exact mass and spectra processing was done by Waters TM Software Masslynx V4.1 SCN871. Sa-5, Sa-7 and Sa-8 were also analyzed similarly in addition to GC-MS of Sa-7 and Sa-8

Results

Sa-5

The results from NMR analysis of Sa-5 (See Appendix A, Sa-5) are in part displayed in Tables 4.1 and 4.2. Summarized in the tables are data obtained from ^{1}H, ^{13}C, and ^{1}H-^{13}C edited HSQC. The first step after peak picking in both 1D spectra, was pairing ^{1}H and ^{13}C with edited HSQC. By cross-referencing the HSQC signal and the corresponding signal's split in the ^{1}H spectrum, the degree of substitution of individual carbons was also established. Using this information in tandem with ^{1}H-^{13}C HMBC, fragments of the structure were assembled, displayed in Figure 4.1. Starting with the prominent high-intensity peaks in the ^{1}H spectrum in the 0.50-2.25 ppm region, corresponding to CH_3 ^{1}H-signals, HMBC was used to established $^{2}J(C,H)$ and $^{3}J(C,H)$ couplings. These couplings are particularly strong for methyl ^{1}H peaks, but the HMBC spectrum revealed couplings for other ^{1}H signals too.

Table 4.1: Extracted data from the ^{1}H spectrum of Sa-5, including chemical shifts, multiplicity, integral, and *J* constants where applicable.

δ ^{1}H (ppm)	**m**	**I**	***J* (Hz)**
0.83	s	3	
0.85	d	3	6.2
1.12	s	3	
1.39 – 1.48	m, 2xdd	3	4.3 12.5 5.2 12.7
1.48 – 1.55	m	4	
1.82	t	1	3.0
1.84	d	1	3.6
1.86	d	1	3.9
1.89	d	4	1.2
2.02	td	1	4.1 13.1
2.15	d	3	1.1
2.32	dd	1	3.7 17.6
2.37	dd	1	13.9 17.5
5.67	q	1	1.1
5.73	t	1	1.1
10.7	s	1	

Table 4.2: Extracted data from the ^{13}C spectrum of Sa-5, including ^{1}J(C,H) couplings as established by HSQC along with the carbon degree of substitution.

δ ^{13}C (ppm)	**δ ^{1}H, HSQC (ppm)**	**Comment**
15.9	0.85	CH_3
18.1	0.83	CH_3
18.6	1.12	CH_3
19.2	1.89	CH_3
19.7	2.15	CH_3
27.1	1.52	CH_2
34.5	2.02	CH_2
35.1	2.37	CH_2
35.7	1.44	CH_2
35.8	1.82	CH_2
36.3	1.51	CH
39.0		q
40.1		q
45.9	1.85	CH
115.1	5.67	CH
125.8	5.73	CH
163.3		q
171.0		COOH
172.7		q
203.0		C=O

Most of the assembled fragments displayed in Figure 4.1 are directly connected, as the fragments share common carbons, with the last fragment being connected with the aid of HMBC and COSY as illustrated in Figure 4.2. Once assembled, this combined fragment accounts for nearly all protons and carbons in the compound. The ^{1}H signal of a COOH group appears as a very broad singlet in the 10-12 ppm area. Such a signal is in fact present in the ^{1}H spectrum of Sa-5 (see Table 4.1), and the corresponding carboxy-^{13}C carbon must be with chemical shift 171.0 ppm, as this is the only carbon with an appropriate shift not fully elucidated. The presence of a carboxylic acid is also supported by IR analysis (See Appendix B, Sa-5). The molecular formula for Sa-5 has been determined from MS analysis as $C_{20}H_{30}O_3$ with a molecular weight of 318 Da, which is consistent with NMR data.

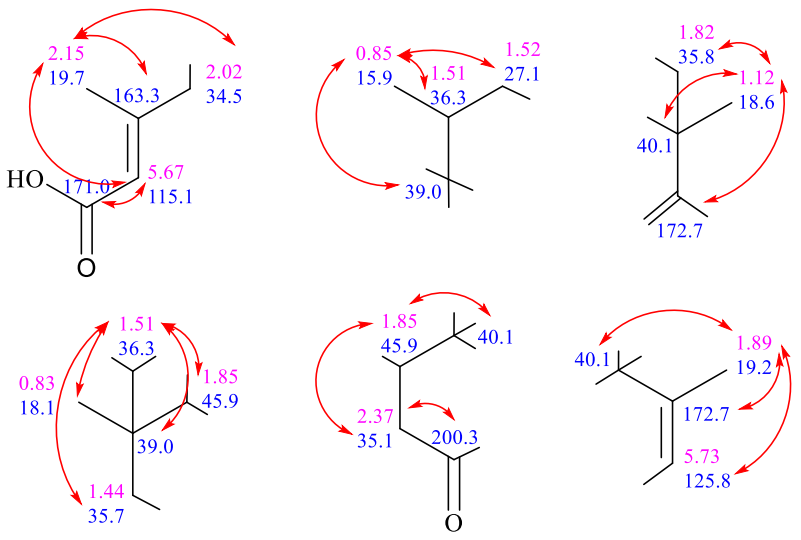

Figure 4.1: Fragments assembled using HMBC signals, indicated with red arrows.

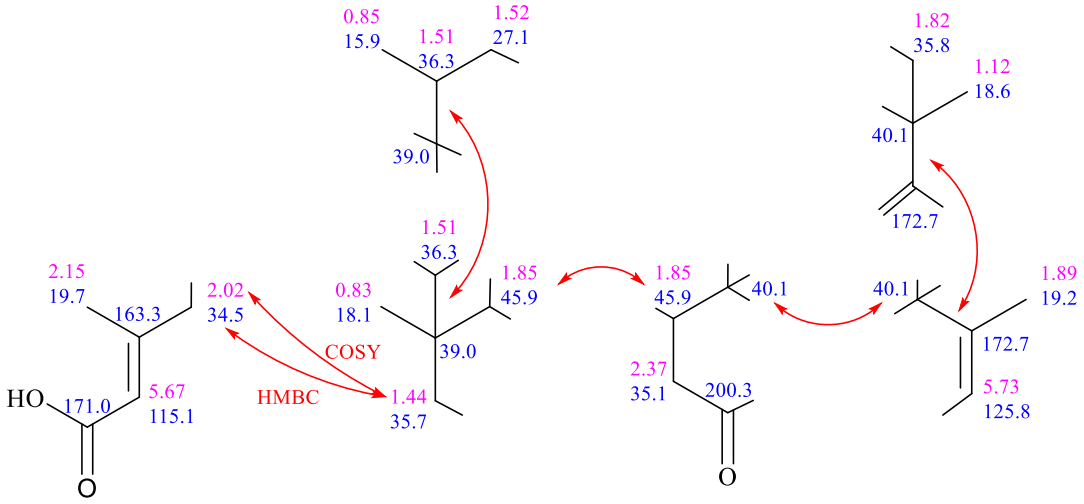

Figure 4.2: The fragments from Figure 4.1 can be directly connected by shared carbons, indicated by the red arrows. COSY and HMBC correlations are also indicated.

The last piece of the puzzle comes with the elemental composition analysis performed on the sample, which corroborates the molecular formula (Appendix C, Sa-5). With the molecular formula the HDI is also uncovered, being 6; 4 are due to double bonds, either in the form of alkene groups or C=O groups. Closure of the larger fragment gives a structure with two 6-membered rings, which is shown in Figure 4.3. The stereochemistry was determined with 2D ^{1}H-^{1}H NOESY and the ^{4}J(H,H) constants, also illustrated in Figure 4.3, and the structure was determined to be (E)-3-methyl-5-((1R,2S,4aS,8aR)-1,2,4a,5-tetramethyl-7-oxo-1,2,3,4,4a,7,8,8a-octahydronaphthalen-1-yl)pent-2-enoic acid.

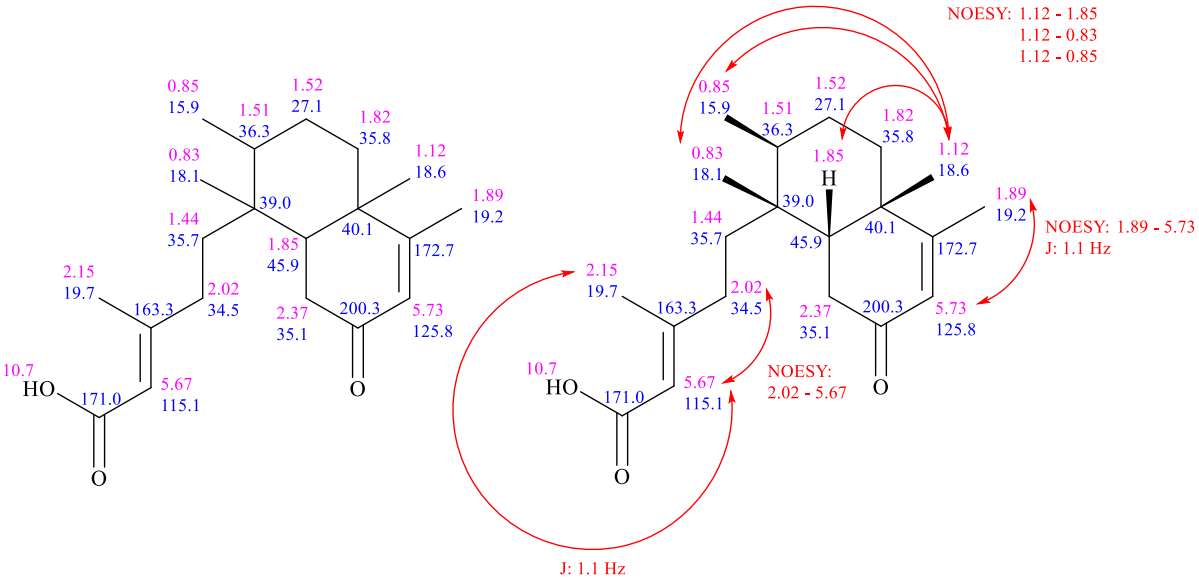

Figure 4.3: The elucidated structure, (E)-3-methyl-5-((1R,2S,4aS,8aR)-1,2,4a,5-tetramethyl-7-oxo-1,2,3,4,4a,7,8,8a-octahydronaphthalen-1-yl)pent-2-enoic acid, with stereochemistry being determined by *J* couplings constants and NOESY signals as indicated.

Sa-6

Sa-6 shows two distinct "layers" of ^{13}C, as illustrated in in Figure 4.4. While ^{13}C spectra are not strictly quantitative, a spectrum that contains two sets of signals with significant difference in intensity between signal sets but decent uniformity within sets, suggests a mixture of two compounds at different concentrations. MS analysis corroborates this notion, revealing two separate compounds with MS peaks of m/z 301 and 303, respectively. For reasons that will be elaborated on shortly, it is assumed that the 301 fragment corresponds to a (M+H) ion with formula $C_{20}H_{29}O_2$, which is the molecular formula minus the loss of H_2O after ionization.

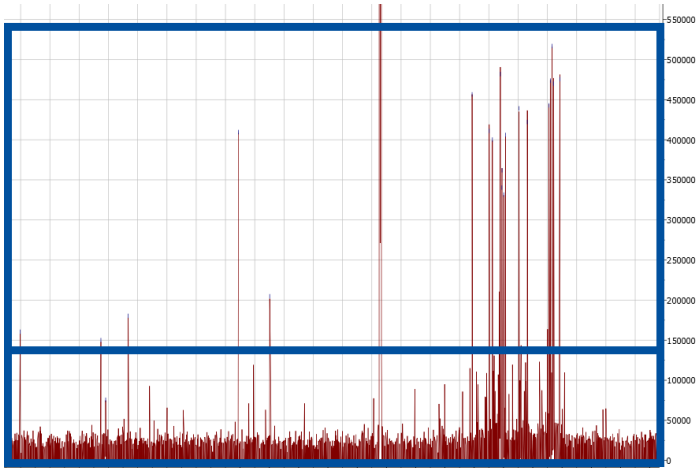

Figure 4.4: The ^{13}C spectrum of Sa-6 shows what appear to be two separate sets of signals with relatively uniform intensity among the sets. The intensity disparity is particularly noticeable in the 10-70 ppm region of the spectrum.

As previously established, Sa-5 has a molecular formula of $C_{20}H_{30}O_3$. Assuming the loss of H_2O, which is possible in positive mode when the analyte contains a carboxylic acid group, the (M + H) ion of Sa-5 would have molecular formula $C_{20}H_{29}O_2$ and a corresponding molecular mass of 301 Da. Indeed, such a m/z peak is observed in the elemental composition analysis of Sa-5. Furthermore, the ^{1}H, ^{13}C, HSQC and HMBC spectra of Sa-6 reveal a great degree of similarity with the corresponding spectra of Sa-5, the most notable similarities are illustrated in Tables 4.3 and Figure 4.5. This suggests that one of the components in the mixture of Sa-6 is either (E)-3-methyl-5-((1R,2S,4aS,8aR)-1,2,4a,5-tetramethyl-7-oxo-1,2,3,4,4a,7,8,8a-octahydronaphthalen-1-yl)pent-2-enoic acid, or a highly similar structural isomer. The remaining component could not be identified due to its lower concentration, however, evidence points to this being kaur-16-en-oic acid, the likely structure of the comparably pure Sa-8.

Table 4.3: A comparison between high-shift ^{13}C signals from Sa-5 and Sa-6's highest intensity set of signals.

δ ^{13}C (Sa-5)	**δ ^{13}C (Sa-6)**
115.1	114.9
125.8	125.5
163.3	163.2
171.0	170.1
172.7	172.6
200.3	200.1

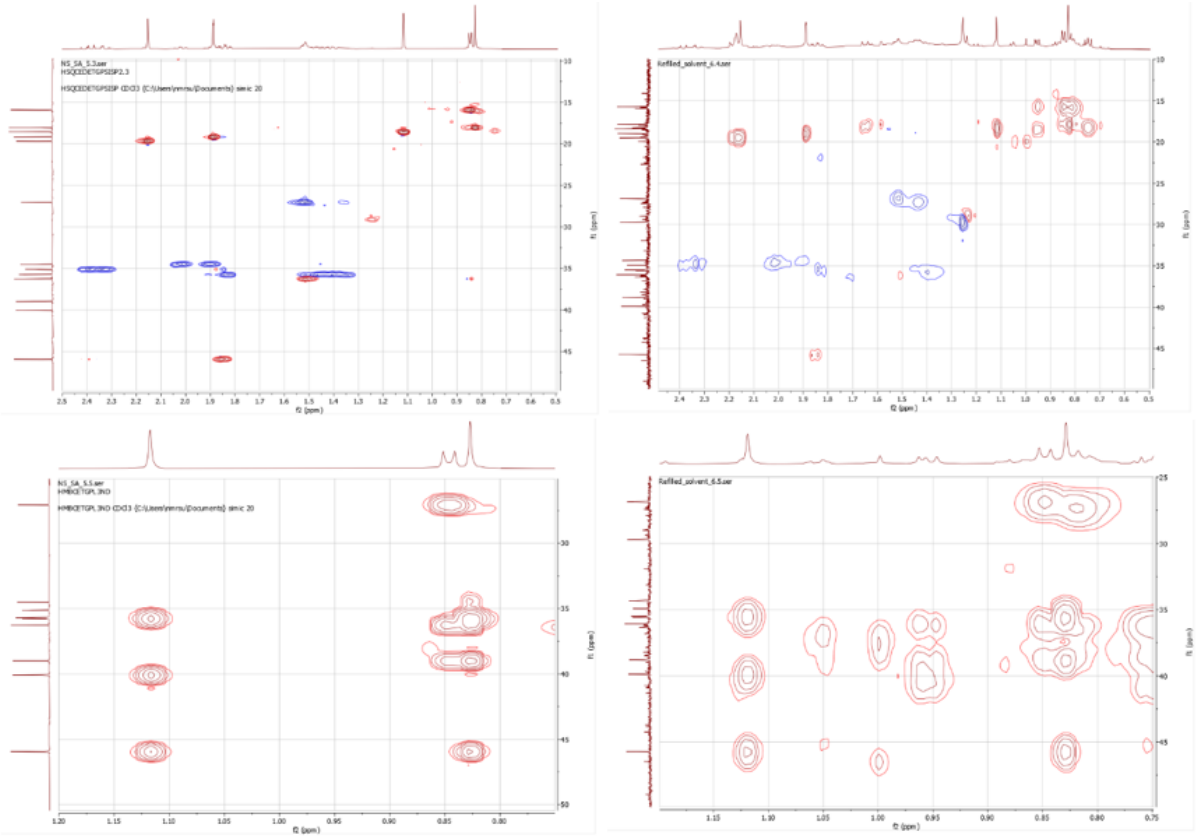

Figure 4.5: A side-by-side comparison of selected sections of the HSQC (above) and HMBC (below) spectra of Sa-5 (left) and Sa-6 (right). While Sa-6 contains more signals on account of being a mixture, the similarities with Sa-5 are evident.

Sa-7

Similarly to Sa-6, MS analysis of the sample revealed Sa-7 is a mixture of two different compounds which appear with ostensible molecular ions with molecular weights 301 Da and 303 Da. Inspecting and comparing the ^{1}H, ^{13}C, and HSQC spectra of Sa-5, Sa-7 and Sa-8 reveals a significant amount of overlap which is illustrated in Tables 4.4 and 4.5.

It bears mentioning that both Sa-5 and the proposed structure for Sa-8 could potentially yield the respective (M + H) peaks with m/z 301 and 303, assuming the loss of H_2O from Sa-5 after ionization. Furthermore, Sa-7 contains ^{13}C with highly similar shifts to that of both Sa-5 and Sa-8 in the 100-200 ppm region of the spectrum, as displayed in Table 4.5. The lower shift range of the spectrum also has many similar peaks, though their suitedness as identifiers of structure similarity is more contestable, given the relative commonality of aliphatic carbons in organic compounds.

Subtracting the Sa-5 and Sa-8 ^{13}C signals from the ^{13}C spectrum of Sa-7 still leaves signals in the 100-210 ppm region, and it is therefore reasonable to assume there could be a third component in the sample, though it did not distinction itself from the other components in GC-MS, and NMR spectra are too contaminated by the other two components to attempt elucidation.

Table 4.4: Comparison of selected ^{13}C signals observed in Sa-5, Sa-7, and Sa-8.

Sa-5	Sa-7	Sa-8
δ ^{13}C (ppm)	**δ ^{13}C (ppm)**	**δ ^{13}C (ppm)**
	103.0	103.0
115.1	114.9	
125.8	125.4	
	155.8	155.9
163.3	163.1	
171.0	171.9	
172.7	173.1	
	184.5	184.8
200.3	200.6	

Table 4.5: Comparison between selected ^{1}H signals and their corresponding ^{13}C as shown by HSQC.

Sa-5		Sa-7		Sa-8	
δ ^{1}H (ppm)	**δ ^{13}C, HSQC (ppm)**	**δ ^{1}H (ppm)**	**δ ^{13}C, HSQC (ppm)**	**δ ^{1}H (ppm)**	**δ ^{13}C, HSQC (ppm)**
0.83	18.1	0.83	18.1		
		0.96	15.8	0.95	15.6
1.12	18.6	1.12	18.3	1.13	
		1.23	29.0	1.24	29.0
1.89	19.2	1.89	19.2	1.89	19.1
2.15	19.7	2.17	19.6		
		4.73	103.0	4.74	103.0
		4.79	103.0	4.80	103.0
5.67	115.1	5.68	114.9		
10.7		10.0		11.8	

Sa-8

GC-MS of SA-8 revealed again a mixture of two compounds with peaks of m/z ratios 301 and 303. The 301 peak appears as well in Sa-6 and Sa-7, but as opposed to those samples, the clear major component in Sa-8 is 303. ^{1}H and ^{13}C NMR corroborate the presence of a carboxylic acid group, which means a (M+H) ion of m/z = 303 would correspond to a molecular formula of $C_{20}H_{30}O_2$. These numbers of carbon and hydrogen atoms are in agreement with the number suggested by NMR, as seen in Table 4.7.

Table 4.6: Extracted data from the ^{1}H spectrum of Sa-8, including chemical shifts, multiplicity, integral, and *J* constants where applicable.

δ ^{1}H (ppm)	**m**	**I**	***J* (Hz)**
0.77 – 0.86	m	2	
0.88	s	1	
0.95	s	3	
0.97 – 1.04	m	2	
1.04 – 1.09	m	2	
1.12 – 1.16	m	2	
1.21	s	1	
1.24	s	3	
1.37 – 1.50	m	4	
1.50 – 1.54	m	1	
1.54 – 1.63	m	3	
1.80 – 1.92	m	5	
1.99	dd	1	2.1 11.4
2.03 – 2.07	m	2	
2.12 – 2.18	m	1	
2.64	t	1	4.2
4.74	s	1	
4.80	s	1	
11.9	s	1	

Table 4.7: Extracted data from the ^{13}C spectrum of Sa-8, including ^{1}J(C,H) couplings as established by HSQC along with the carbon degree of substitution.

δ ^{13}C (ppm)	**δ ^{1}H, HSQC (ppm)**	**Comment**
15.6	0.95	CH_3
18.5	1.57	CH_2
19.1	1.47 + 1.89	CH_2
21.8	1.83	CH_2
29.0	1.24	CH_3
33.1	1.50 + 1.63	CH_2
37.8	1.05 + 2.17	CH_2
39.7	1.15 + 2.00	CH_2
39.7		q
40.7	0.83 + 1.89	CH_2
41.3	1.47 + 1.55	CH_2
43.8		q
43.9	2.64	CH
44.2		q
49.0	2.04	CH_2
55.1	1.06	CH
57.1	1.07	CH

103.0	4.74 + 4.80	CH_2
155.9		q
184.8		COOH

HSQC and HMBC correlations allowed the elucidation of fragments shown in Figure 4.6. Two fragments are directly connected (Figure 4.7) and hint toward a 3-cyclic structure, while the third fragment could not be connected in a similar manner.

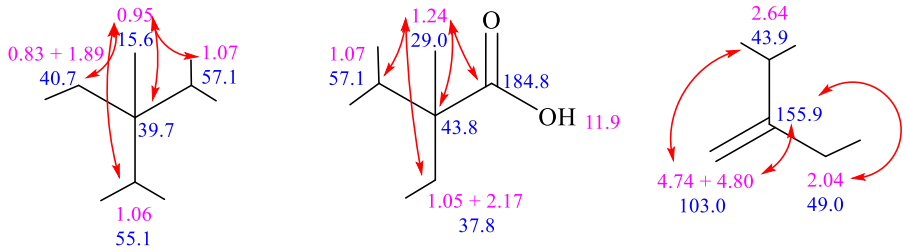

Figure 4.6: HMBC correlations, indicated by arrows, reveal fragments of the structure.

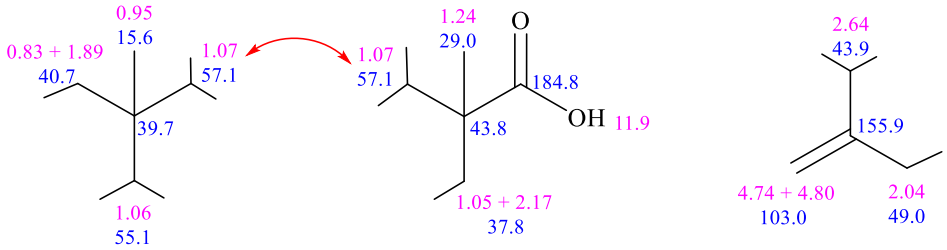

Figure 4.7: The assembled fragments are displayed, two of which are directly connected. No evidence was found to elucidate connection with the third fragments.

In addition to the fragments there remain 6 CH_2 groups as well as 1 quaternary carbon. Available data was not sufficient to elucidate the structure further, but arranging the already known fragments appropriately revealed a potential similarity to kaur-16-en-18-oic acid, see Figure 4.8. Upon inspection the unaccounted CH_2 groups and quaternary carbon complement this structure very well, and the obtained ^{1}H and ^{13}C spectra for Sa-8 correspond extremely well with previously reported NMR data for kaur-16-en-oic acid (See Appendix D, kaur-16-en-18-oic acid)

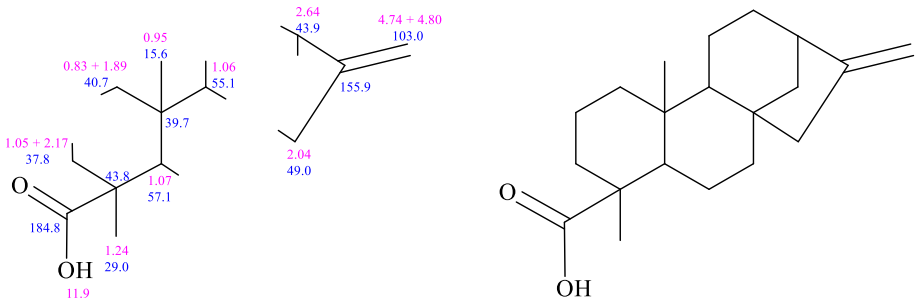

Sa-8 fragments kaur-16-en-18-oic acid

Figure 4.8: The elucidated fragments compared side-by-side with kaur-16-en-18-oic acid. While direct supporting evidence was not found, the remaining CH_x groups not in the fragments can be fitted into the structure as to yield kaur-16-en-18-oic acid.

Sa-10

By use of 1D ^{1}H and ^{13}C, and 2D ^{1}H-^{13}C HSQC (Appendix A, Sa-10) information was extracted that allowed the assembly of multiple fragments. The data are summarised in tables 4.8 and 4.9.

Table 4.8: Extracted data from the ^{1}H spectrum of Sa-10, including chemical shifts, multiplicity, integral, and *J* constants where applicable.

δ ^{1}H (ppm)	**m**	**I**	***J* (Hz)**
0.73	s	3	
0.87	s	6	
0.88	d		7.3
0.95	s	3	
1.00	s	6	
1.01	s		
1.05	s	3	
1.18	s	3	
1.19 – 1.23	dd	1	6.0 13.7
1.23 – 1.33	m	5	
1.33 – 1.42	m	6	
1.42 – 1.60	m	11	
1.69	qd	1	5.1 13.0
1.73 – 1.78	m	1	
1.94 – 1.99	m	1	
2.22 – 2.33	td + q	2	7.3 13.6 6.7
2.37 – 2.42	ddd	1	1.7 5.1 13.7

Table 4.9: Extracted data from the ^{13}C spectrum of Sa-10, including ^{1}J(C,H) couplings as established by HSQC along with the carbon degree of substitution.

δ ^{13}C (ppm)	**δ ^{1}H, HSQC (ppm)**	**Comment**
6.8	0.88	CH_3
14.7	0.73	CH_3
18.0	0.87	CH_3
18.3	1.40 + 1.50	CH_2
18.7	1.05	CH_3
20.3	1.01	CH_3
22.3	1.69 + 1.97	CH_2
28.2		q
30.0		q
30.5	1.35	CH_2
31.8	1.00	CH_3
32.1	1.18	CH_3
32.4	1.31 + 1.52	CH_2
32.8	1.27 + 1.48	CH_2
35.0	0.95	CH_3
35.4	1.21 + 1.38	CH_2
35.6	1.27 + 1.46	CH_2
36.0	1.37 + 1.57	CH_2
37.5		q
38.3		q
39.3	0.94 + 1.50	CH_2

39.7		Q
41.3	1.28 + 1.75	CH_2
41.6	2.30 + 2.40	CH_2
42.2		q
42.8	1.56	CH
53.1	1.40	CH
58.2	2.25	CH
59.5	1.54	CH
213.3		C=O

Cross-referencing with data obtained from GC-MS analysis (Appendix C, Sa-10) the mass spectrum shows a molecular ion of 426 Da, corresponding to the molecular formula $C_{30}H_{50}O$. This is corroborated by the ^{1}H and ^{13}C NMR spectra and the IR spectrum (Appendix B, Sa-10), which indicates the presence of a C=O group with characteristic absorption bands at 1750 cm^{-1} and 1100-1250 cm^{-1}. Furthermore, the molecular formula reveals an HDI of 6.

The assembled fragments are displayed in Figure 4.9. Upon closer inspection several fragments are interconnected and can be combined into a larger fragment, illustrated in Figure 4.10. A NIST library search was run on the fragmentation of the sample, which returned friedelan-3-one as the most likely compound in the database. This is a triterpene, which seems a likely structure given the molecular formula and HDI. Arranging the larger fragment into a triterpene-like skeleton, the remaining smaller fragments readily fit into the structure, corroborated by ^{1}H-^{1}H COSY and to a lesser extent NOESY as visualized in Figure 4.11.

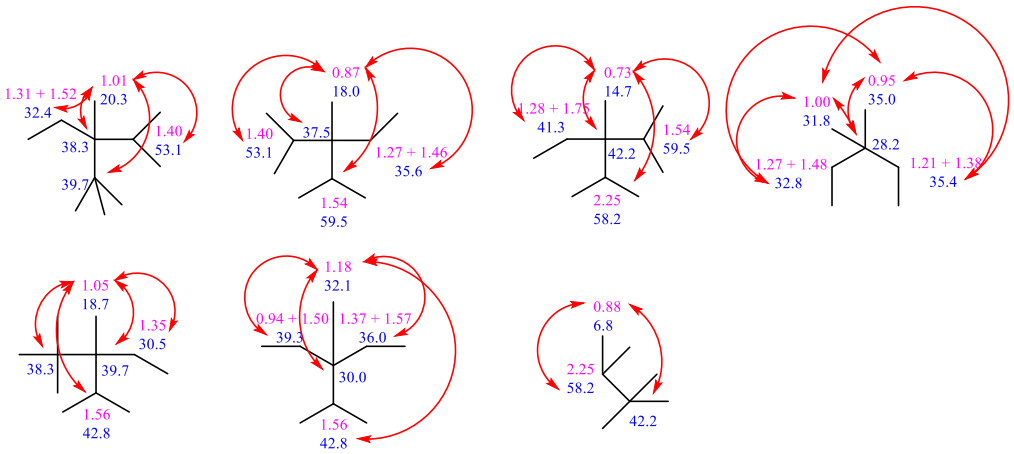

Figure 4.9: Fragments assembled based on HMBC signals, indicated by the arrows.

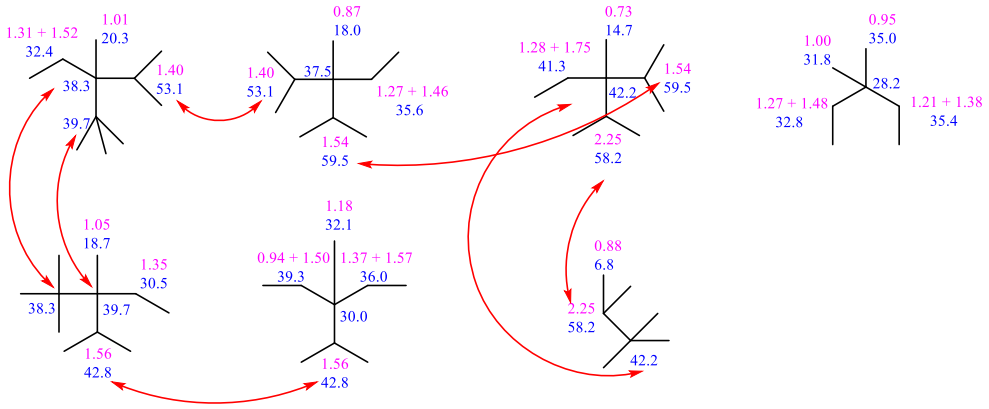

Figure 4.10: Here illustrated are the direct connections between assembled fragments. Apart from one fragment, all could be connected directly.

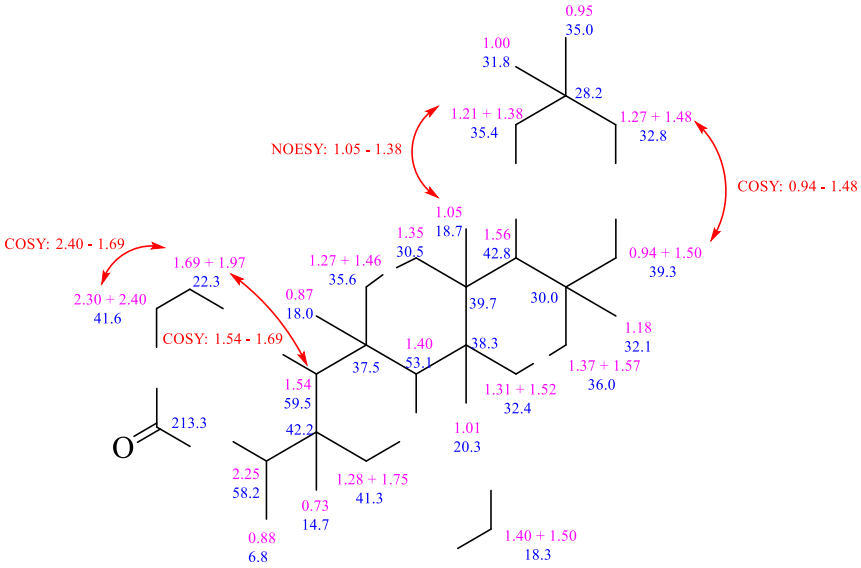

Figure 4.11: The connected fragments from Figure 4.10 oriented to accommodate a triterpene-like structure. The remaining atoms can be fitted on this skeleton by the correlations indicated.

The only remaining parts of the compound as of yet unaccounted for are the C=O and one CH_2 group. Triterpenes will almost always as a product of their biosynthesis from 2,3-oxidosqualene have oxygen in some form on C3, and the protons in the immediate vicinity of this position have a higher shift (2.30 + 2.40 and 2.25 ppm) than protons elsewhere, suggesting some amount of de-shielding not present in the other available "slot" in the structure. Barring any other possibilities, this de-shielding must be assumed due to effects from the C=O group, which leaves only one possible location for the last remaining CH_2 group.

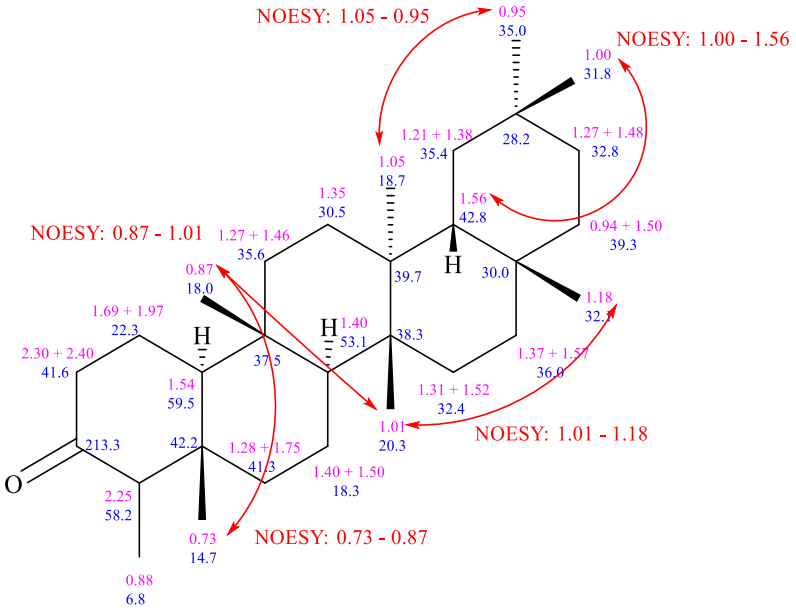

Figure 4.12: The final elucidated structure of Sa-10, *4,4a,6b,8a,11,11,12b,14a-octamethylicosahydropicen-3(2H)-one*, with partial stereochemistry.

Suggested stereochemistry of (compound name) was based on 2D NOESY as shown in Figure 4.12, and it must be noted that this makes tenuous evidence for a polycyclic compound of this fashion. Each ring could be in a chair or boat conformation, with methyl substituents in an equatorial or axial conformation, which yields several possible combinations of such orientations to allow for the NOESY signals observed. Using *J* coupling constants to determine axial/equatorial orientations of substituents proved extremely difficult due to both the placement of substituents and chemical shift similarity in the cyclic hydrogens. Consider the ^{1}H with shift 2.25 ppm: It has no vicinal hydrogens (methyl excluded) with which a coupling constant could yield a dihedral angle to determine equatorial or axial configuration with. Since it is unknown whether the hydrogen occupies the axial or equatorial position, it is also unknown which of these positions the methyl occupies. Similarly, none of the bridgeheads in the structure contain hydrogens with which the ring conformations can be determined, since both bridgeheads would need a hydrogen to produce a usable coupling constant.

The opposite is the case with ^{1}H 1.56 ppm; since it has 2 vicinal protons, useful information might be had from its coupling constants. If a dihedral angle of 180° can be indicated with either of the vicinal protons, that means the neighbouring ring would have to occupy the equatorial position. However, the 1.56 ppm signal in the 1D ^{1}H spectrum is part of a multiplet of superimposed signals from which no coupling constant can be discerned. Using Chemdraw 3D software, the stereochemistry in Figure 4.12 was selected based on the given NOESY signals, and what orientation of the rings and remaining substituents allowed for the most stable structure. NOESY yielded little information about the ^{13}C 6.8 ppm methyl, although the *(S)* conformation is the more reported variant of its adjacent stereocenter, ^{13}C 58.2 ppm, in literature.

Sa-11

As with previous samples, the ^{1}H and ^{13}C spectra were evaluated and the information extracted from them is summarized in tables 4.10 and 4.11 along with ^{1}J(C,H) couplings extracted from HSQC in the latter table.

Evaluating the HMBC spectrum revealed inconsistencies. These inconsistencies arise from HMBC cross peaks which indicate that a methyl group is part of two different chemical environments simultaneously. This could be a consequence of sample impurity, which GC-MS analysis confirmed. “Valid” cross peaks were evaluated based on whether the connections was demonstrated by the methyl group in question. For example, the ^{1}H peak with δ = 1.01 ppm is bonded to the ^{13}C with δ = 31.8 ppm as shown by HSQC – a methyl group. HMBC reveals these same protons have geminal and vicinal carbons with chemical shifts 30.7, 38.4, 39.7, and 53.2. On the other hand, the protons with shift 0,94 ppm, another methyl group, have similar couplings with carbons 28.2, 31.8, 32.9, and 35.4. But 31.8 is our first methyl group, whose ^{1}H signal shows no correlations whatsoever with any of the carbons 28.2, 31.8, 32.9, and 35.4 in HMBC. This is conflicting information, so methyl 31.8’s environment is evaluated based on its own cross peaks, rather than that of another methyl group.

The ^{1}H integrals also dispel the notion that there are two distinct methyl groups with similar shifts. Such inconsistencies were encountered relating to the HMBC peaks of methyl groups with ^{1}H shift 1.00 ppm and 0.94 ppm. These two methyl groups do share common carbons which do not lead to contradictions, and could be combined into a presumed fragment which eventually proved to fit the structure without further complications as seen in Figures 4.14 and 4.15.

Table 4.10: Extracted data from the ^{1}H spectrum of Sa-11, including chemical shifts, multiplicity, integral, and *J* constants where applicable.

δ ^{1}H (ppm)	**m**	**I**	***J* (Hz)**
0.86	s	3	
0.88 – 0.92	m	2	
0.93	d	6	7.6
0.94	s		
0.96	s	3	
0.99	s	9	
1.00	s		
1.01	s		
1.09 – 1.16	m	2	
1.17	s	3	
1.18 – 1.22	dd	1	5.9 13.8
1.22 – 1.33	m	7	
1.33 – 1.41	m	5	
1.41 – 1.50	m	5	
1.50 – 1.60	m	9	
1.71 – 1.76	dt	1	3.2 12.8
1.88 – 1.92	m	1	
3.74	q	1	2.6

Table 4.11: Extracted data from the ^{13}C spectrum of Sa-11, including ^{1}J(C,H) couplings as established by HSQC along with the carbon degree of substitution.

δ ^{13}C (ppm)	**δ ^{1}H, HSQC (ppm)**	**Comment**
11.7	0.93	CH_3
15.8	1.42 + 1.54	CH_2
16.4	0.96	CH_3
17.6	1.37	CH_2
18.3	0.86	CH_3
18.7	1.00	CH_3
20.2	0.99	CH_3
28.2		q
30.1		q
30.7	1.32	CH_2
31.8	1.01	CH_3
32.1	1.17	CH_3
32.4	1.29 + 1.49	CH_2
32.9	1.27 + 1.47	CH_2
35.1	0.94	CH_3
35.2	1.57 + 1.91	CH_2
35.4	1.21 + 1.37	CH_2
35.6	1.13 + 1.44	CH_2
36.1	1.35 + 1.55	CH_2
37.1		q
37.9		q
38.4		q
39.3	0.94 + 1.49	CH_2
39.7		q
41.8	0.98 + 1.74	CH_2
42.9	1.55	CH
49.2	1.26	CH
53.2	1.28	CH
61.4	0.90	CH
72.8	3.74	CH, OH

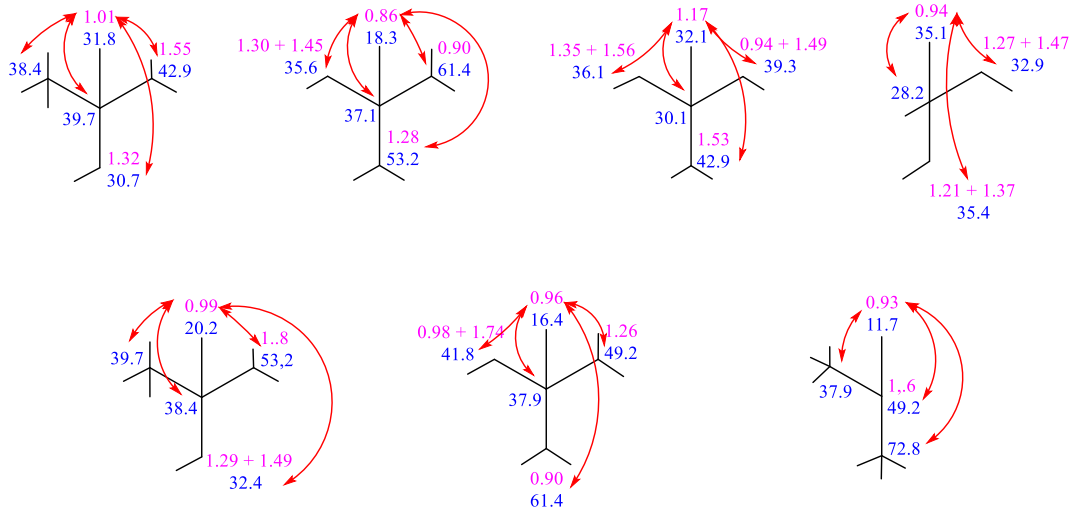

Figure 4.13: Fragments of Sa-11's structure assembled based on HMBC signals, indicated by the arrows.

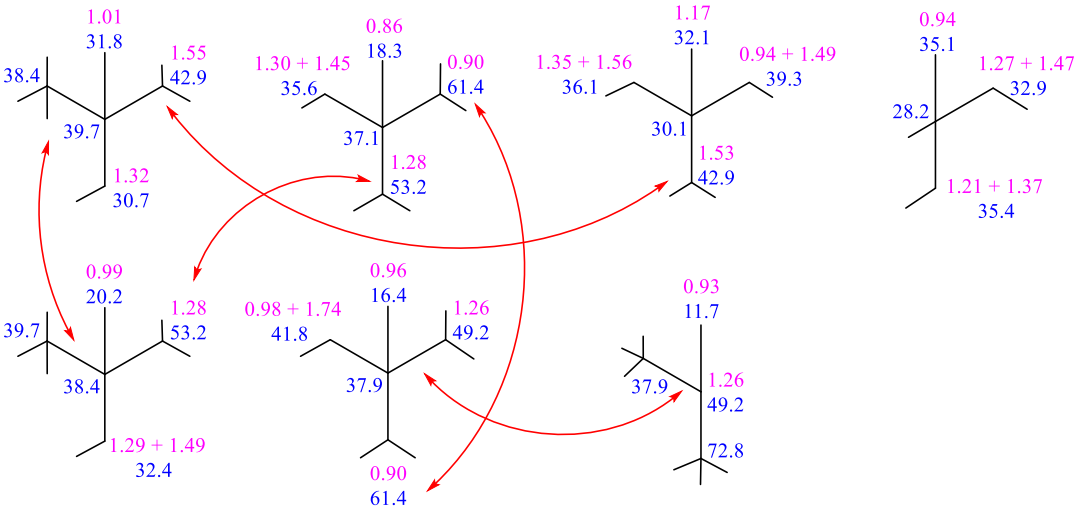

Figure 4.14: The assembled fragments elucidated by HMBC are shown, and common carbons that connect them are indicated by arrows.

After assembly of the fragments, the rest of the carbons and hydrogens could be fitted into the structure with the help of COSY as seen in Figure 4.15. Finally, the structure was closed as to result in 5 stable 6-membered rings in accordance with the HDI shown below and the suggested structure skeleton from the MS NIST library (See Appendix C, Sa-11).

In addition, IR suggests a hydroxyl group; C-O stretching vibrations typically have strong absorption bands in the 1000-1260 cm^{-1} region of the spectrum, which were also observed in Sa-11. Another common absorption band for OH groups is due to O-H stretching vibrations and can be found in the 3200-3550 cm^{-1} region. This absorption band is absent in Sa-11's IR spectrum, however, MS corroborates the presence of at least 1 oxygen atom which by process of elimination has to be assigned to the carbon with δ = 72.8 ppm. This carbon is not fully saturated yet and the shift is in line with expected values for C-O carbons. Lacking any other carbons that could be part of an ether moiety, a hydroxyl group is the only explanation. This sets the theoretical molecular formula and mass at $C_{30}H_{52}O$ and 428 Da, respectively, which

are confirmed by MS (See Appendix C, Sa-11). The resulting HDI of 5 is also in line with the pentacyclic structure arrived at in Figure 4.16.

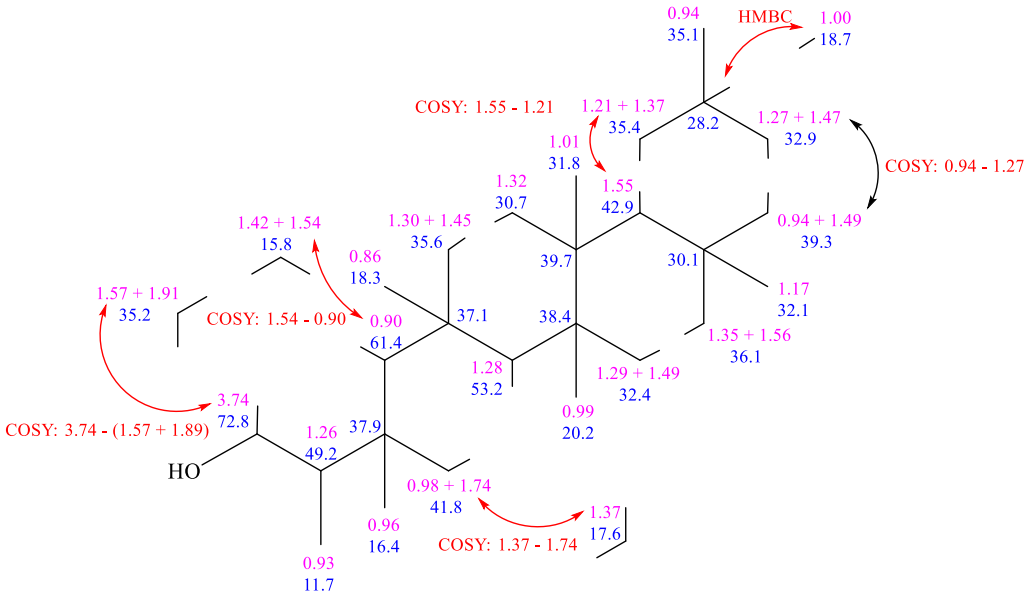

Figure 4.15: The larger fragment from Figure 4.15 oriented to fit onto a triterpene skeleton, with the remaining atoms and fragments being connected through correlations indicated by the arrows.

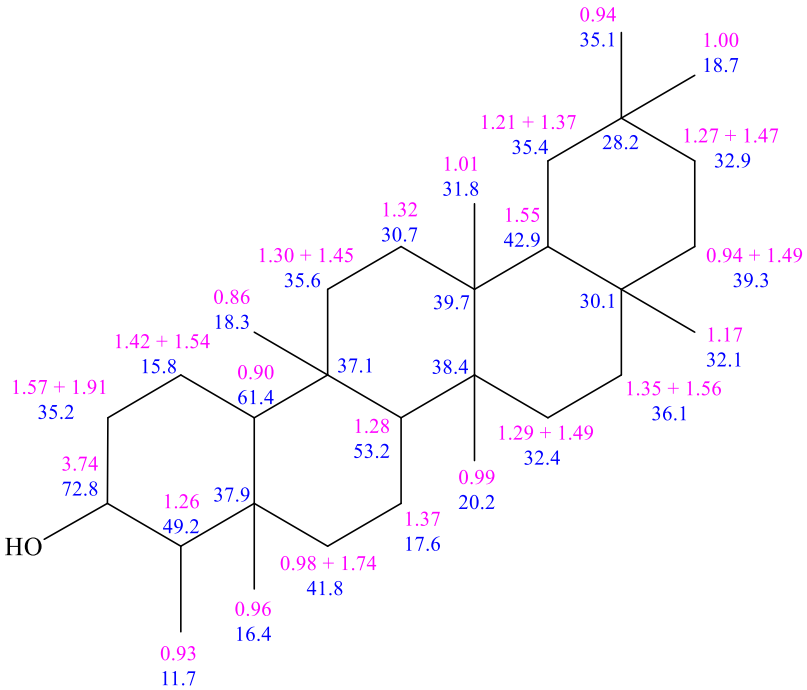

Figure 4.16: The elucidated structure of Sa-11, *4,4a,6b,8a,11,11,12b,14a-octamethyldocosahydropicen-3-ol*.

Using the 2D NOESY spectra and obtained *J* constants in Table 4.10, the compound's stereochemistry was investigated, but could not be elucidated with available data for similar reason as discussed for Sa-10.

Sa-12

The ^{1}H, ^{13}C, and HSQC spectra of Sa-8 were evaluated and relevant data is summarized in tables 4.12 and 4.13. As per the standard procedure, this data was used to assemble fragments which are displayed in Figure 4.17. Several of the fragments have common atoms and can thus be connected, and additional connections between fragments were demonstrated using COSY, and are illustrated in Figures 4.18 and 4.19.

Table 4.12: Extracted data from the ^{1}H spectrum of Sa-12, including chemical shifts, multiplicity, integral, and *J* constants where applicable.

δ ^{1}H (ppm)	**m**	**I**	***J* (Hz)**
0.65 – 0.67	m	2	
0.67 – 0.71	m	2	
0.71 – 0.75	m	6	
0.72	s		
0.75 – 0.77	m	4	
0.76	s		
0.78 – 0.82	m	7	
0.85 – 0.97	m	21	
0.87	s		
0.90	s		
0.93	s		
0.95	s		
0.99 – 1.05	m	4	
1.07	s	3	
1.15	dt	2	3.3 13.8
1.17 – 1.22	m	3	
1.22 – 1.30	m	5	
1.30 – 1.39	m	5	
1.39 – 1.52	m	9	
1.52 – 1.60	m	5	
1.60 – 1.63	m	1	
1.65 – 1.74	m	2	
1.78 – 1.82	m	1	
1.82 – 1.96	m	3	
3.10 – 3.18	m	2	
5.11	t	1	3.5

Table 4.13: Extracted data from the ^{13}C spectrum of Sa-12, including ^{1}J(C,H) couplings as established by HSQC along with the carbon degree of substitution.

δ ^{13}C (ppm)	**δ ^{1}H, HSQC (ppm)**	**Comment**
15.5	0.87	CH_3
15.6	0.72	CH_3
16.8	0.90	CH_3
18.4	1.33 + 1.47	CH_2
23.6	1.80	CH_2
23.7	0.80	CH_3
26.0	1.07	CH_3
26.2	0.90 + 1.70	CH_2
27.0	0.73 + 1.92	CH_2
27.3	1.53	CH_2
28.1	0.93	CH_3
28.4	0.76	CH_3

31.2		q
32.5		q
32.7	1.27 + 1.44	CH_2
33.4	0.80	CH_3
34.8	1.03 + 1.26	CH_2
37.0		q
37.2	1.14 + 1.36	CH_2
38.6	0.90 + 1.56	CH_2
38.8		q
39.8		q
41.8		q
46.9	0.95 + 1.61	CH_2
47.3	1.88	CH
47.7	1.49	CH
55.2	0.67	CH
79.0	3.15	CH, OH
121.8		CH
145.2		q

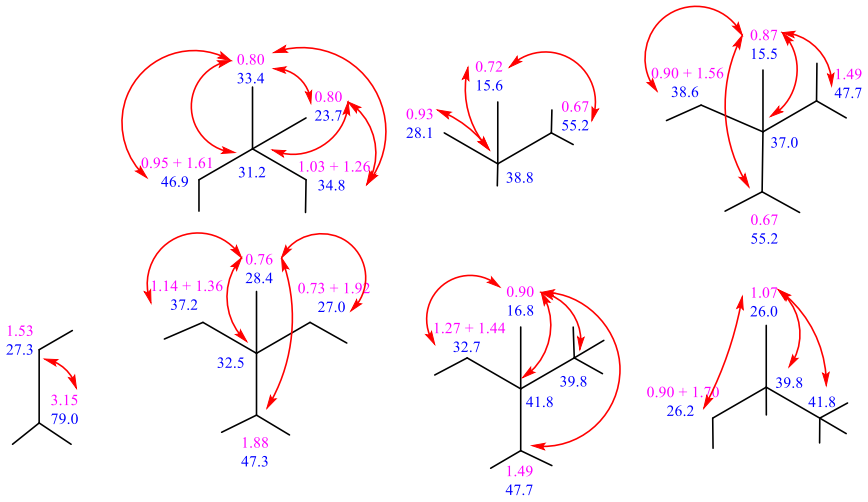

Figure 4.17: Fragments of Sa-12's structure assembled based on HMBC signals, indicated by the arrows.

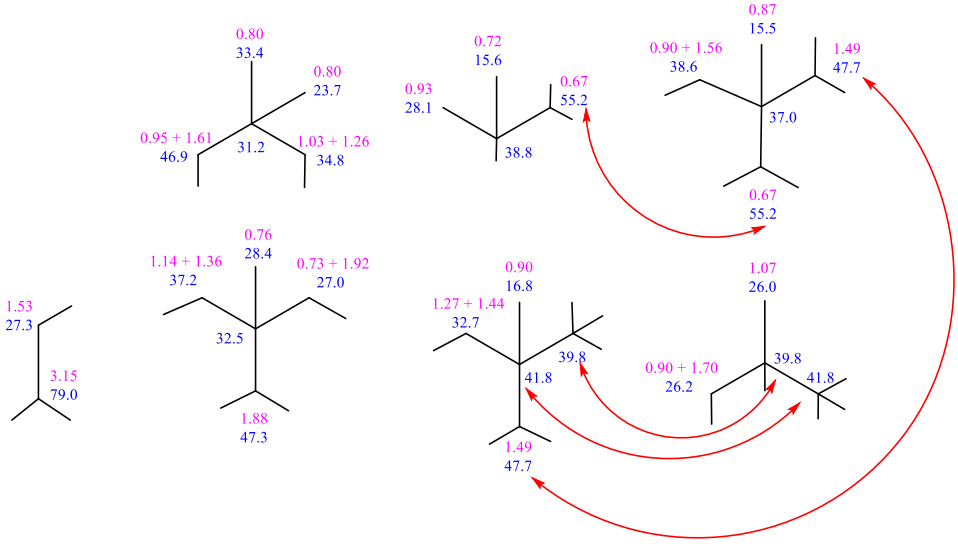

Figure 4.18: The fragments assembled from HMBC correlations are shown, along with indication of common carbons between fragments that connect them.

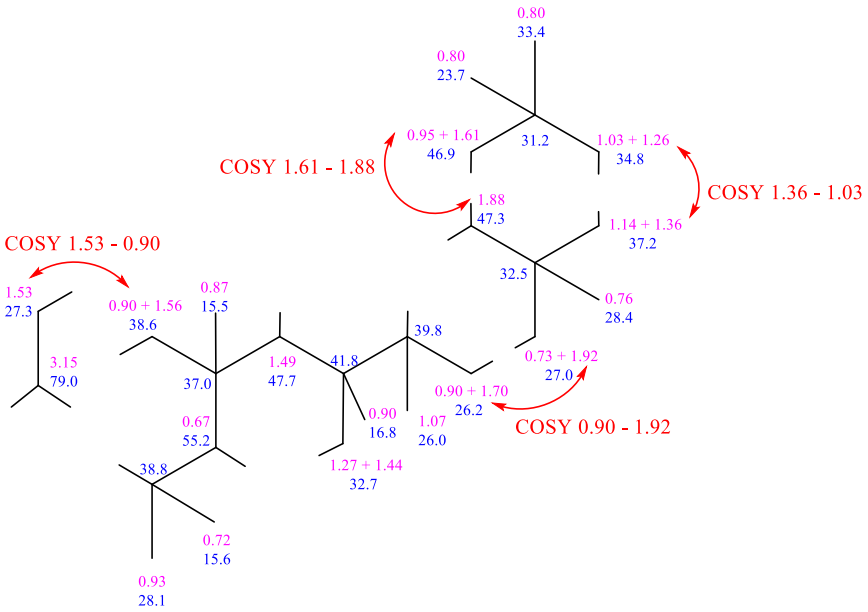

Figure 4.19: The larger fragment from Figure 4.18 oriented to fit onto a triterpene skeleton, with the remaining atoms and fragments being connected through correlations indicated by the arrows.

Additional COSY-peaks show an allylic moiety which can be directly connected to the larger structure, see Figure 4.20. The carbon with δ = 125.8 ppm has a shift that matches expected values for alkenes, and thus has to be connected with quaternary carbon with δ = 145.2, which also matches expected values for alkene carbons. The slightly higher shift can be attributed to its quaternary nature, and its placement in the structure suggests it is the missing carbon required for closure of rings C and D. The only unaccounted carbon is a CH_2 group, which readily fit into the structure as a closing link for ring B. Lastly, the carbon with δ = 79.0 is still missing a substituent. The observed shift corresponds to expected values for C-O, suggesting the substituent may be a hydroxyl group. This is supported by IR and MS.

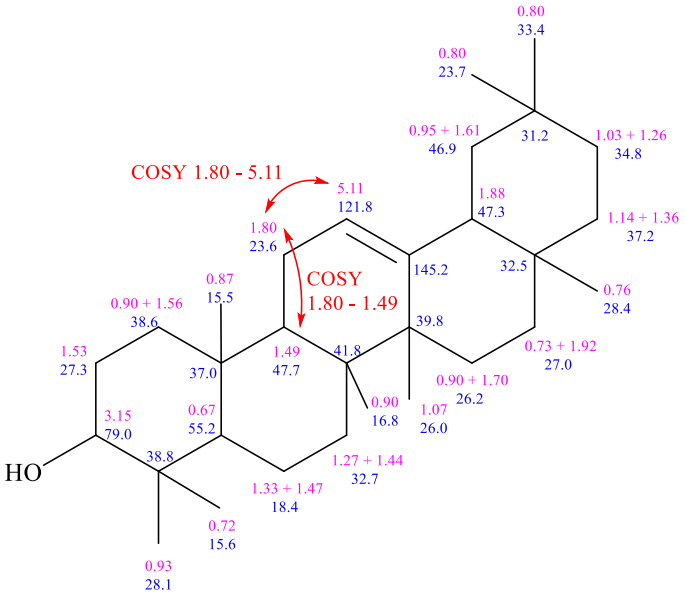

Figure 4.20: The final elucidated structure. Indicated are the final supporting signals.

The IR spectrum contains a broad absorption ban in the 3200-3550 cm^{-1} region, corresponding to O-H stretching vibrations. C-O stretching vibrations yield strong absorption bands in the 1000-1260 cm^{-1} region of the spectrum and are also observed. There is also a strong absorption band around 1750 cm^{1}, which can be attributed to C=C stretching vibrations for alkenes. Additionally, GC-MS analysis suggests a molecular ion with m/z = 426. Accounting for the known number of carbon and hydrogen atoms as established by NMR, $C_{20}H_{27}$, the addition of a hydroxyl group yields the molecular formula of $C_{30}H_{50}O$ with a molecular formula of 426 Da. The corresponding HDI = 6 is also in agreement with the elucidated structure. Using 2D NOESY the stereochemistry of the molecule was investigated, but for similar reasons encountered with Sa-11, the attempt was unsuccessful.

Discussion

It must be considered that in addition to the expected complications and difficulties tied to the extraction and isolation of compounds from plants, these samples in particular have been stored away for an extended amount of time, 2 years. It is possible that some compounds have degraded during this time, despite being stored at low temperature in absence of light. It is also possible, although less likely, that potentially unstable compounds could have undergone reactions with their environment upon evaporation of the initial solvent and subsequent exposure to air in the NMR tube. While these suspicions are impossible to confirm, their possibility can not be discarded entirely either, as a consequence of the extended timeframe separating their isolation and identification.

Another issue encountered during the elucidation of the structures is tied to their concentration; several of the compounds made up less than the recommended 5 mg for NMR analysis. Indeed, for Sa-3, Sa-4, and Sa-13, the concentration of sample was too low to be detected in ^{13}C NMR at all, and these structures could not be elucidated due to a lack of compelling data. The available amount of sample also meant that all NMR had to be run before MS analysis, which is destructive. This meant that any NMR spectra not obtained before MS analysis could not be obtained at all, which was problematic since any structure arrived at from NMR would have to be confirmed by MS. Sa-11 and Sa-12 could have benefitted from additional NOESY experiments given their poor spectra, which was not possible anymore by the time the respective structures were confirmed.

While sample impurity is not an unknown problem while isolating compounds from plants, and must to some degree be expected, this proved a particularly prevalent problem for Sa-6 and Sa-7. While several of the other samples displayed some minor impurities, these were relatively easy to distinguish from the sample's main constituent. In the case of Sa-6 and Sa-7 however, the constituent compounds were of a too similar concentration to readily distinguish between them. Comparison with spectra obtained from Sa-5 and Sa-8 hints that they may in fact be components present in both Sa-6 and Sa-7 in different ratios, although actual elucidation from what effectively would be 2 – or 3 – superimposed spectra of comparable intensity is infeasible. Lacking a better hypothesis, it is the most likely conclusion that Sa-6 and Sa-7 are mixtures of *(E)-3-methyl-5-((1R,2S,4aS,8aR)-1,2,4a,5-tetramethyl-7-oxo-1,2,3,4,4a,7,8,8a-octahydronaphthalen-1-yl)pent-2-enoic acid* and *kaur-16-en-18-oic acid*, but lacking hard evidence this notion must sadly be resigned to the realm of speculation.

Several samples were not possible to elucidate, like the aforementioned Sa-6 and Sa-7, which are assumed to be mixtures of other elucidated structures. Sa-3, Sa-4, and Sa-13 were not present in sufficient concentration, not even with 3mm NMR tubes, to be sufficiently detected in ^{13}C NMR. Sa-2 and Sa-9 remain unknown, as no structures for these samples were arrived at, nor was there found evidence to suggest mixtures. Their elucidation may be possible with the data obtained and provided in the appendices of this thesis, but this task eventually proved undoable within an appropriate timeframe and might be subject for later work. MS analysis on these compounds were initially non-conclusive, as the initial GC-MS analysis with ESI ionization didn't yield much result. After switching to direct mass analysis using an ASAP probe, which uses APCI ionization, results were obtained. APCI ionization is well-suited for non-polar analytes, and it stands to reason that compounds 2 and 9 were too non-polar to be

ionized with the previous ESI method. Sa-02's ^{1}H spectrum in particular contains signals with chemical shift in the 7.0-8.0 ppm region, which is in agreement with expected values for aromatic hydrogen.

While the development and improvement of NOAH-sequences are a considerable and important development toward cheaper, more efficient, and more sustainable structure elucidation, satisfactory results could not be obtained using them with the samples analysed here. Spectra developed from NOAH experiments were plagued poor resolution and unclear/blurry 2D signals. Additionally, all elucidated structures required selective HSQC and HMBC experiments, which required running traditional and separate HSQC and HMBC to set up. These experiments were considerably higher quality than most corresponding NOAH spectra that were obtained.

References

1. Brunken, U., Schmidt, M., Dressler, S., Janssen, T., Thiombiano, A. & Zizka, G. *East African Plants - A Photo Guide*. 2010 [cited 2022 28.06]; Available from: http://www.eastafricanplants.senckenberg.de.
2. Brunken, U., Schmidt, M., Dressler, S., Janssen, T., Thiombiano, A. & Zizka, G. *West African Plants - A Photo Guide*. 2008 [cited 2022 28.06]; Available from: http://www.westafricanplants.senckenberg.de.
3. Bray, F., et al., *The ever-increasing importance of cancer as a leading cause of premature death worldwide.* Cancer, 2021. **127**(16): p. 3029-3030.
4. Organization, W.H., *Global health estimates 2015: deaths by cause, age, sex, by country and by region, 2000–2015.* Geneva: WHO, 2016: p. 2016.
5. Bhaskaran, K., et al., *Air pollution as a carcinogen*. 2013, British Medical Journal Publishing Group.
6. Nobili, S., et al., *Natural compounds for cancer treatment and prevention.* Pharmacological Research, 2009. **59**(6): p. 365-378.
7. Chukwuma, E.C., M.O. Soladoye, and R.T. Feyisola, *Traditional medicine and the future of medicinal Plants in Nigeria.* Journal of Medicinal Plants Studies, 2015. **3**(4): p. 23-29.
8. Raphael, E.C., *Traditional medicine in Nigeria: current status and the future.* Research journal of pharmacology, 2011. **5**(6): p. 90-94.
9. Oloyede, G.K., *Toxicity, antimicrobial and antioxidant activities of methyl salicylate dominated essential oils of Laportea aestuans (Gaud).* Arabian Journal of Chemistry, 2016. **9**: p. S840-S845.
10. Oloyede, G.K. and O.E. Ayanbadejo, *Phytochemical, toxicity, antimicrobial and antioxidant screening of extracts obtained from Laportea aestuans (Gaud).* J Med Sci, 2014. **14**(51): p. e59.
11. Adetunji, O.A., et al., *Reno-Hepatoprotective and Antidiabetic Properties of Methanol Leaf Extract of Laportea Aestuans in Wistar Rats.* Journal of Evidence-Based Integrative Medicine, 2021. **26**: p. 2515690X211017464.
12. Okereke, S. and I. Elekwa, *Studies on the in vitro antioxidant activity of Laportea aestuans leaf extract.* IOSR Journal of Environmental Science, Toxicology and Food Technology, 2014. **8**(1): p. 33-41.
13. Tchinda, C.F., et al., *Antibacterial activities of the methanol extracts of Albizia adianthifolia, Alchornea laxiflora, Laportea ovalifolia and three other Cameroonian plants against multi-drug resistant Gram-negative bacteria.* Saudi journal of biological sciences, 2017. **24**(4): p. 950-955.
14. Kashiwada, Y., et al., *Antitumor agents, 129. Tannins and related compounds as selective cytotoxic agents.* Journal of Natural Products, 1992. **55**(8): p. 1033-1043.
15. Podolak, I., A. Galanty, and D. Sobolewska, *Saponins as cytotoxic agents: a review.* Phytochemistry Reviews, 2010. **9**(3): p. 425-474.
16. Rao, A. and M.-K. Sung, *Saponins as anticarcinogens.* The Journal of nutrition, 1995. **125**(suppl_3): p. 717S-724S.
17. Sakagami, H., et al., *Cytotoxic activity of hydrolyzable tannins against human oral tumor cell lines — A possible mechanism.* Phytomedicine, 2000. **7**(1): p. 39-47.
18. Plucknett, D.L., *2 Taxonomy of the Genus Colocasia*, in *Taro: A Review of Colocasia esculenta and Its Potentials*, W. Jaw-Kai, Editor. 2021, University of Hawaii Press. p. 14-19.
19. Kaushal, P., V. Kumar, and H.K. Sharma, *Utilization of taro (Colocasia esculenta): a review.* Journal of Food Science and Technology, 2015. **52**(1): p. 27-40.
20. Rashmi, D., et al., *Taro (Colocasia esculenta): an overview.* Journal of Medicinal Plants Studies, 2018. **6**(4): p. 156-161.
21. Prajapati, R., et al., *Colocasia esculenta: A potent indigenous plant.* International Journal of Nutrition, Pharmacology, Neurological Diseases, 2011. **1**(2): p. 90.

22. Kundu, N., et al., *Antimetastatic activity isolated from Colocasia esculenta (taro).* Anti-cancer drugs, 2012. **23**(2): p. 200-211.
23. Chakraborty, P., et al., *Cytotoxicity and antimicrobial activity of Colocasia esculenta.* J. Chem. Pharm. Res, 2015. **7**(12): p. 627-635.
24. Earnest, E., *Xylopia Aethiopica: A Review of its Ethnomedicinal, Chemical and Pharmacological Properties.* 2014. **4**: p. 22-37.
25. Fetse, J.P., W. Kofie, and K.A. Reimmel, *Ethnopharmacological importance of Xylopia aethiopica (DUNAL) A. RICH (Annonaceae)-A review.* British Journal of Pharmaceutical Research, 2016. **11**(1): p. 1.
26. Yin, X., et al., *Xylopia aethiopica Seeds from Two Countries in West Africa Exhibit Differences in Their Proteomes, Mineral Content and Bioactive Phytochemical Composition.* Molecules (Basel, Switzerland), 2019. **24**(10): p. 1979.
27. Choumessi, A.T., et al., *Characterization of the antiproliferative activity of Xylopia aethiopica.* Cell Division, 2012. **7**(1): p. 8.
28. Adaramoye, O.A., et al., *Antiproliferative Action of Xylopia aethiopica Fruit Extract on Human Cervical Cancer Cells.* Phytotherapy Research, 2011. **25**(10): p. 1558-1563.
29. Bakarnga-Via, I., et al., *Composition and cytotoxic activity of essential oils from Xylopia aethiopica (Dunal) A. Rich, Xylopia parviflora (A. Rich) Benth.) and Monodora myristica (Gaertn) growing in Chad and Cameroon.* BMC Complementary and Alternative Medicine, 2014. **14**(1): p. 125.
30. Ezekwesili, C., et al., *Investigation of the chemical composition and biological activity of Xylopia aethiopica Dunal (Annonacae).* African Journal of Biotechnology, 2010. **9**(43): p. 7352-7356.
31. Avaligbe, C.T., et al., *Antihemolytic properties of extracts of six plants used in the traditional treatment of sickle cell disease in Benin.* Journal of Applied Pharmaceutical Science, 2012(Issue): p. 08-13.
32. Evuen, U.F., et al., *Protective activity of root extract of Rhaphiostylis beninensis against carbon tetrachloride-induced hepatotoxicity in Wistar rats.* Biokemistri, 2021. **32**(2).
33. Lasisi, A., et al., *Phytochemical, antibacterial and cytotoxic evaluation of Raphiostylis beninensis [Hook F. ex Planch] stem bark extracts.* International Journal of Pharma and Bio Sciences, 2011. **2**(3).
34. Usunobun, U., O.J. Ovbokhan, and O.N. Paulinaus, *Hepatoprotective Effect of Raphiostylis Beninensis Ethanol Root Extract on Carbon-tetrachloride (CCl4)-induced Liver Attack and Damage in Rats.* Am. J. Biomed. Sci, 2020. **12**(3): p. 155-163.
35. Sasidharan, S., et al., *Extraction, isolation and characterization of bioactive compounds from plants' extracts.* African journal of traditional, complementary and alternative medicines, 2011. **8**(1).
36. Friebolin, H., *Basic one- and two-dimensional NMR spectroscopy*. 5th completely rev. and enl. ed. Ein- und zweidimensionale NMR-Spektroskopie. 2011, Weinheim: Wiley-VCH.
37. Silverstein, R.M., et al., *Spectrometric identification of organic compounds*. 8th ed. 2015, Hoboken, N.J: Wiley.
38. Parella, T., et al., *A general building block to introduce carbon multiplicity information into multi-dimensional HSQC-type experiments.* Magnetic resonance in chemistry, 1998. **36**(10): p. 715-719.
39. Kupče, Ē. and R. Freeman, *Molecular structure from a single NMR sequence (fast-PANACEA).* Journal of Magnetic Resonance, 2010. **206**(1): p. 147-153.
40. Kupče, Ē., R. Freeman, and B.K. John, *Parallel Acquisition of Two-Dimensional NMR Spectra of Several Nuclear Species.* Journal of the American Chemical Society, 2006. **128**(30): p. 9606-9607.

41. Haasnoot, C.A.G., F.J.M. van de Ven, and C.W. Hilbers, *COCONOSY. Combination of 2D correlated and 2D nuclear overhauser enhancement spectroscopy in a single experiment.* Journal of Magnetic Resonance (1969), 1984. **56**(2): p. 343-349.
42. Kupče, Ē. and T.D.W. Claridge, *NOAH: NMR Supersequences for Small Molecule Analysis and Structure Elucidation.* Angewandte Chemie International Edition, 2017. **56**(39): p. 11779-11783.
43. Claridge, T.D.W., M. Mayzel, and Ē. Kupče, *Triplet NOAH supersequences optimised for small molecule structure characterisation.* Magnetic Resonance in Chemistry, 2019. **57**(11): p. 946-952.

Appendix A: Exhaustive NMR spectra for all compounds

Sa-2

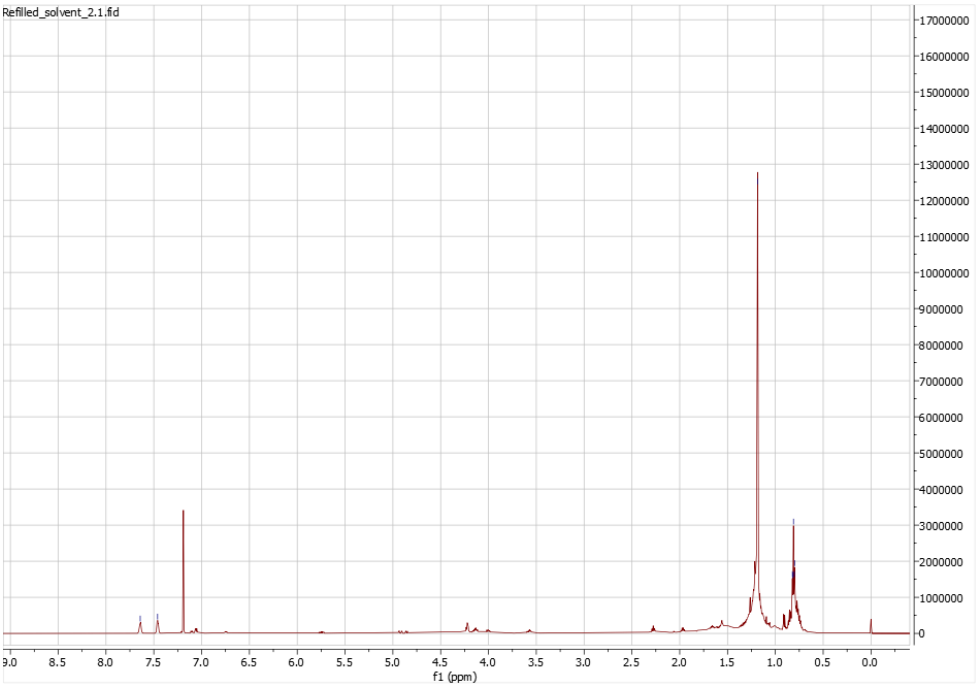

Figure A.2.1: ^{1}H spectrum of Sa-2, acquired with pulse sequence zg30 and 64 scans.

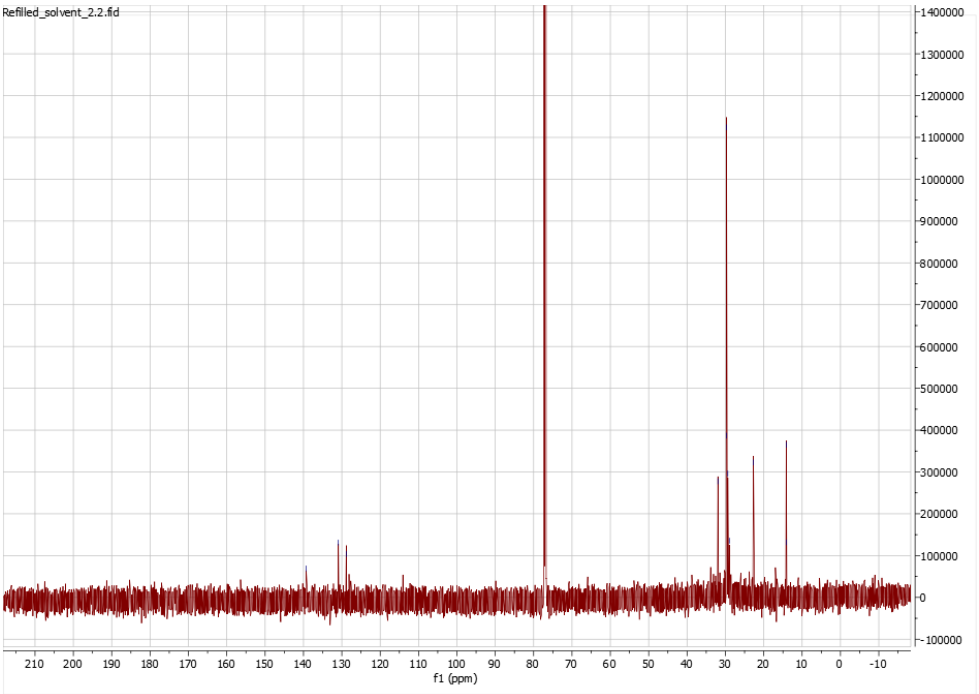

Figure A.2.2: ^{13}C spectrum for Sa-2. The pulse sequence zgpg30 with 4096 scans was used.

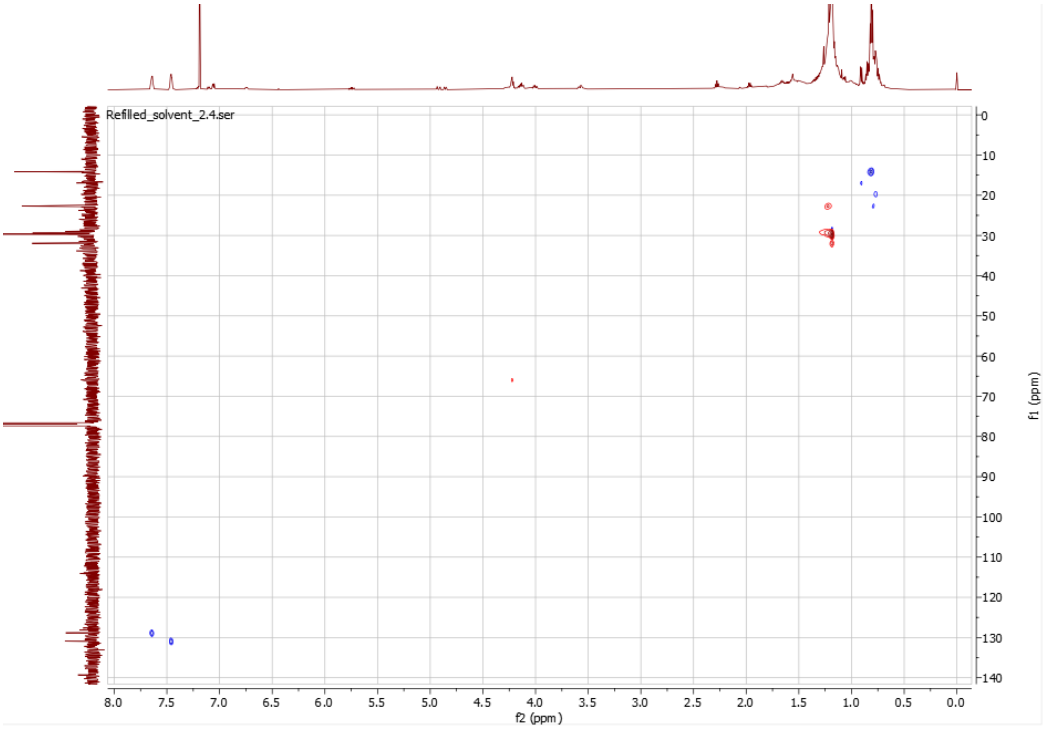

Figure A.2.3: Edited HSQC spectrum obtained with pulse sequence hsqcedetgpsisp2.3 and 8 scans.

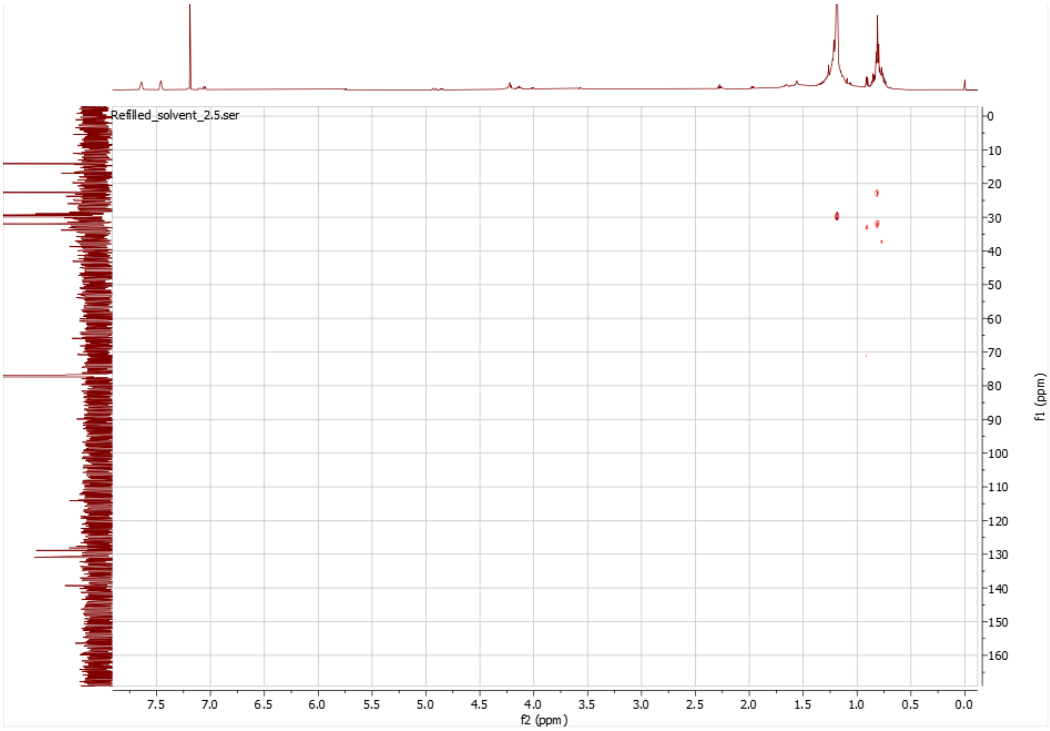

Figure A.2.4: HMBC spectrum of Sa-2, obtained with pulse sequence hmbcetgpl3nd and 8 scans.

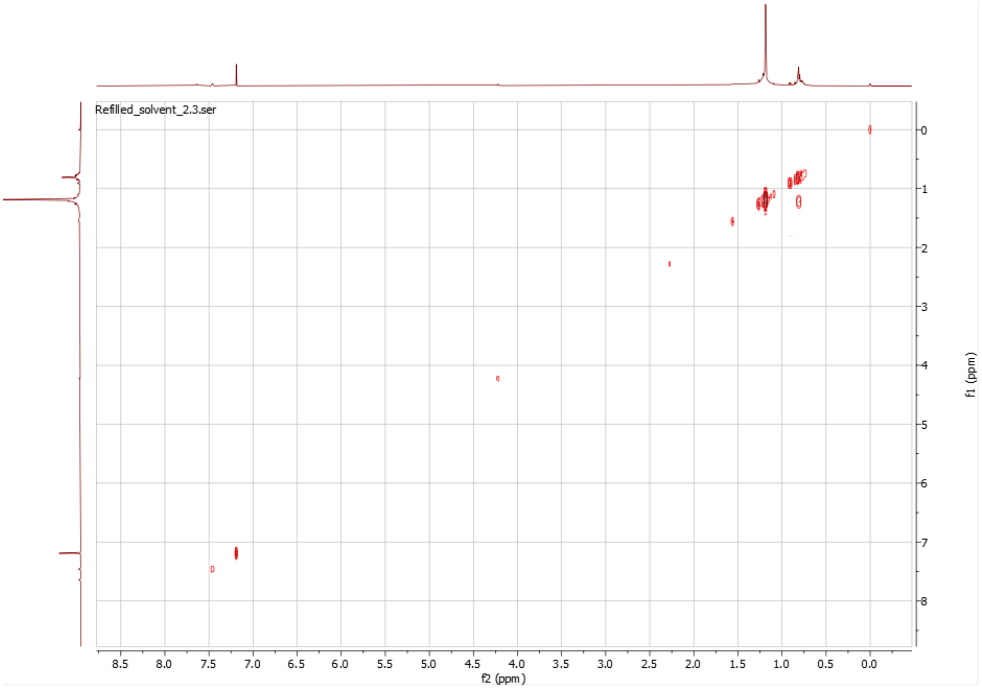

Figure A.2.5: COSY spectrum of Sa-2, obtained with pulse sequence cosygpppqf and 4 scans.

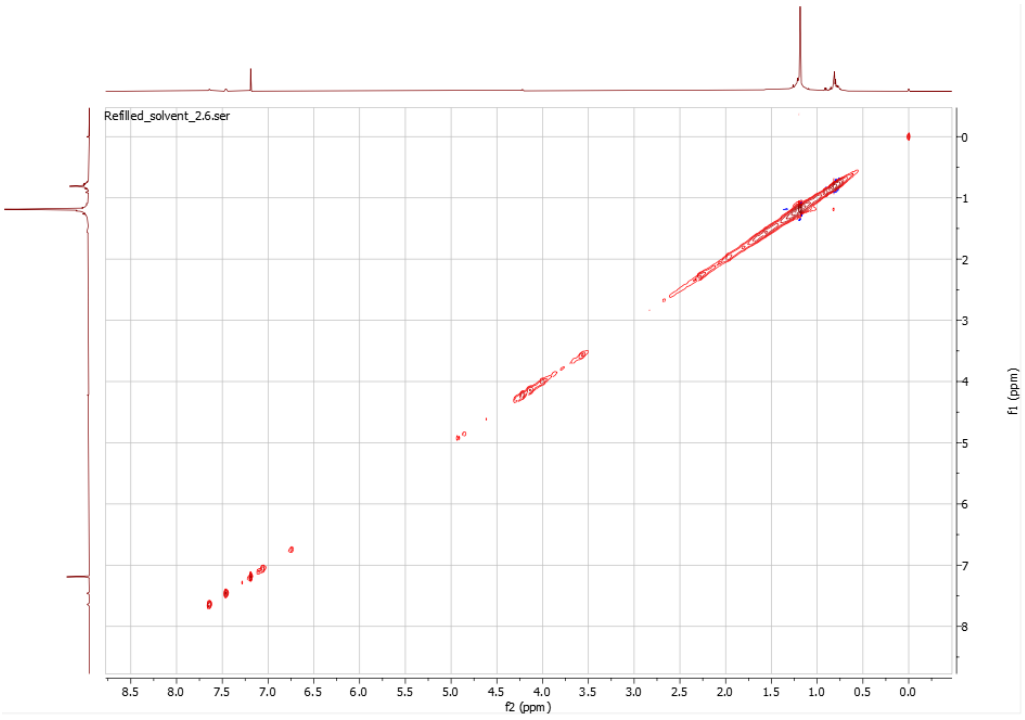

Figure A.2.6: NOESY spectrum of Sa-2. The pulse sequence used was noesygpphpp with a mixing time of 300 ms and 8 scans.

Sa-3

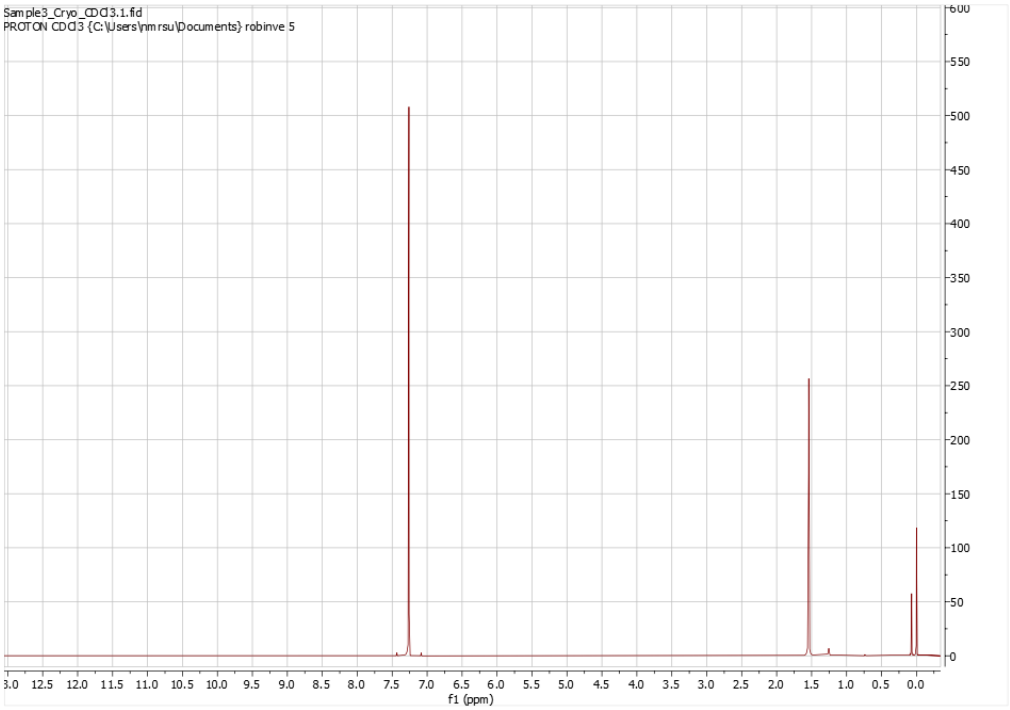

Figure A.3.1: ^{1}H spectrum of Sa-3 obtained with pulse sequence zg30 and 16 scans.

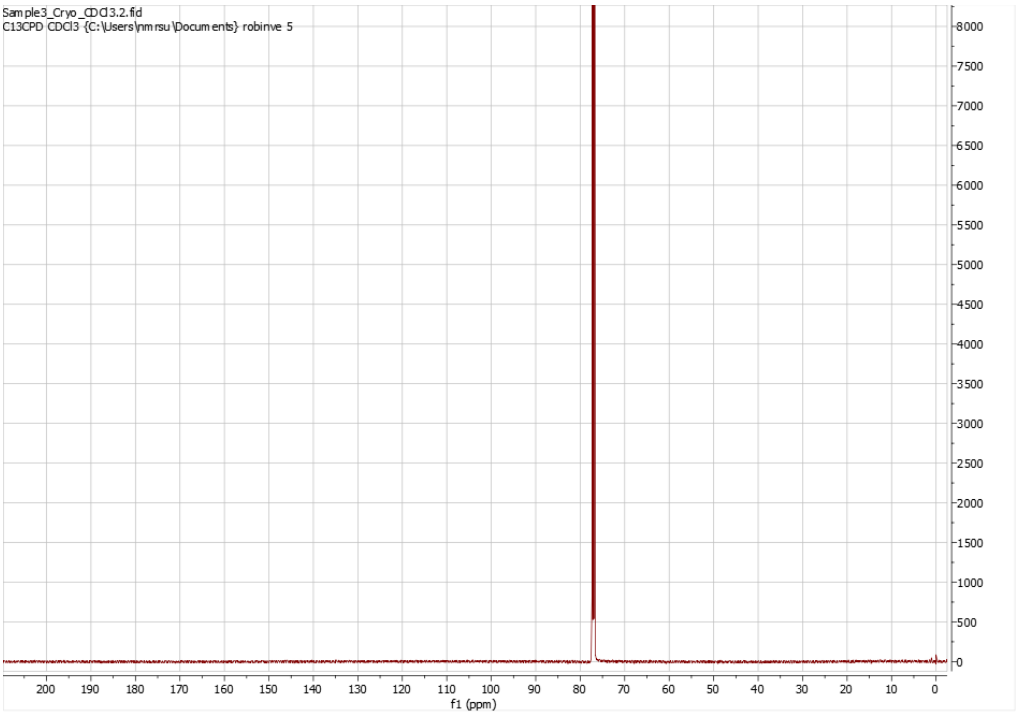

Figure A.3.2: ^{13}C spectrum of Sa-3, acquired with pulse sequence zgpg30 and 2048 scans.

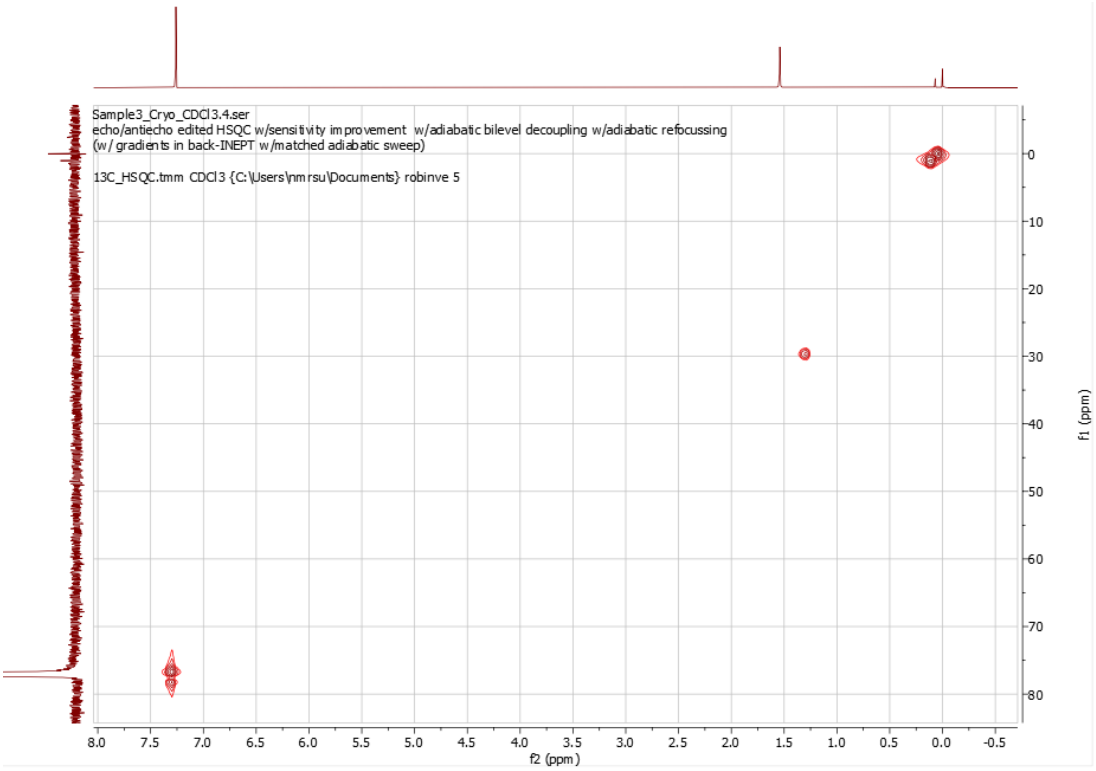

Figure A.3.3: HSQC spectrum for Sa-3 acquired with pulse sequence hsqcedetgpsisp2.3 and 8 scans.

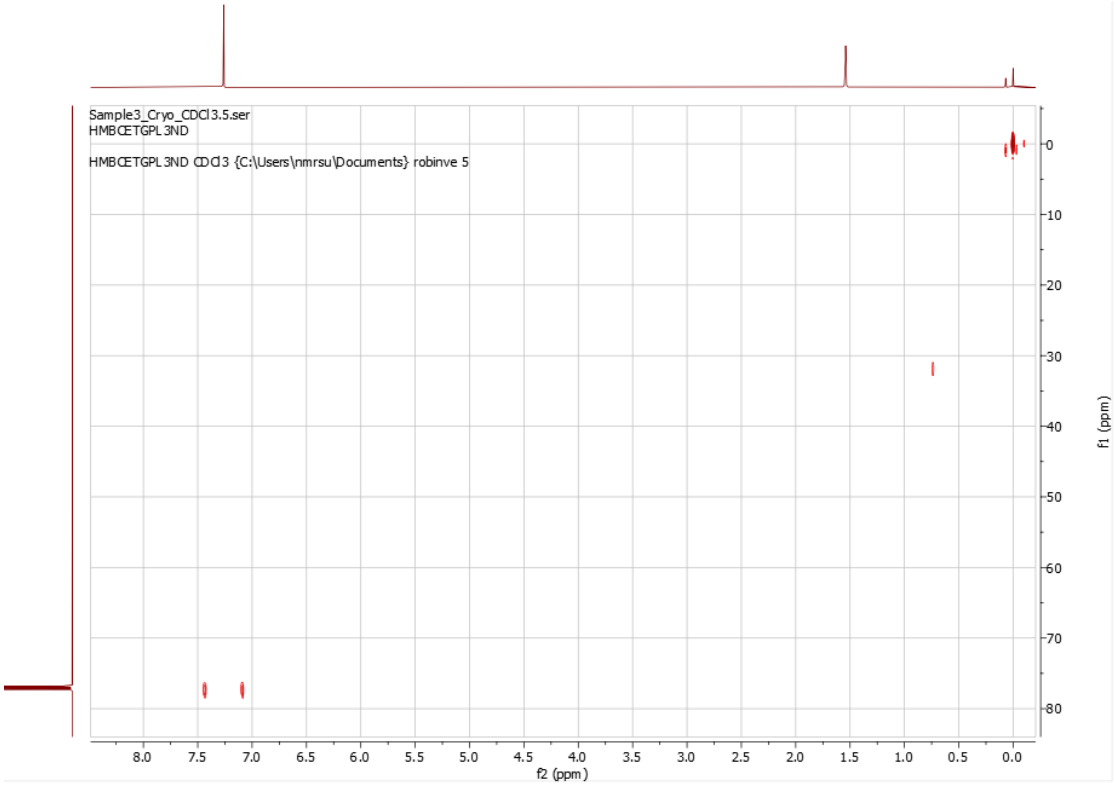

Figure A.3.4: HMBC spectrum for Sa-3. The spectrum was obtained using pulse sequence hmbcetgpl3nd and 8 scans.

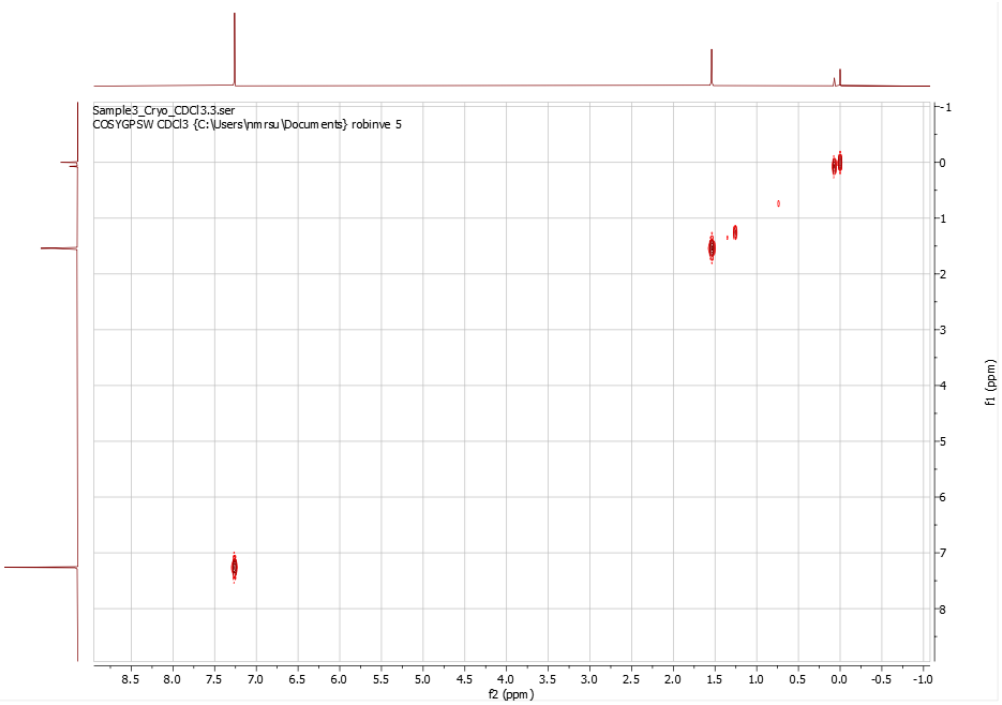

Figure A.3.5: COSY spectrum of Sa-3, obtained with pulse sequence cosygpppqf and 8 scans.

Sa-4

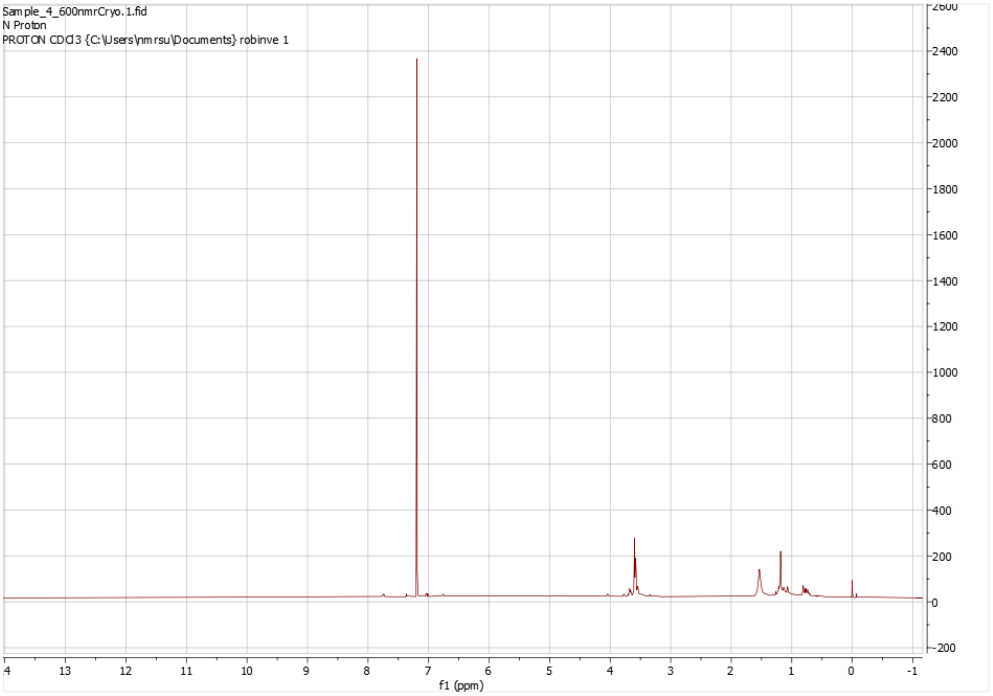

Figure A.4.1: ^{1}H spectrum for Sa-4. The spectrum was obtained with pulse sequence zg30 and 128 scans.

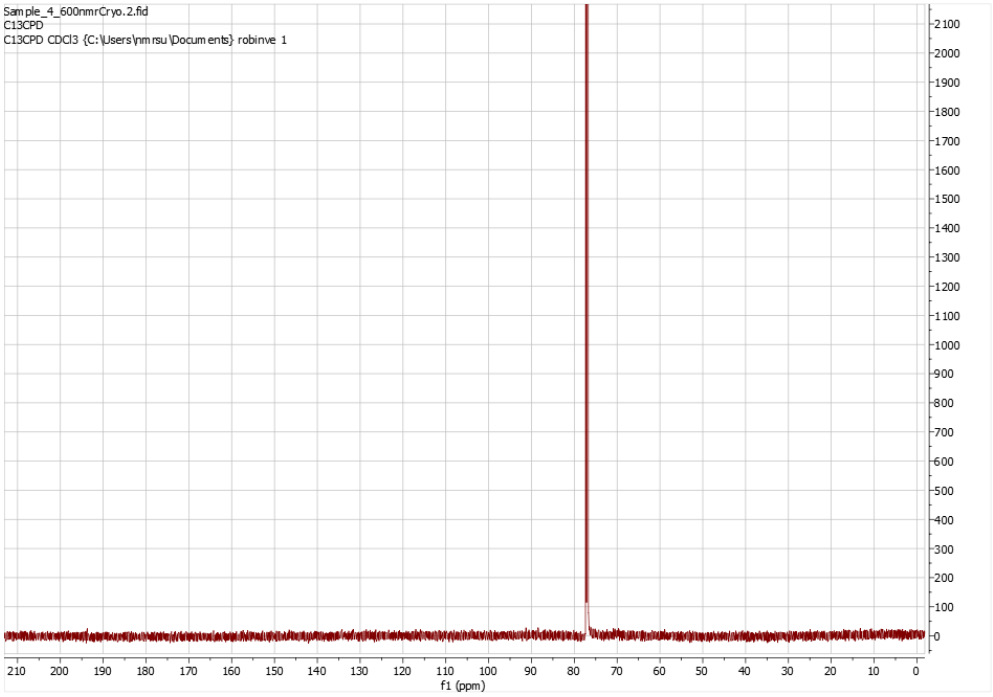

Figure A.4.2: ^{13}C spectrum for Sa-4 acquired with pulse sequence zgpg30 and 2048 scans.

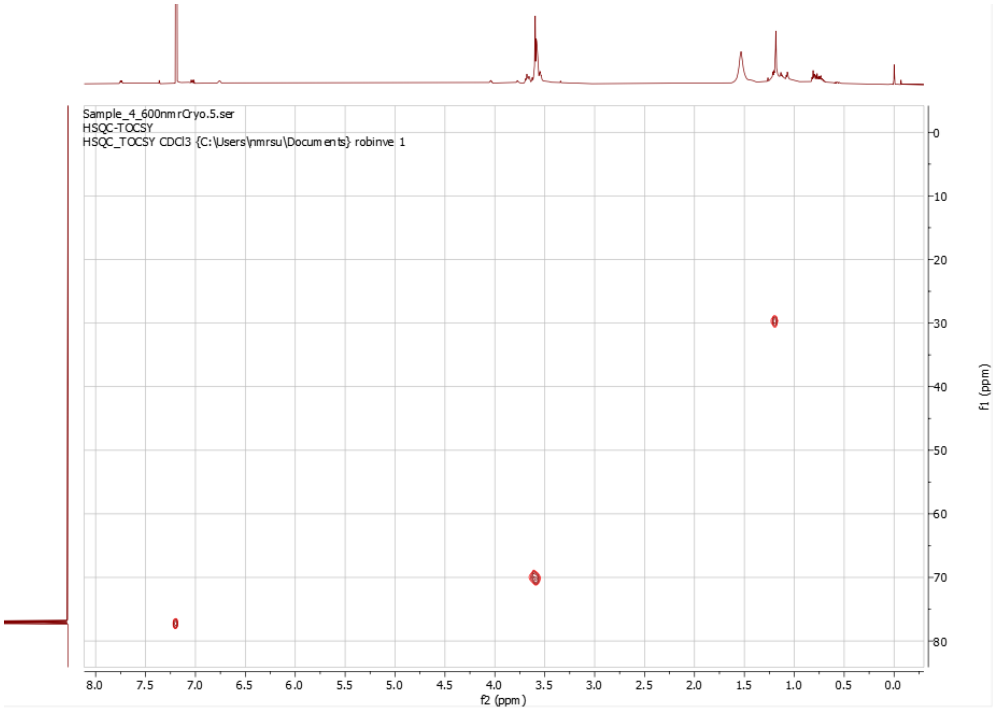

Figure A.4.3: HSQC-TOCSY spectrum for Sa-4 obtained with pulse sequence hsqcdietgpsisp.2 and 8 scans. HSQC-TOCSY was attempted in the stead of HSQC, due to extremely low ^{13}C response.

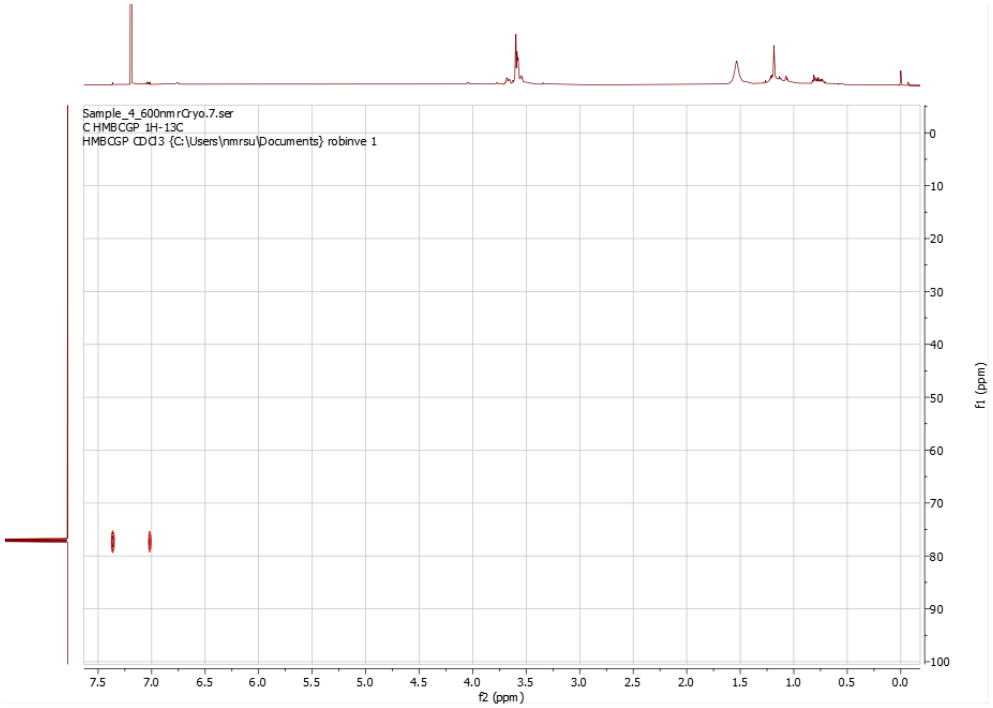

Figure A.4.4: HMBC spectrum for Sa-4, acquired with pulse sequence hmbcgplpndqf and 4 scans.

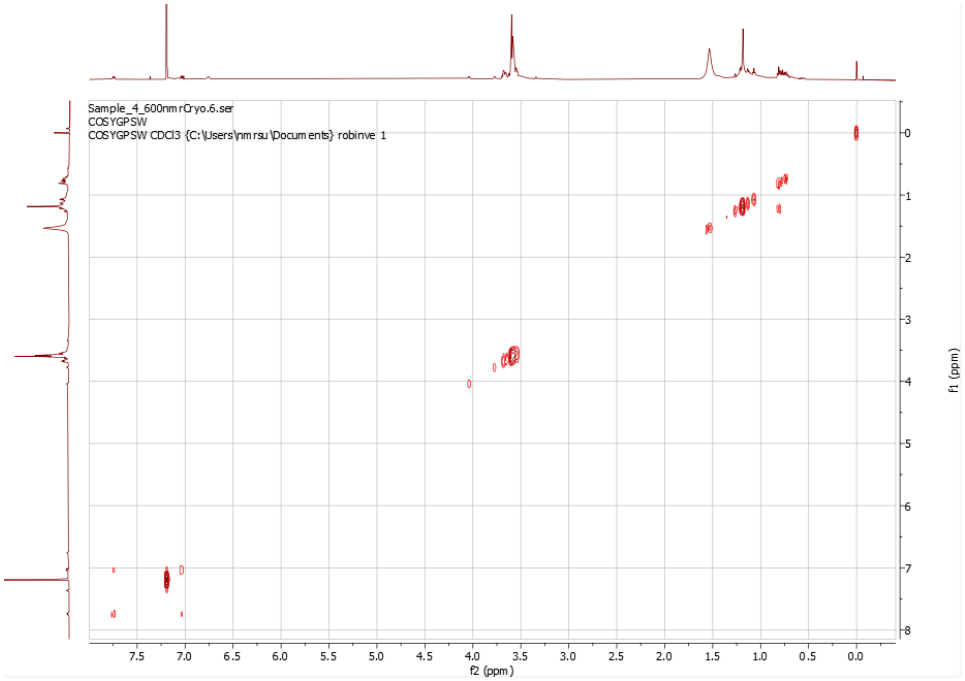

Figure A.4.5: COSY spectrum of Sa-4, obtained with the pulse sequence cosygpppqf and 1 scan.

Sa-5

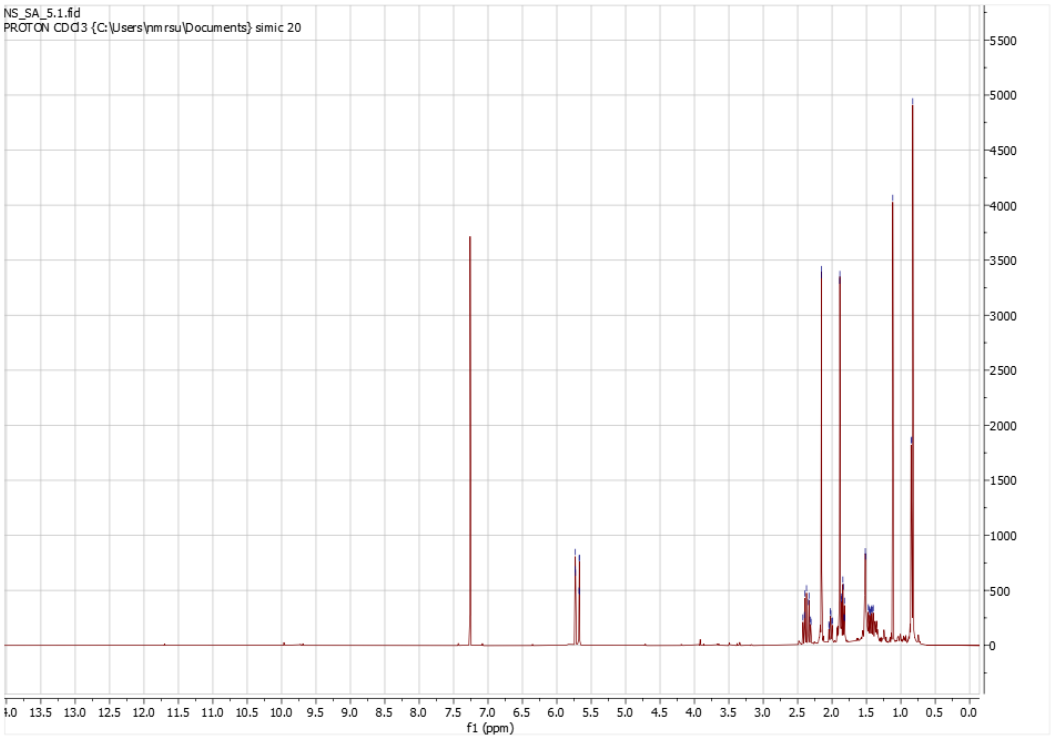

Figure A.5.1: ^{1}H spectrum for Sa-5 obtained with pulse sequence zg30 and 64 scans.

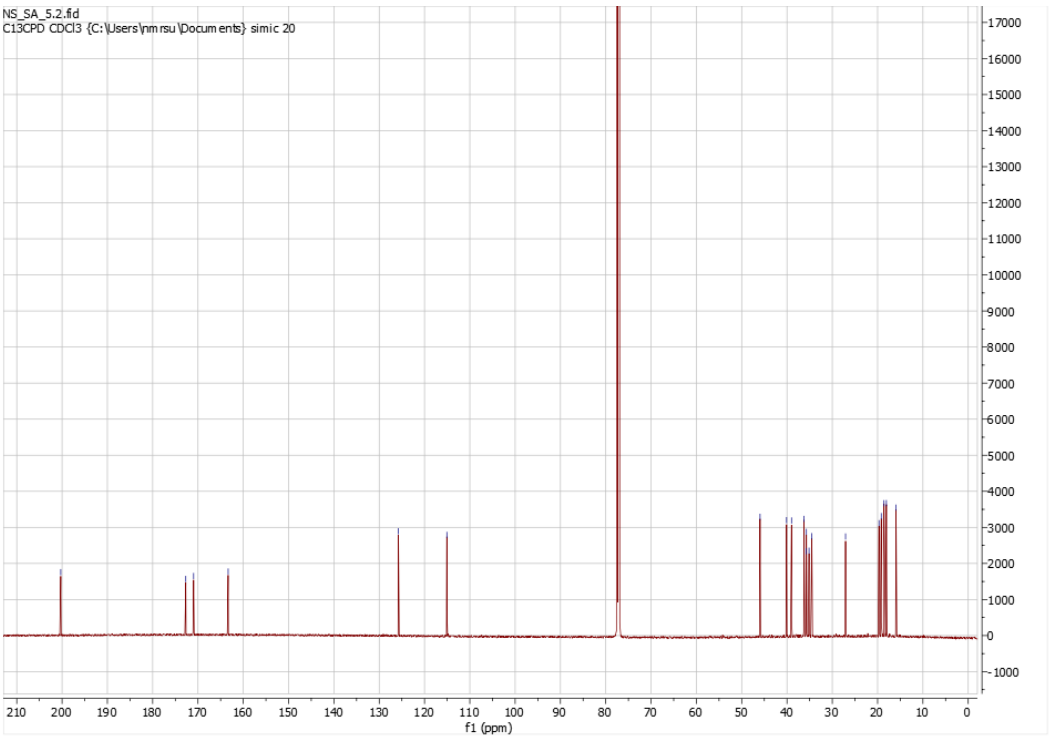

Figure A.5.2: ^{13}C spectrum for Sa-5, obtained with pulse sequence zgpg30 and 4096 scans.

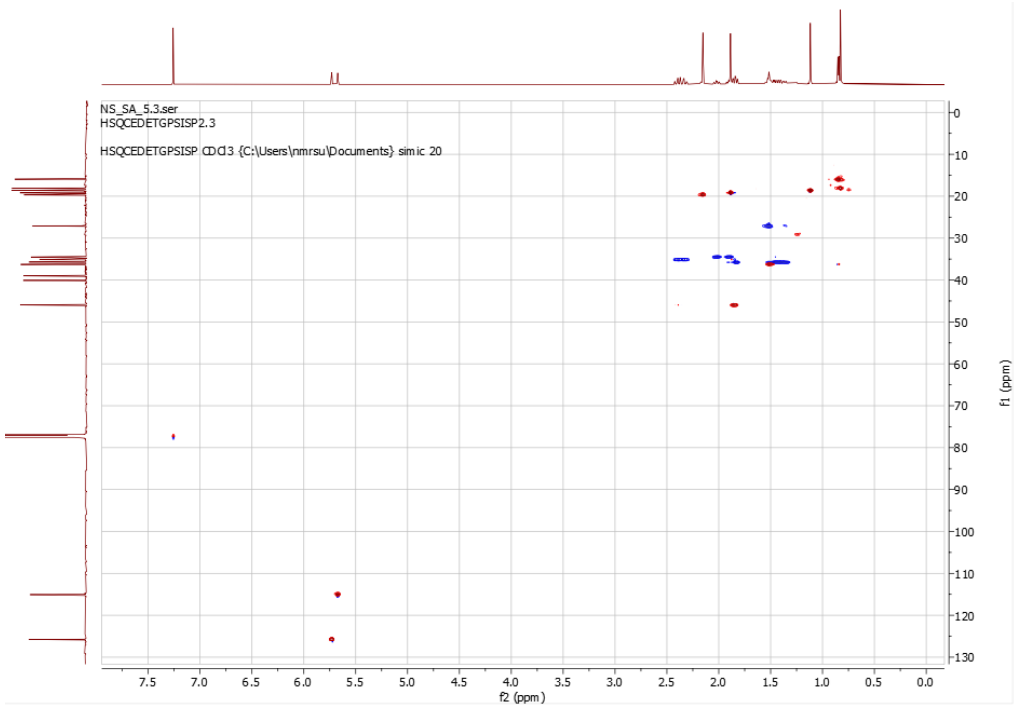

Figure A.5.3: Edited HSQC spectrum of Sa-5. The pulse sequence used was hsqcedetgpsisp2.3 with 8 scans.

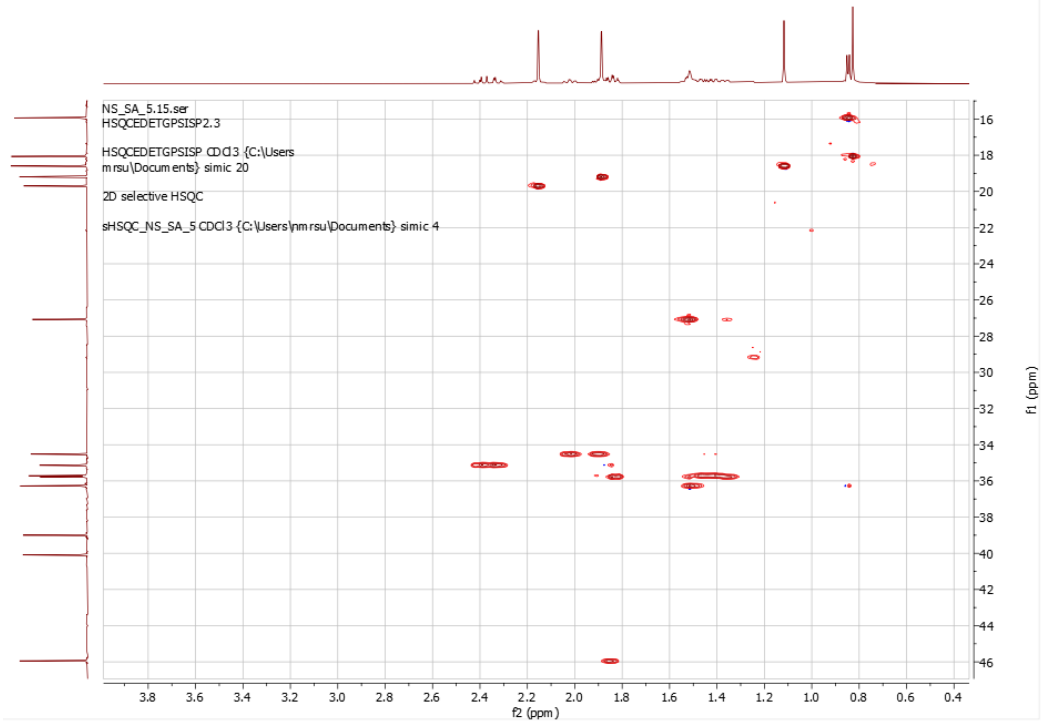

Figure A.5.4: Edited HSQC spectra for Sa-5 in the 15,5-46,5 ppm f1 range, acquired with pulse sequence hsqcedetgpsisp2.3 and 8 scans.

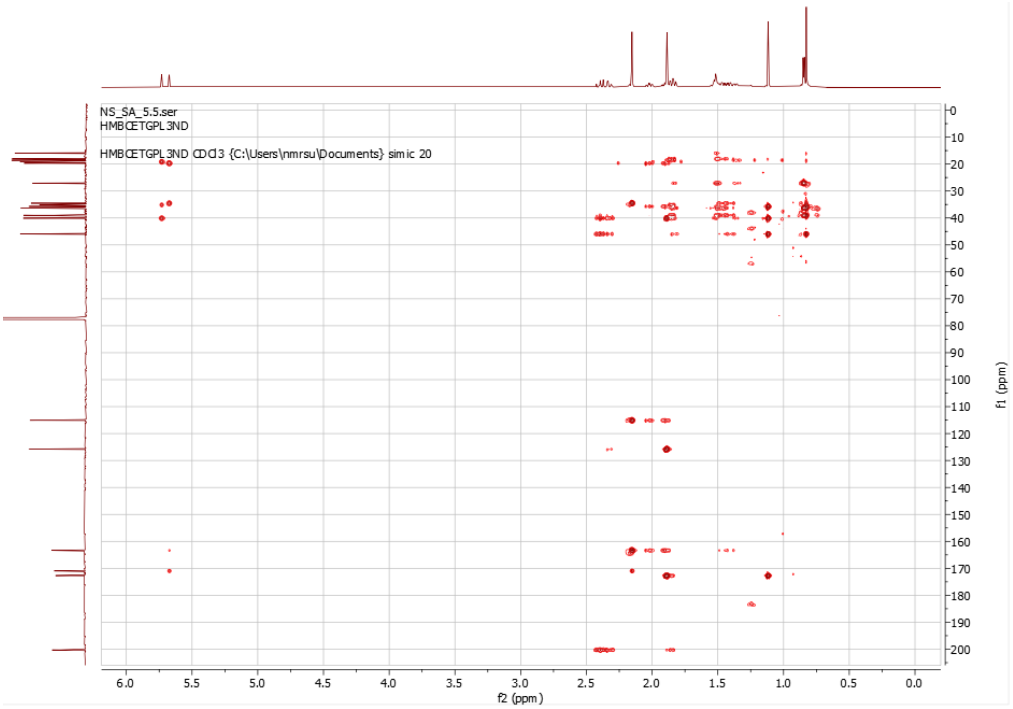

Figure A.5.5: HMBC spectrum for Sa-5 obtained with pulse sequence hmbcetgpl3nd and 14 scans.

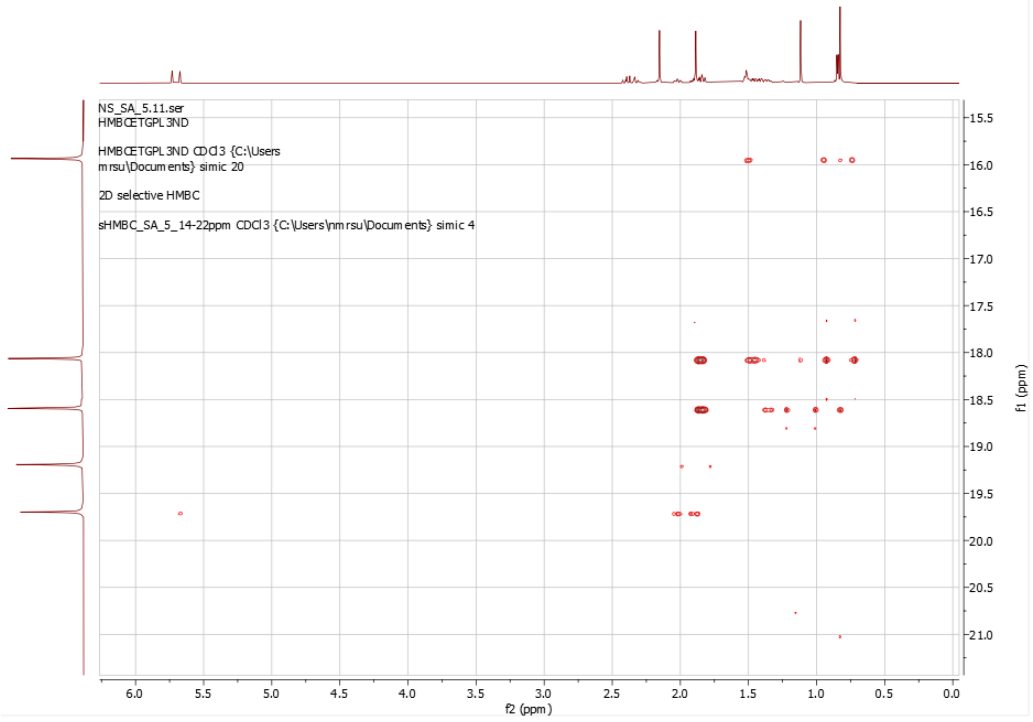

Figure A.5.6: Edited HMBC spectrum of Sa-5 in the 15,5-22,0 ppm f1 range. The pulse sequence used was shmbcctetgpl2nd with 16 scans.

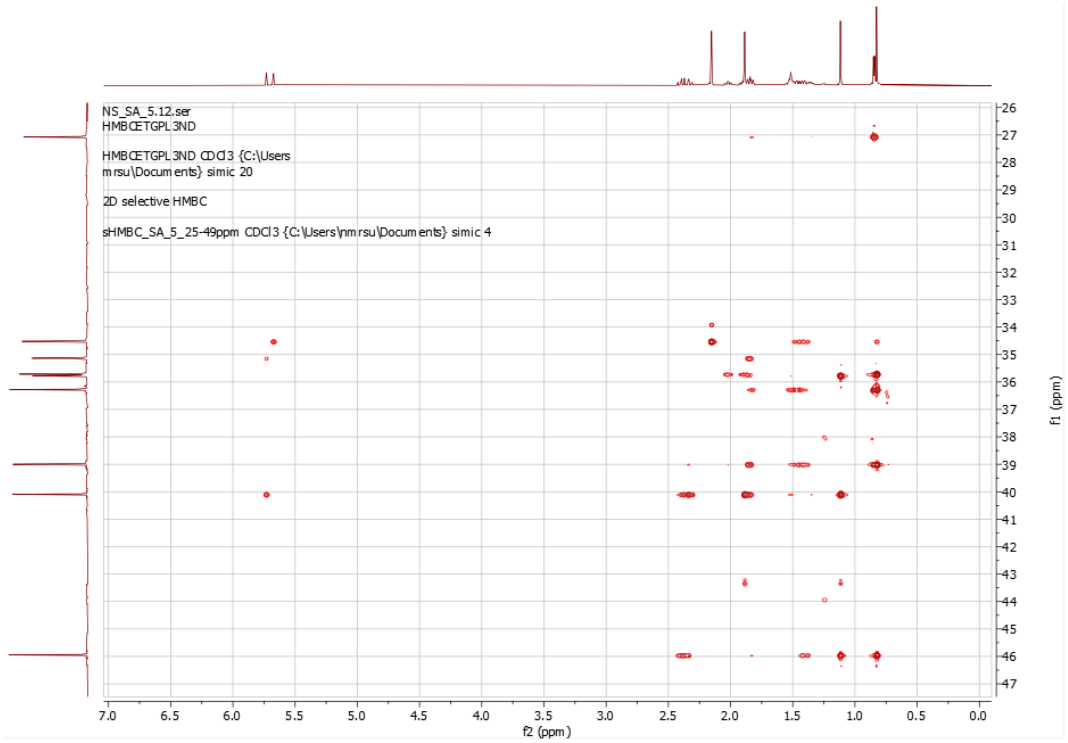

Figure A.5.7: Edited HMBC spectrum of Sa-5 in the 26,0-47,5 ppm f1 range. The pulse sequence used was shmbcctetgpl2nd with 16 scans.

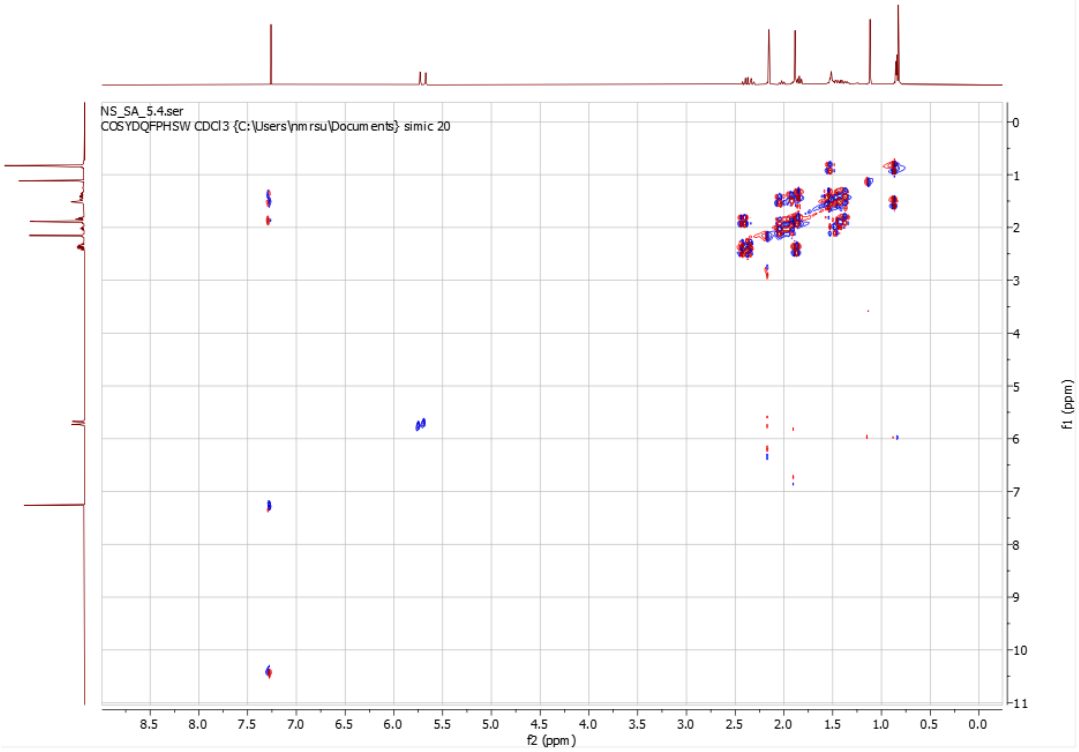

Figure A.5.8: COSY spectrum for Sa-5, obtained with pulse sequence cosydfph and 32 scans.

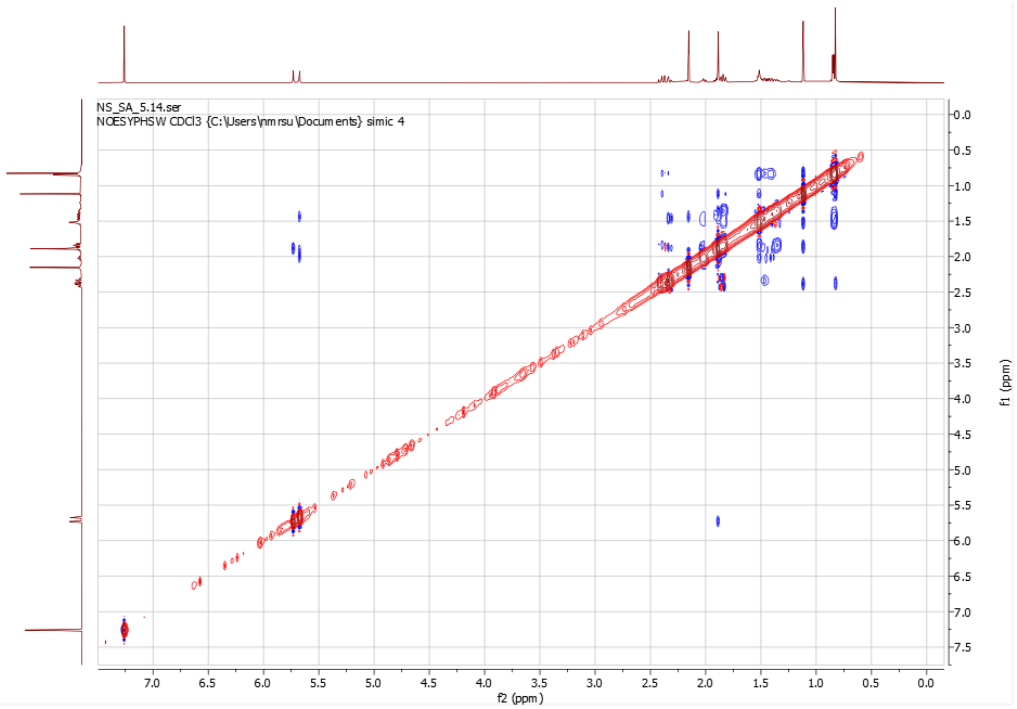

Figure A.5.9: NOESY spectrum for Sa-5, acquired with pulse sequence noesygpphpp and 24 scans.

Sa-6

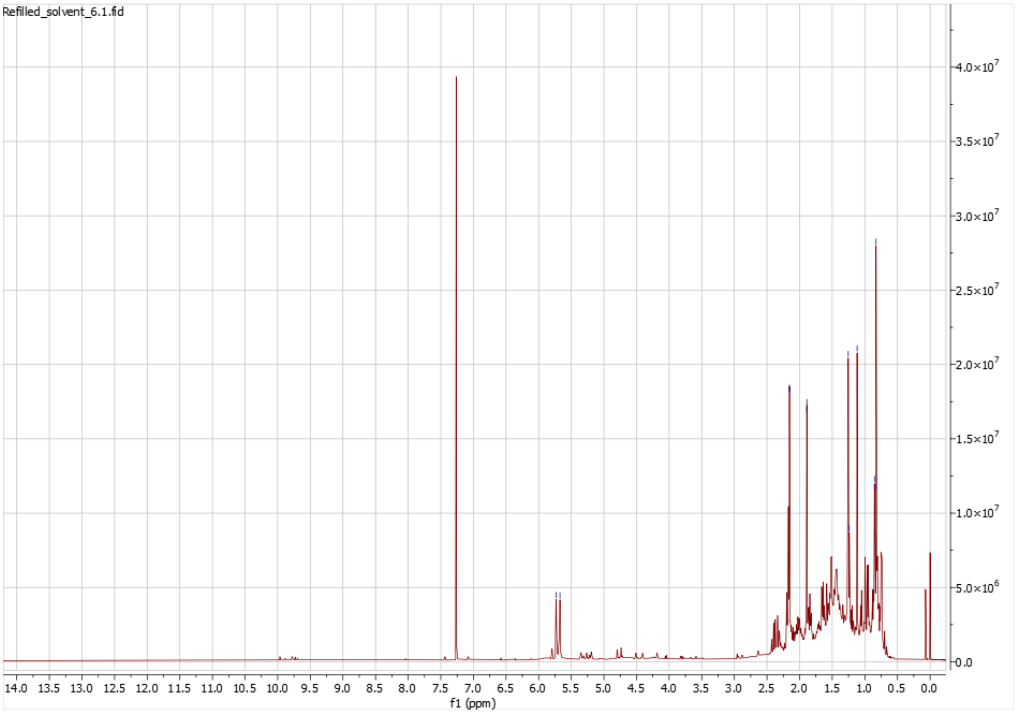

Figure A.6.1: ^{1}H spectrum of Sa-6, acquired with pulse sequence zg30 and 256 scans.

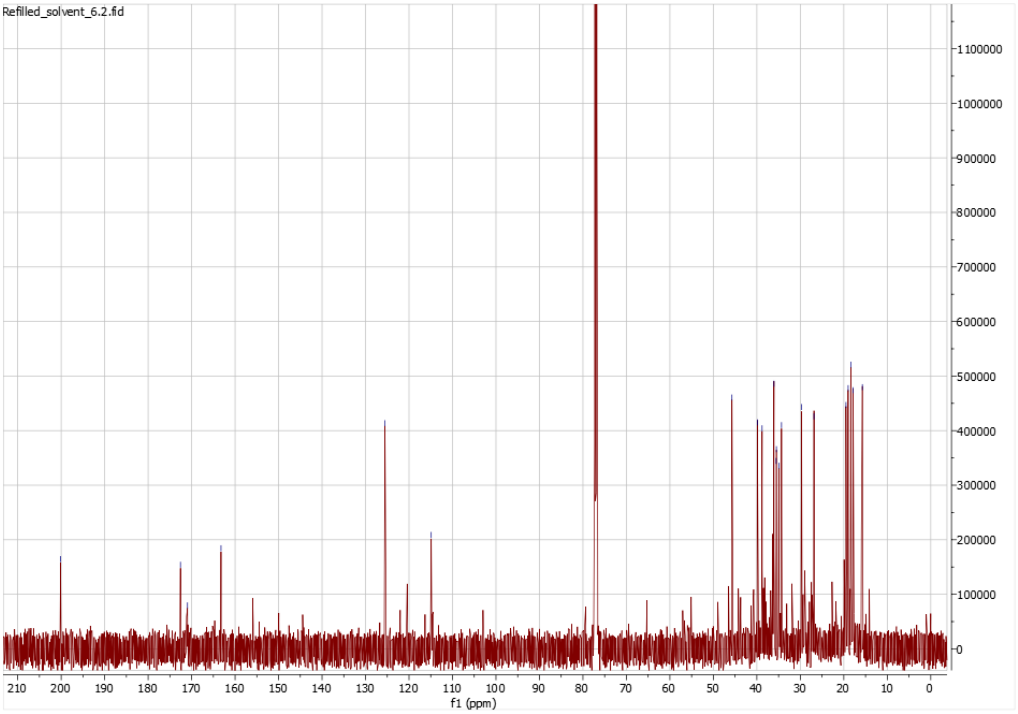

Figure A.6.2: ^{13}C spectrum for Sa-5, aquired with pulse sequence zgpg30 and 4096 scans.

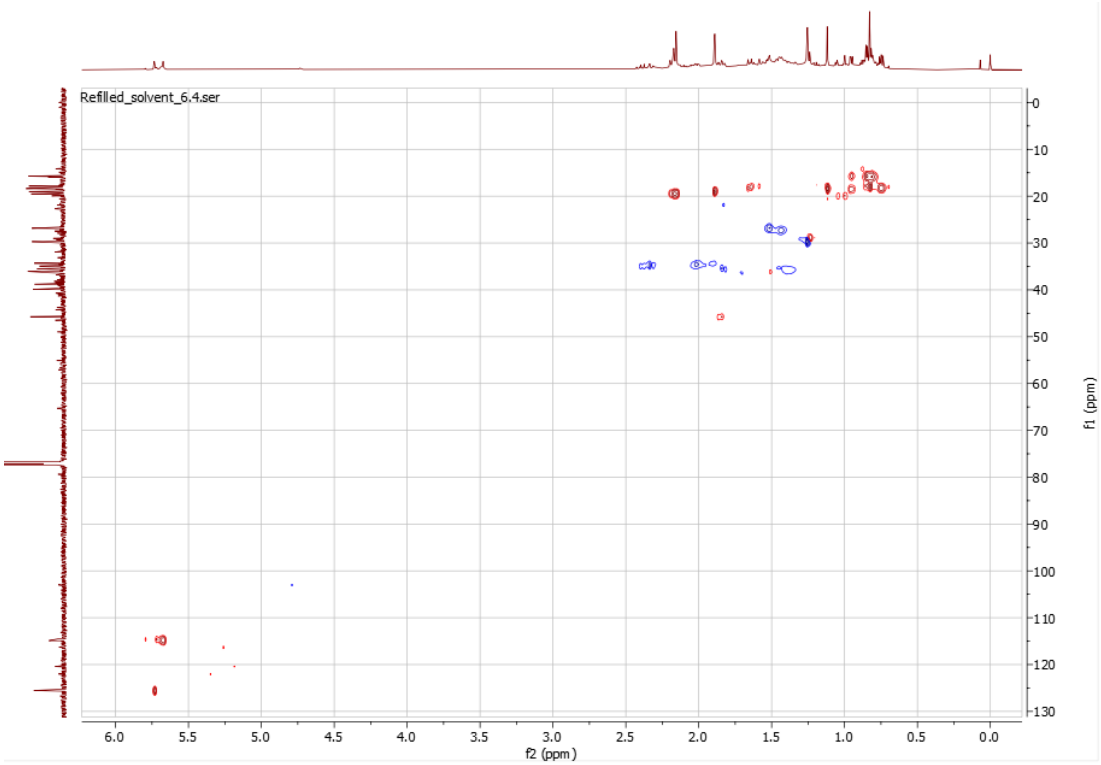

Figure A.6.3: Edited HSQC spectrum of Sa-6 obtained with pulse sequence hsqcedetgpsisp2.3 and 8 scans.

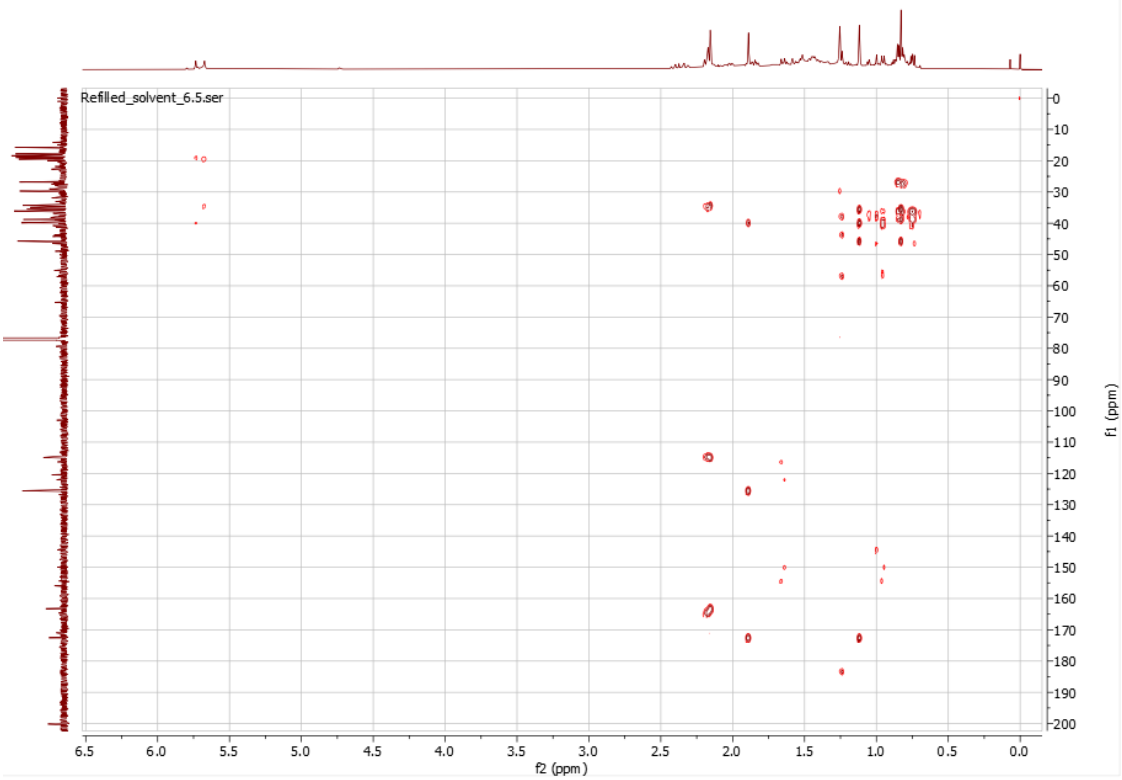

Figure A.6.4: HMBC spectrum of Sa-6, obtained with pulse sequence hmbcetgpl3nd and 8 scans.

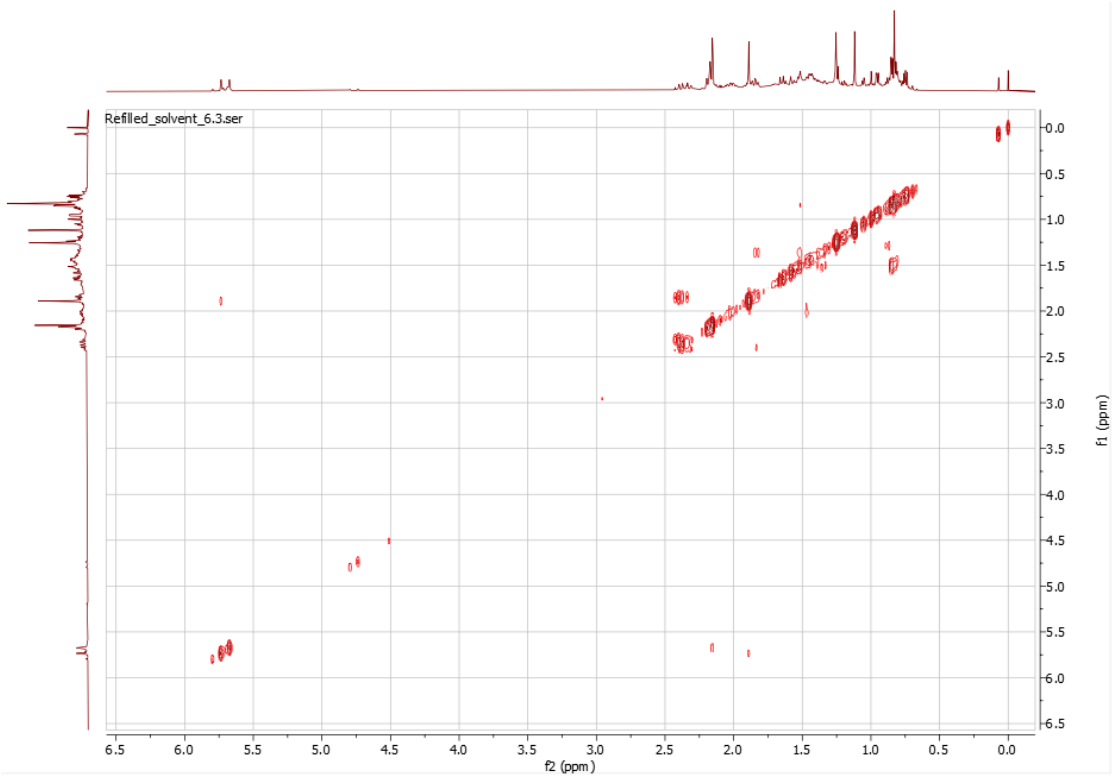

Figure A.6.5: COSY spectrum of Sa-6. The spectrum was obtained with the pulse sequence cosygpppqf and 4 scans.

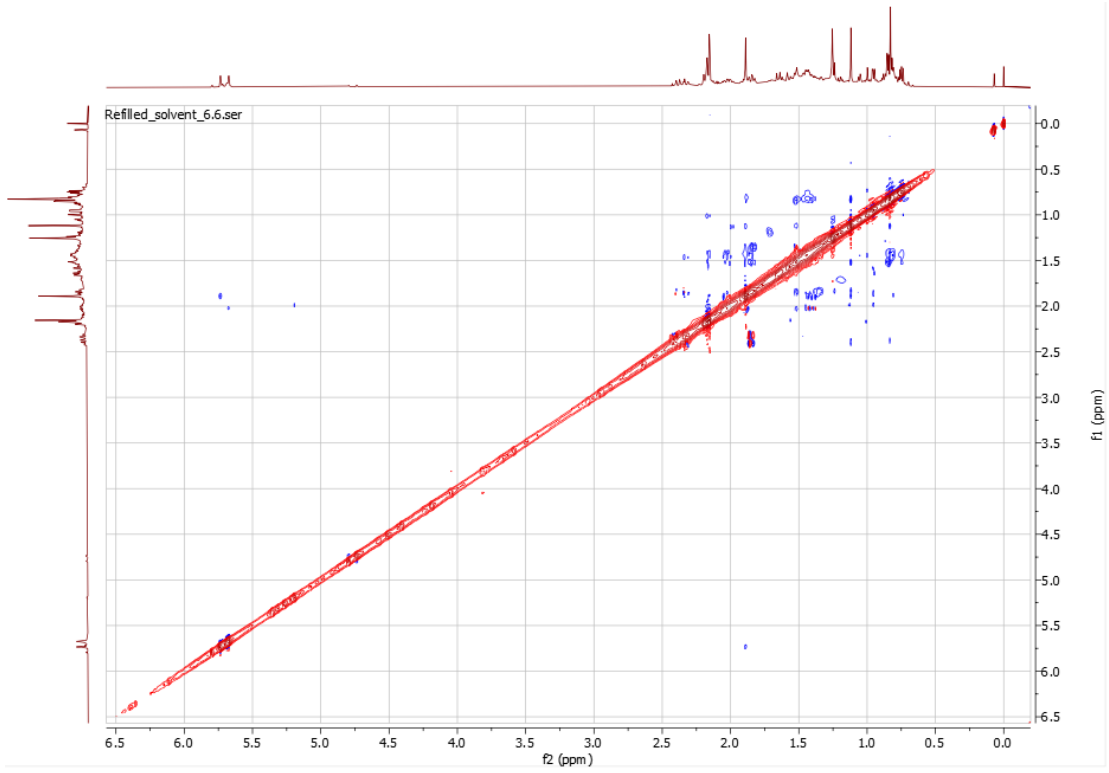

Figure A.6.6: NOESY spectrum of Sa-6 obtained with pulse sequence noesygpphpp and 8 scans.

Sa-7

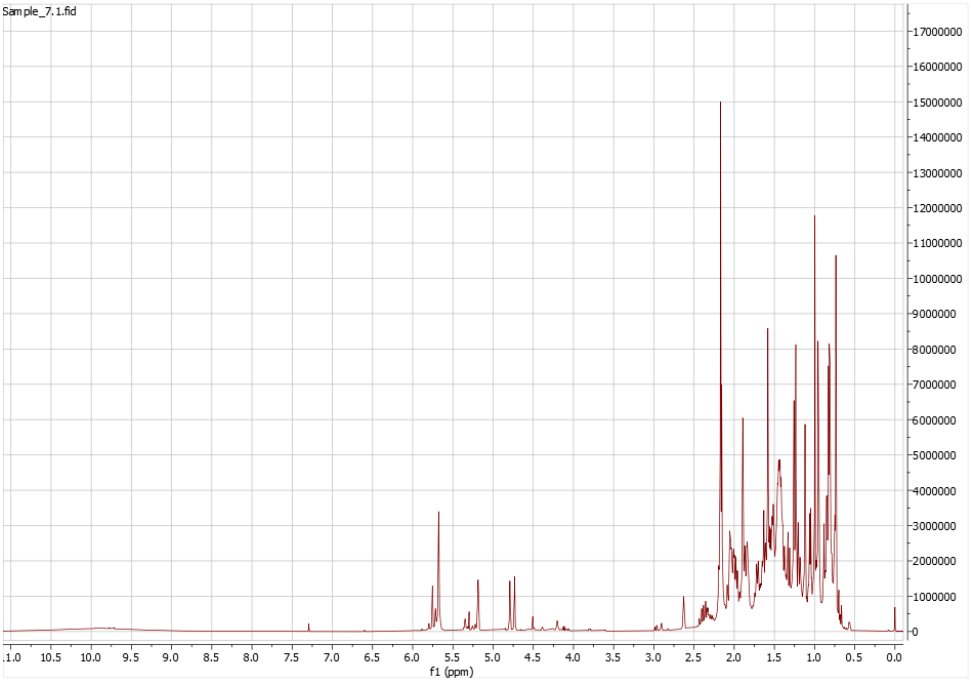

Figure A.7.1: ^{1}H spectrum for Sa-7, obtained with pulse sequence zg30 and 128 scans.

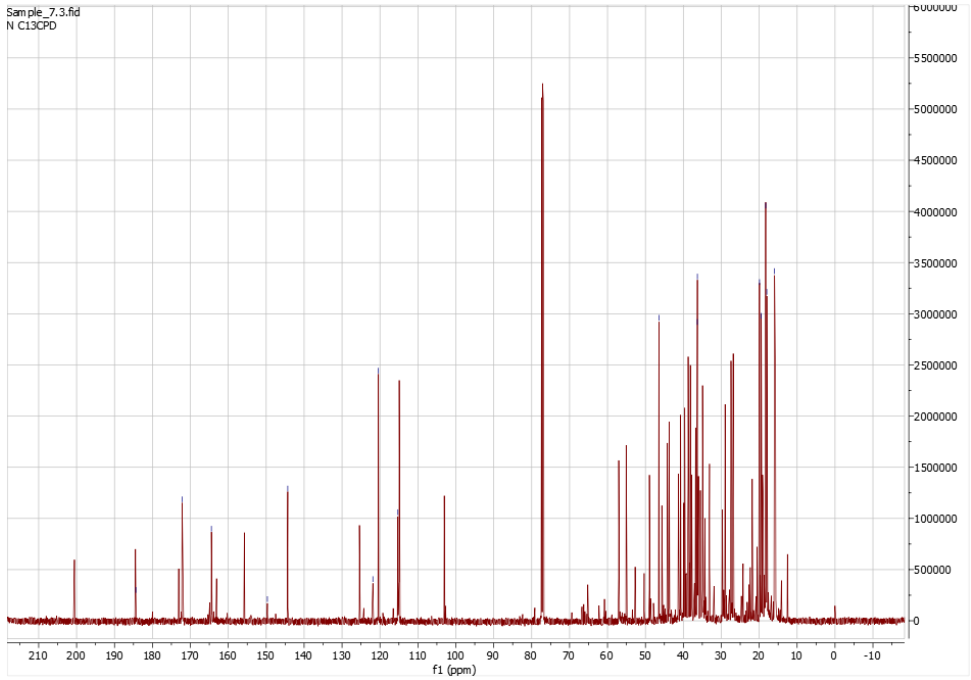

Figure A.7.2: ^{13}C spectrum for Sa-7, acquired with pulse sequence zgpg30 and 4096 scans.

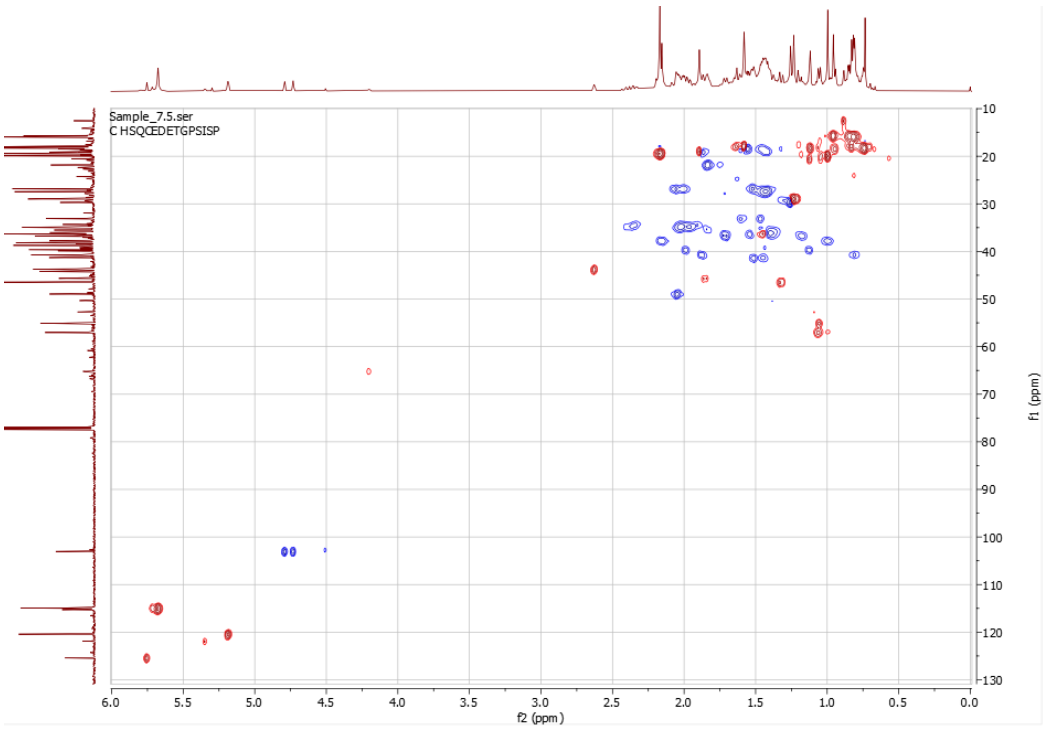

Figure A.7.3: Edited HSQC spectrum of Sa-7. The pulse sequence utilized was hsqcedetgpsisp2.3 with 4 scans.

Figure A.7.4: Selective HSQC spectrum of Sa-7 in the 12,0-52,0 ppm f1 range. The pulse sequence used was shsqcetgpsisp2.2 and 16 scans.

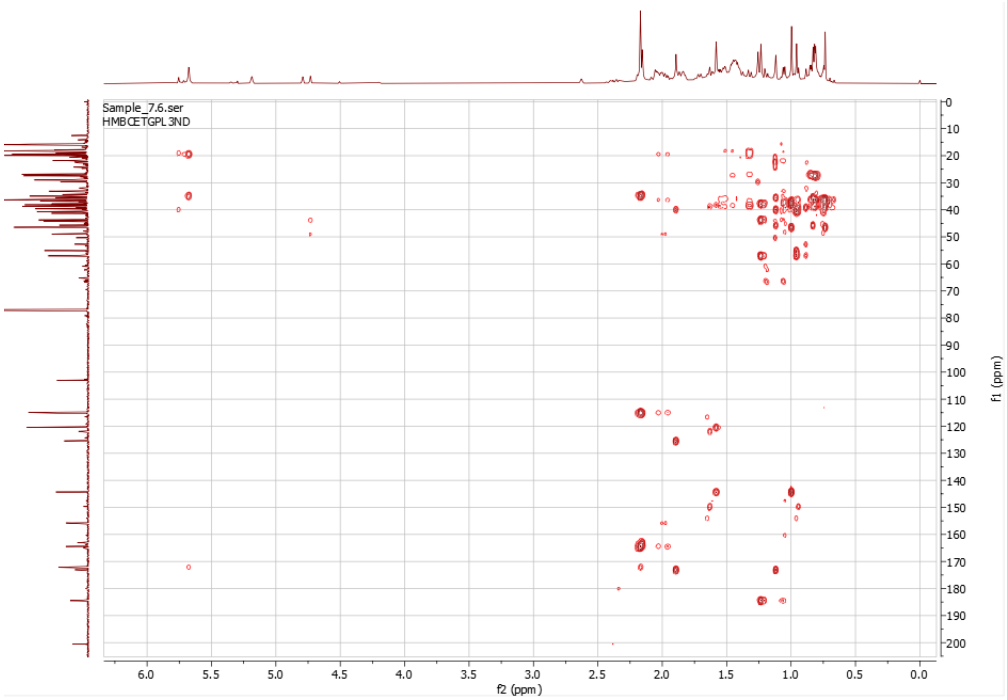

Figure A.7.5: HMBC spectrum of Sa-7 aquired with pulse sequence hmbcetgpl3nd and 4 scans.

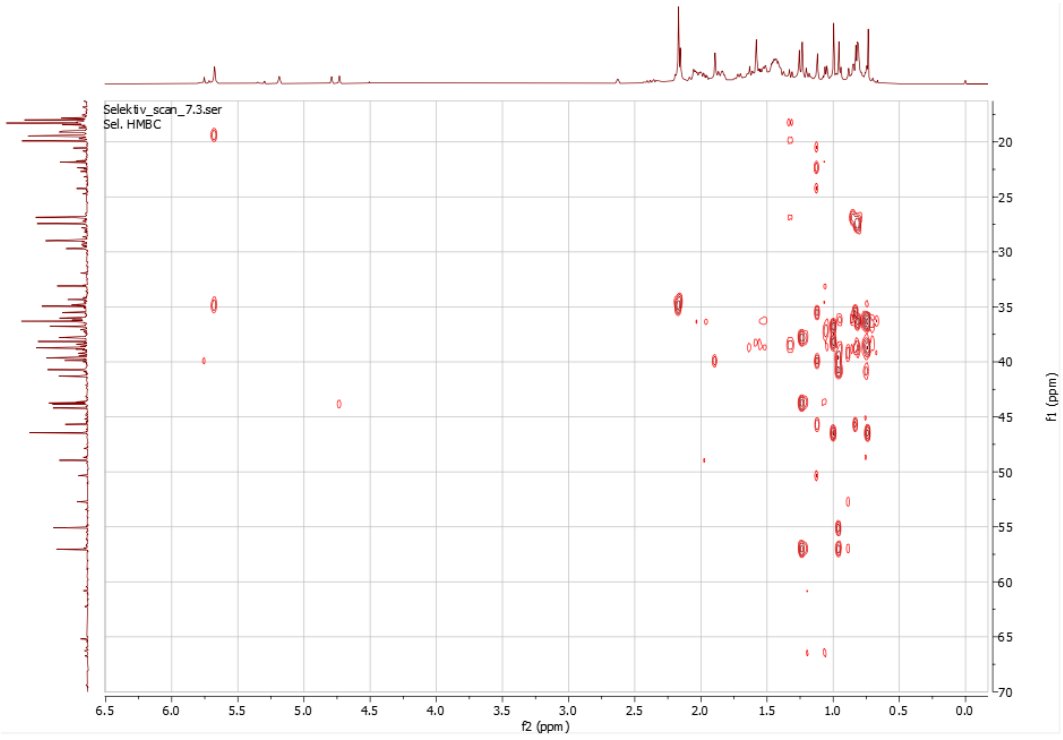

Figure A.7.6: Selective HMBC spectrum of Sa-7 in the 16,0-70,0 ppm f1 range. The utilized pulse sequence was shmbcctetgpl2nd with 16 scans.

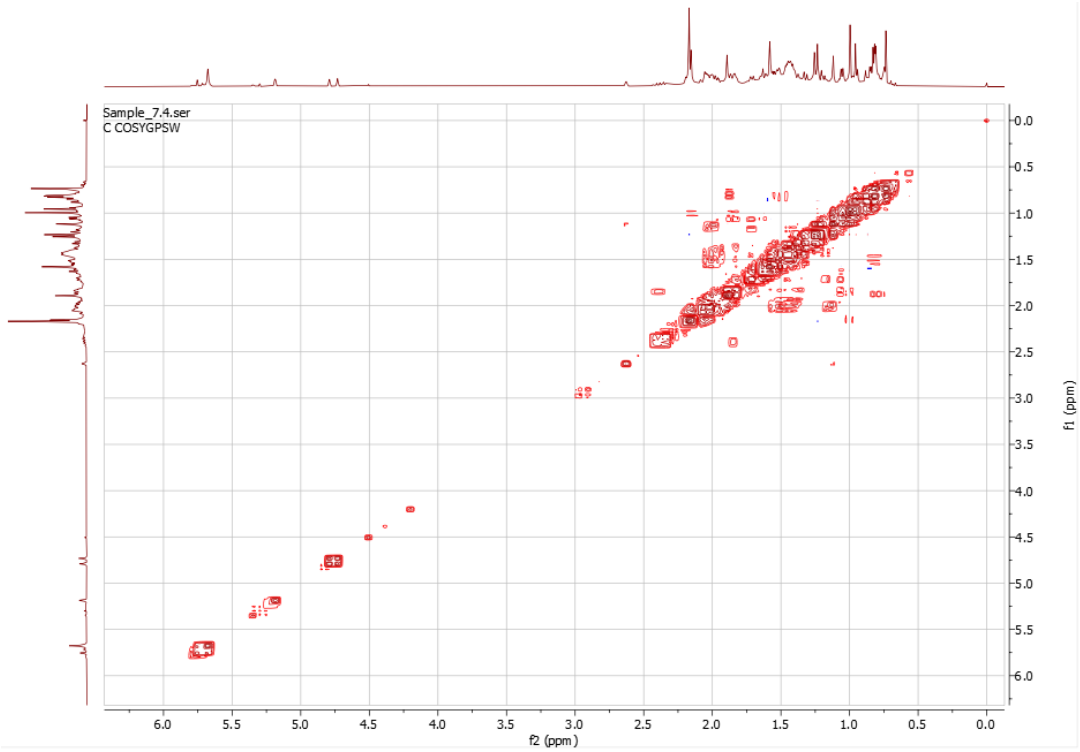

Figure A.7.7: COSY spectrum for Sa-7 acquired with pulse sequence cosygpppqf and 1 scan.

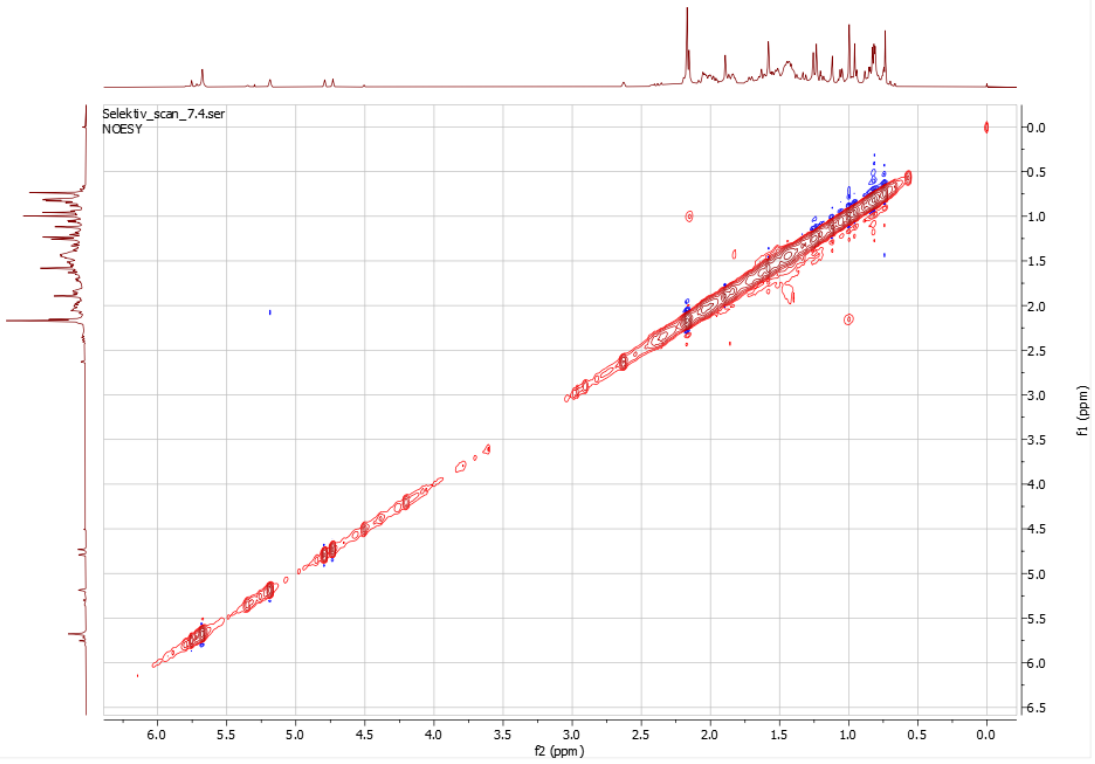

Figure A.7.8: NOESY spectrum for Sa-7 obtained with pulse sequence noesygpphpp, 16 scans, and a mixing time of 300 ms.

Sa-8

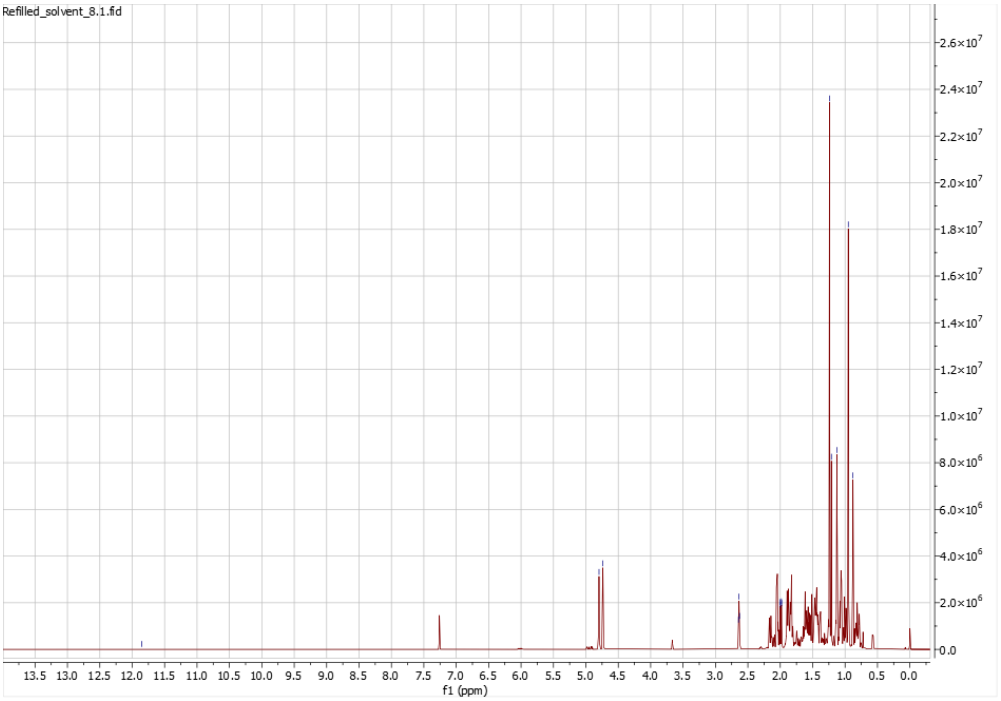

Figure A.8.1: ^{1}H spectrum for Sa-8, obtained with pulse sequence zg30 and 64 scans.

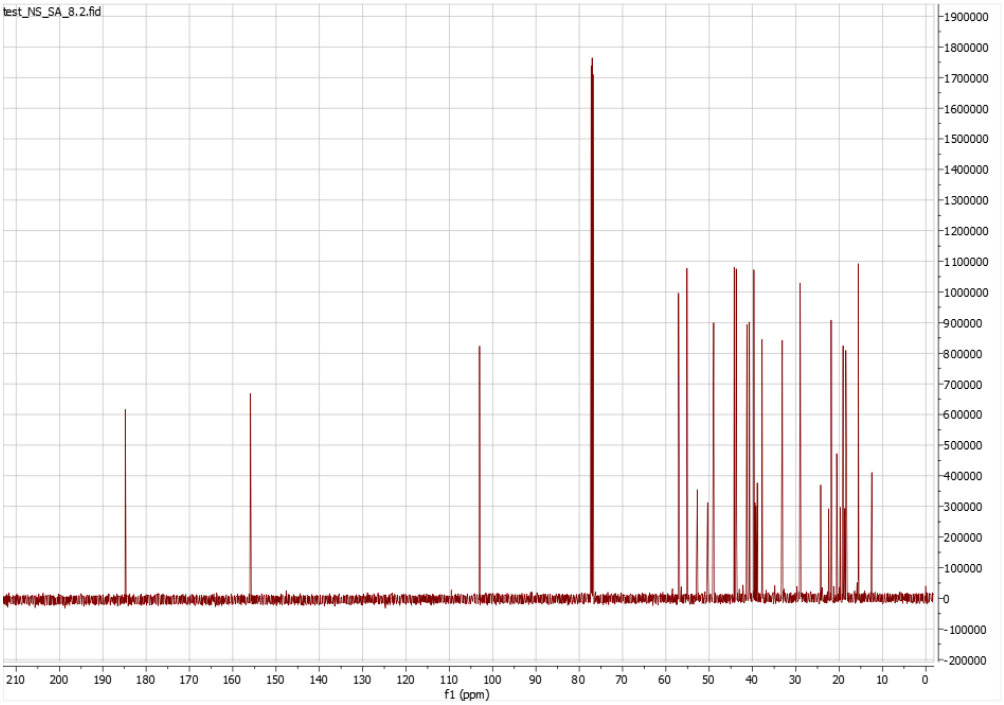

Figure A.8.2: ^{13}C spectrum for Sa-8 aquired with pulse sequence zgpg30 and 1024 scans.

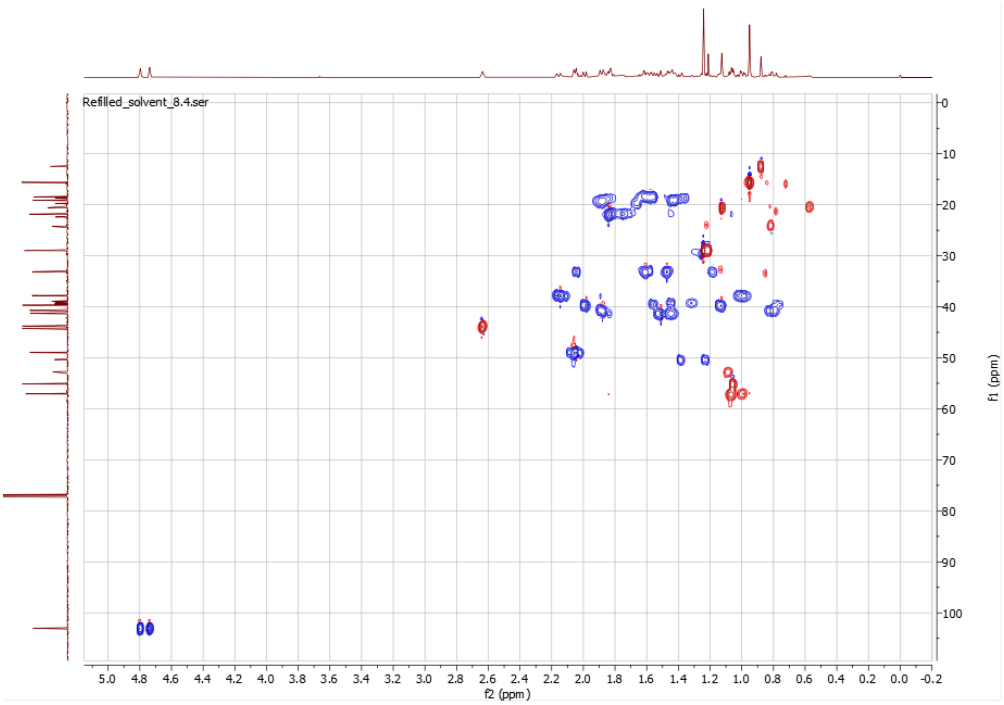

Figure A.8.3: Edited HSQC spectrum for Sa-8. The spectrum was obtained with pulse sequence hsqcedetgpsisp2.3 and 8 scans.

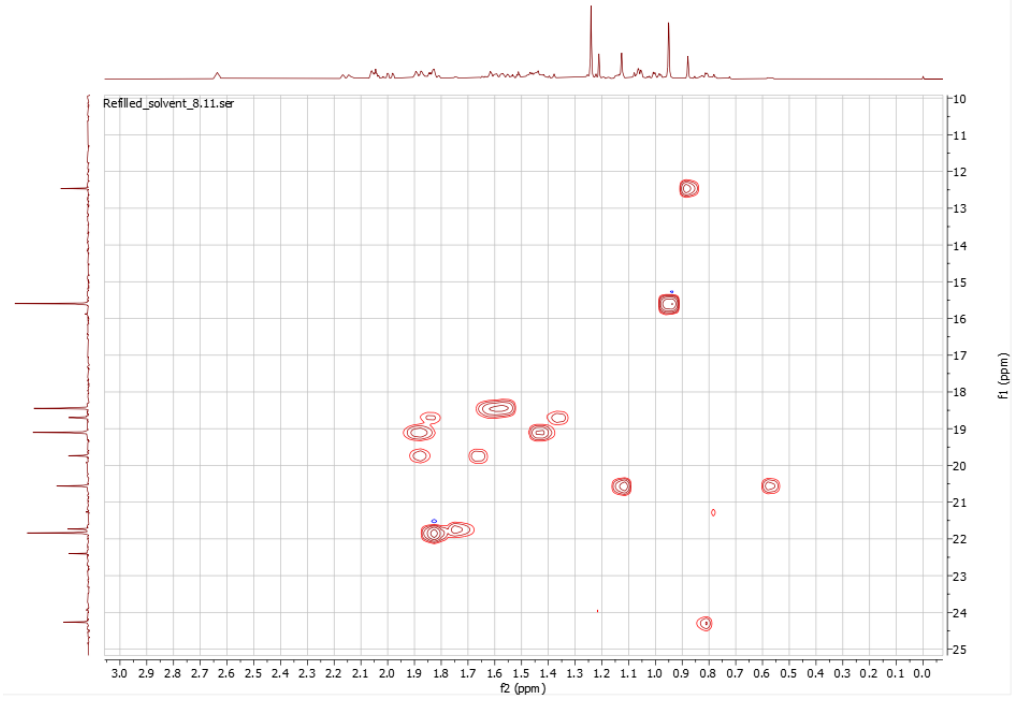

Figure A.8.4: Selective HSQC spectrum for Sa-8 in the 10,0-25,0 ppm f1 range. The pulse sequence used was shsqcetgpsisp2.2 with 16 scans.

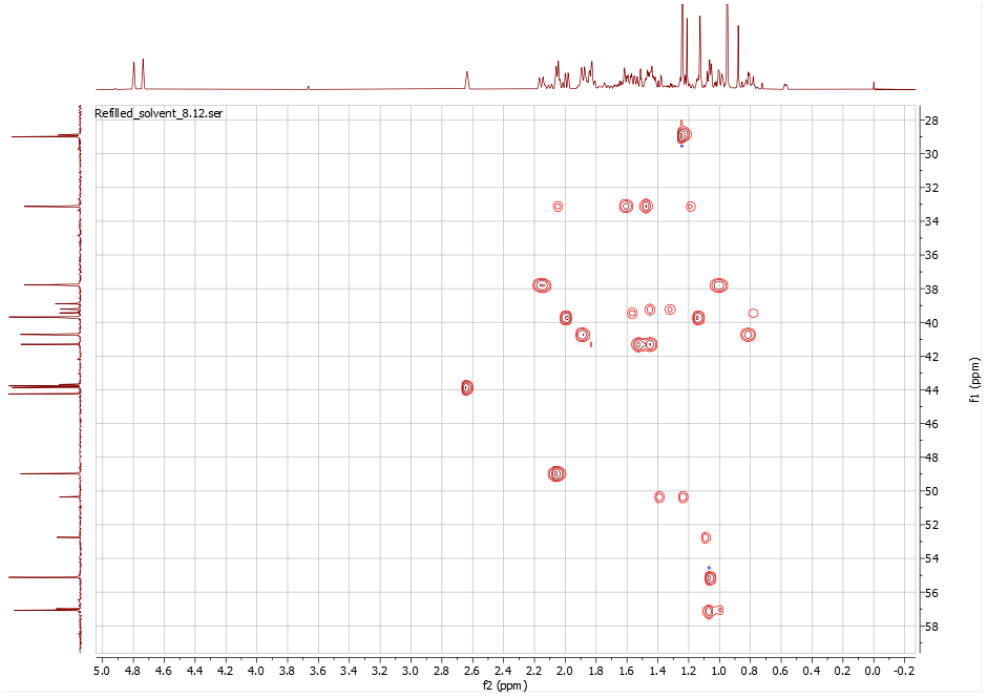

Figure A.8.5: Selective HSQC spectrum for Sa-8 in the 27,5,0-59,0 ppm f1 range. The pulse sequence used was shsqcetgpsisp2.2 with 16 scans

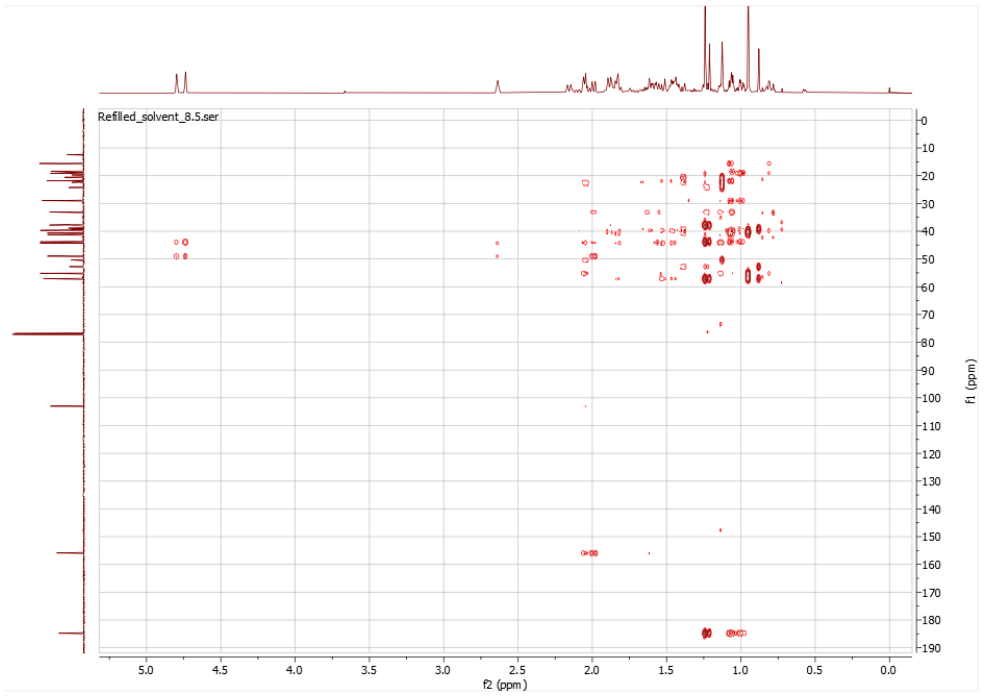

Figure A.8.6: HMBC spectrum of Sa-8, obtained with pulse sequence hmbcetgpl3nd and 8 scans.

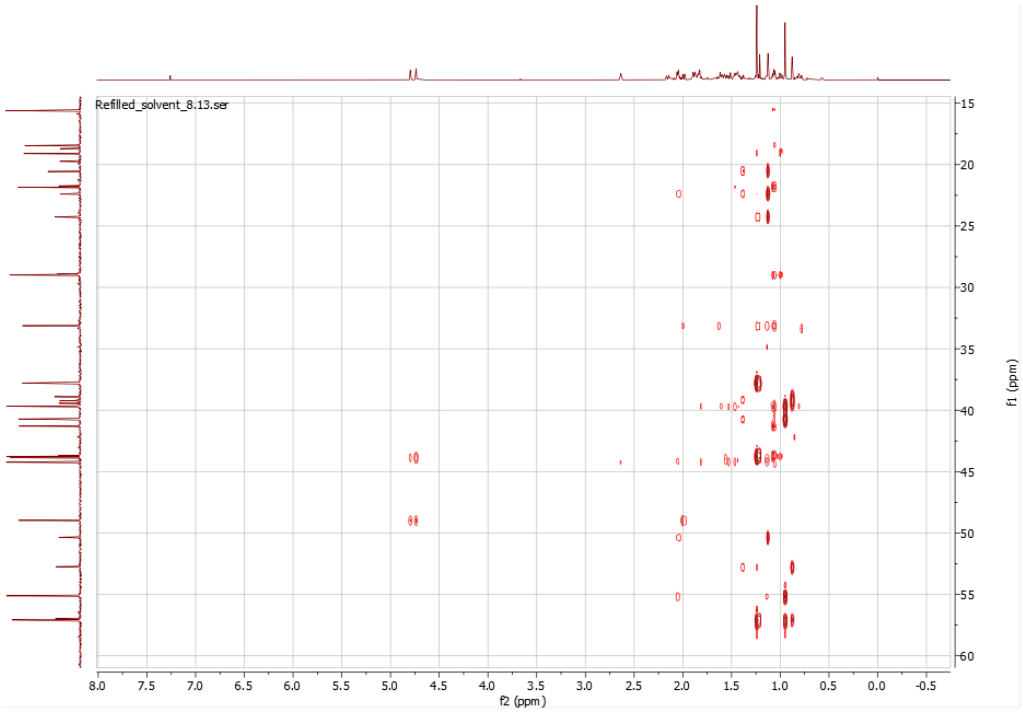

Figure A.8.7: Selective HMBC spectrum of Sa-8 in the 15,0-61-1 ppm f1 range. The utilized pulse sequence was hmbcctetgpl2nd with 16 scans.

Figure A.8.8: COSY spectrum of Sa-8 obtained with pulse sequence cosygpppqf and 4 scans.

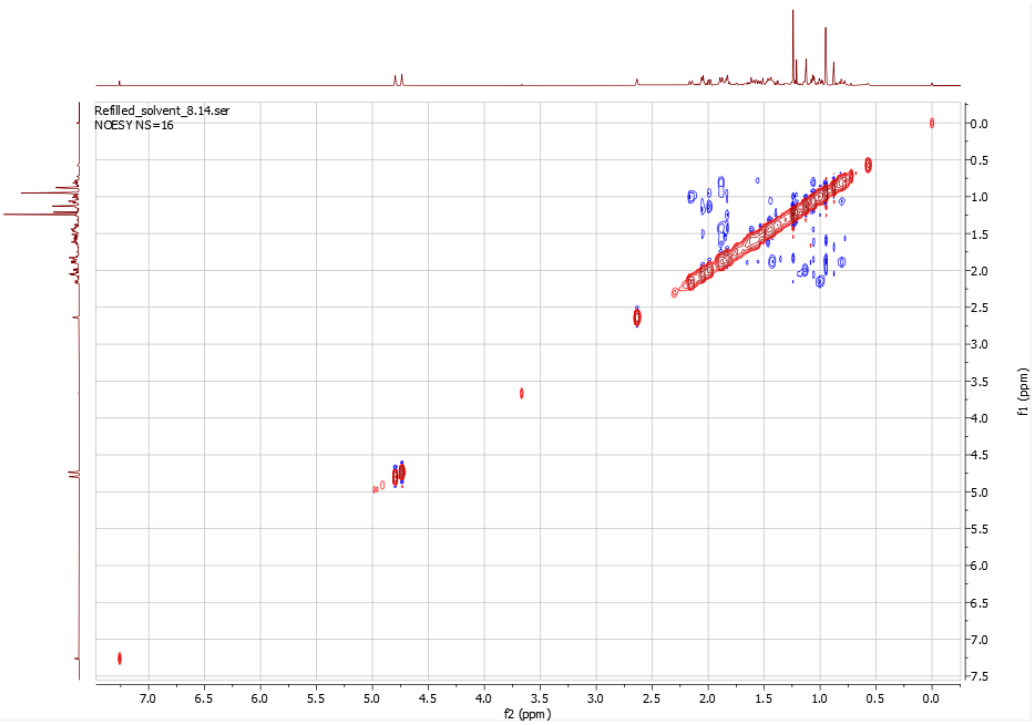

Figure A.8.9: NOESY spectrum of Sa-8 obtained with pulse sequence noesygpphpp, 16 scans, and a mixing time of 300 ms.

Sa-9

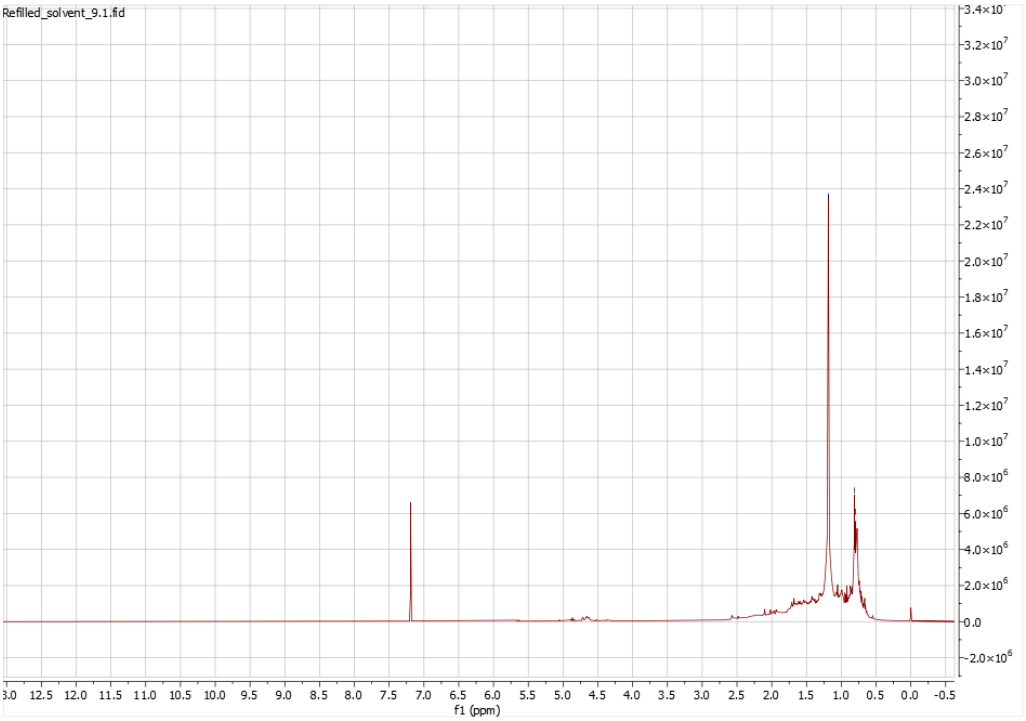

Figure A.9.1: ^{1}H spectrum of Sa-9, obtained with pulse sequence zg30 and 128 scans.

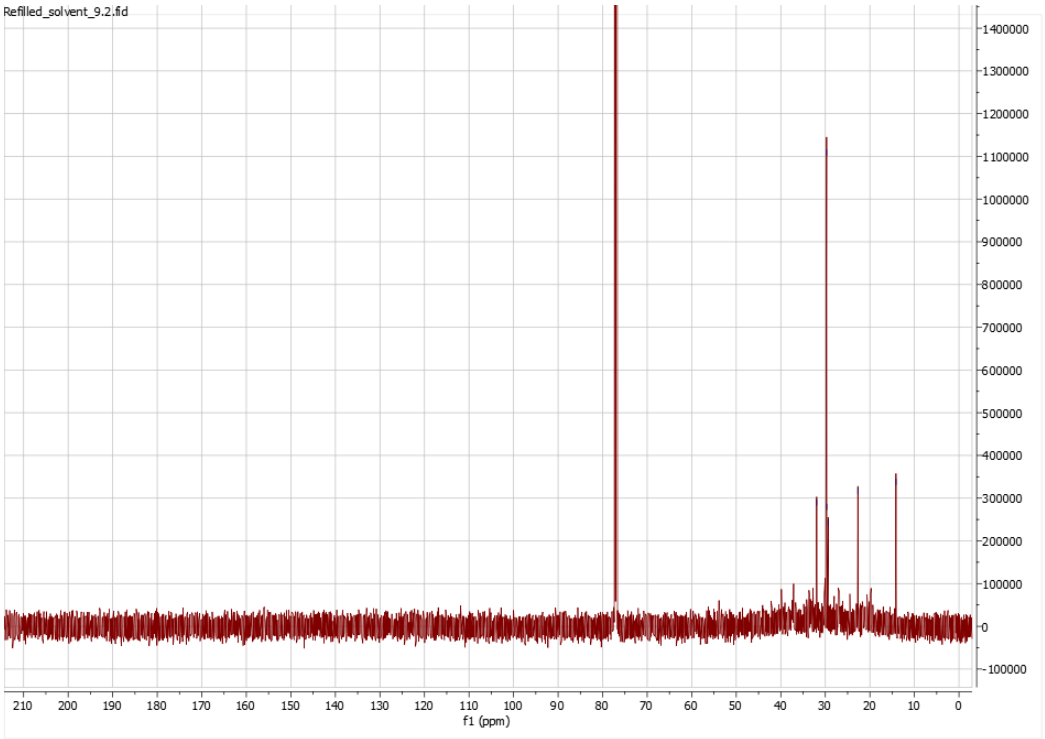

Figure A.9.2: ^{13}C spectrum of Sa-9, acquired with pulse sequence zgpg30 and 4096 scans.

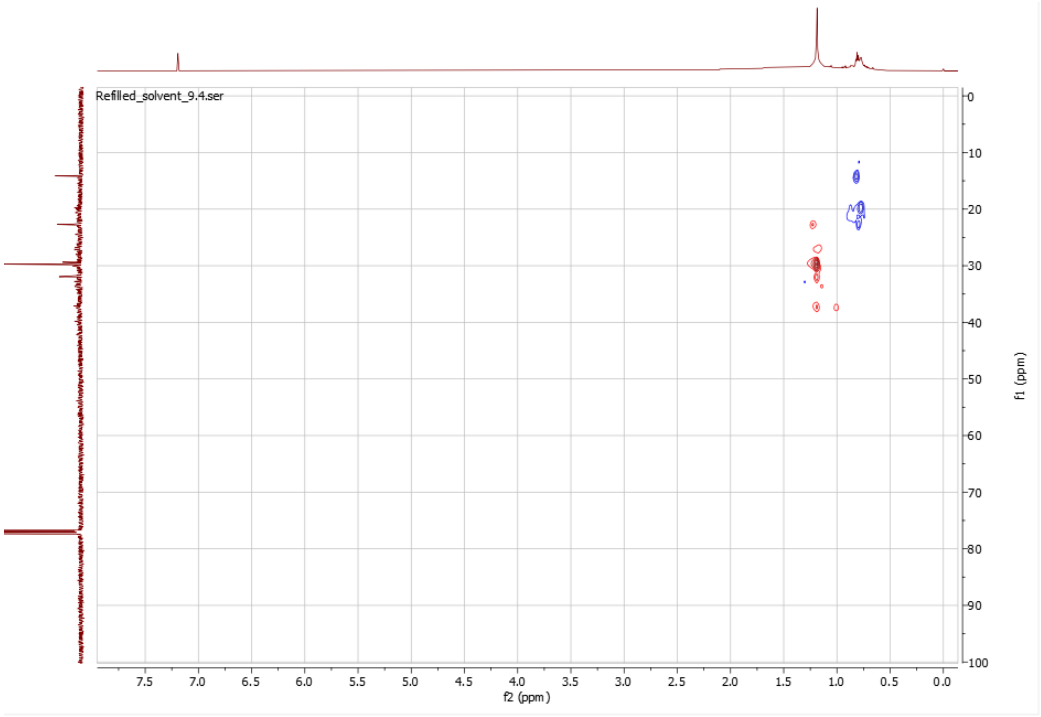

Figure A.9.3: Edited HSQC spectrum for Sa-9. The utilized pulse sequence was hsqcedetgpsisp2.3 and 8 scans.

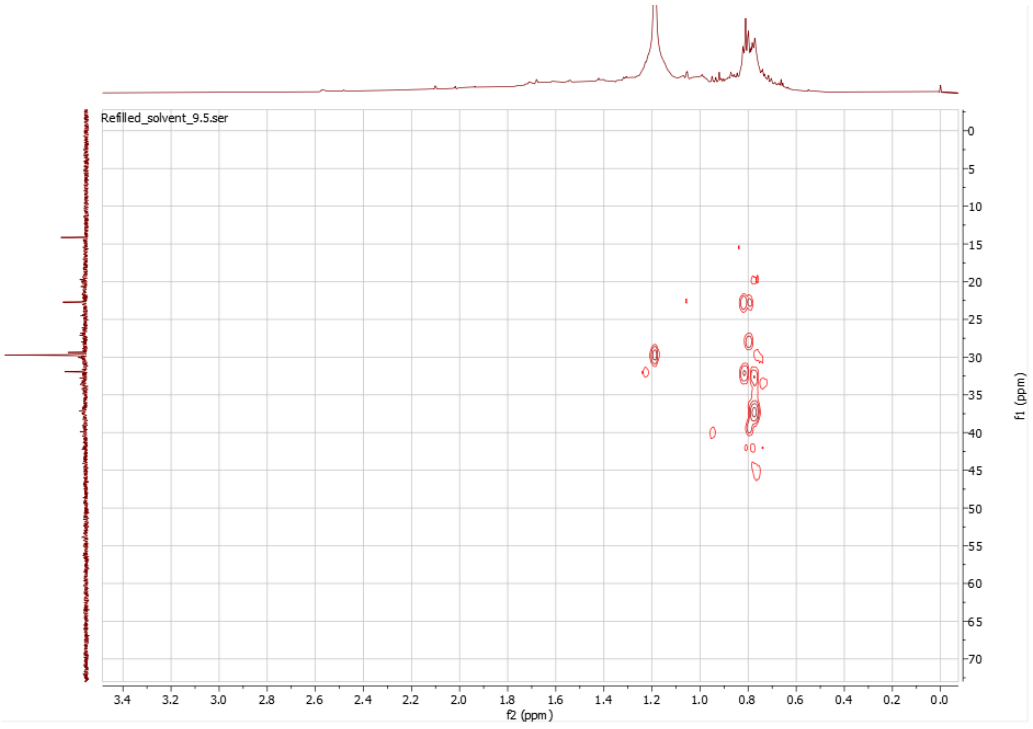

Figure A.9.4: HMBC spectrum for Sa-9, acquired with pulse sequence hmbcetgpl3nd and 8 scans.

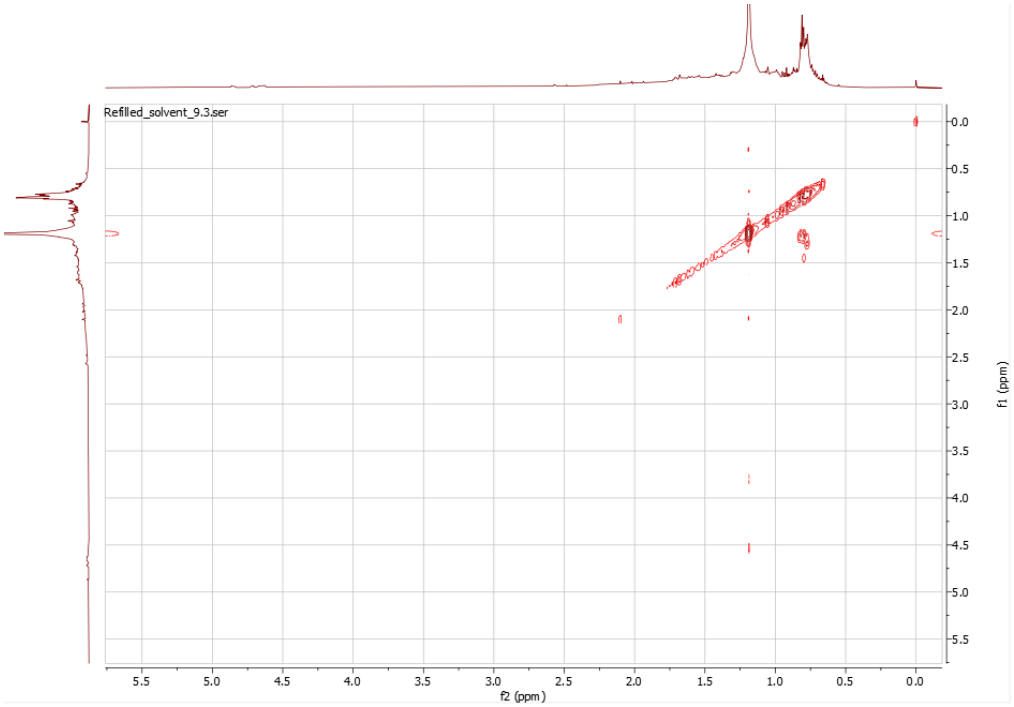

Figure A.9.5: COSY spectrum of Sa-9, obtained using pulse sequence cosygpppqf and 4 scans.

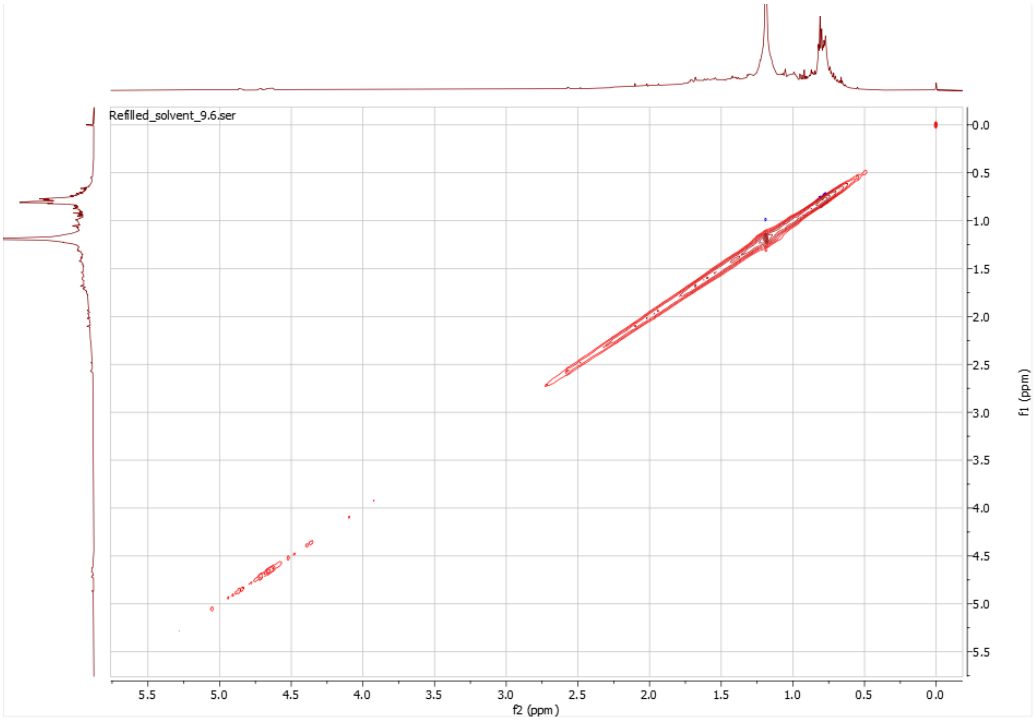

Figure A.9.6: NOESY spectrum of Sa-8. The utilized pulse sequence was noesygpphpp with 8 scans and a mixing time of 300 ms. No non-diagonal signals were detected without signal enhancement which resulted in inseparable t1 noise.

Sa-10

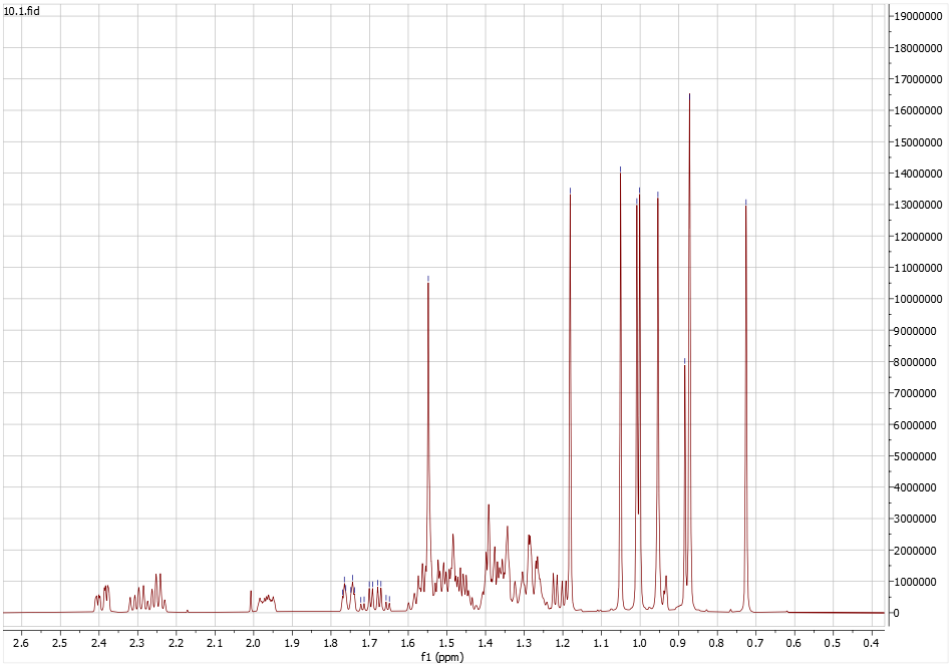

Figure A.10.1: ^{1}H NMR spectrum of Sa-10. The sample was analyzed with 256 scans and the pulse sequence zg30 was utilized.

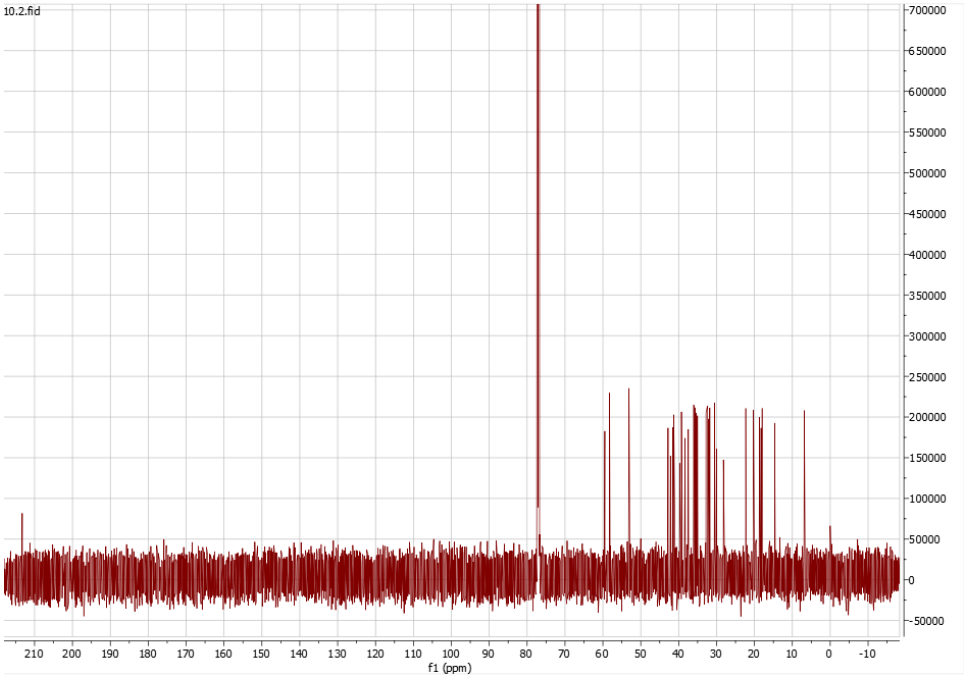

Figure A.10.2: ^{13}C NMR spectrum for Sa-10. The experiment was run with 4096 scans and pulse sequence zgpg30.

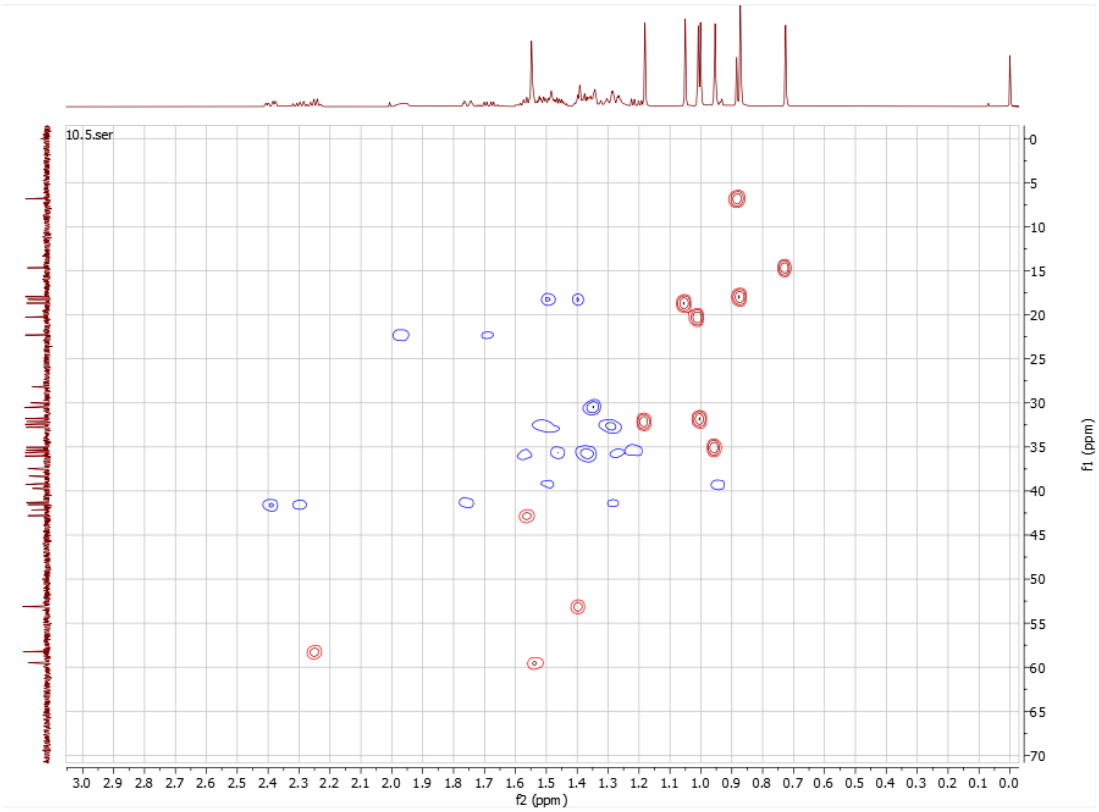

Figure A.10.3: Edited ^{1}H-^{13}C HSQC spectrum for Sa-10. The experiment was run with 16 scans and pulse sequence hsqcedetgpsisp2.3.

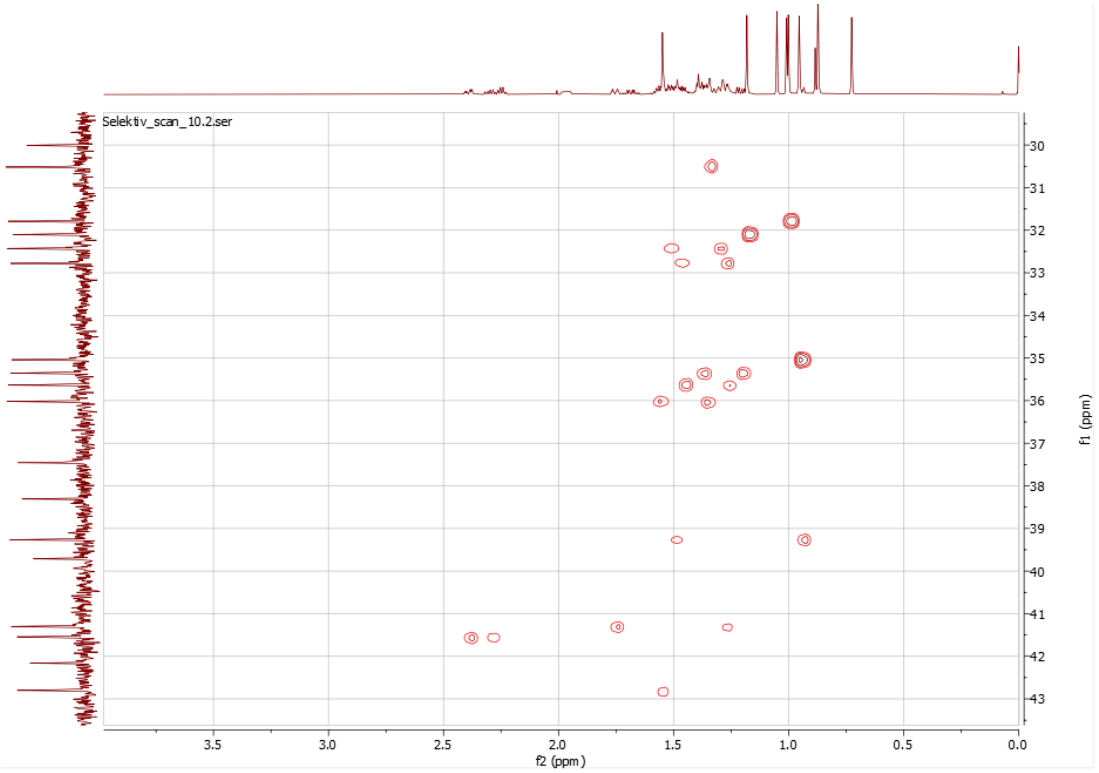

Figure A.10.4: Selective HSQC performed on the 29,0-43,5 ppm area (f1 axis) of the spectrum in Figure A.10 3. Pulse sequence shsqcedetgpsisp2.2 was used, with 16 scans.

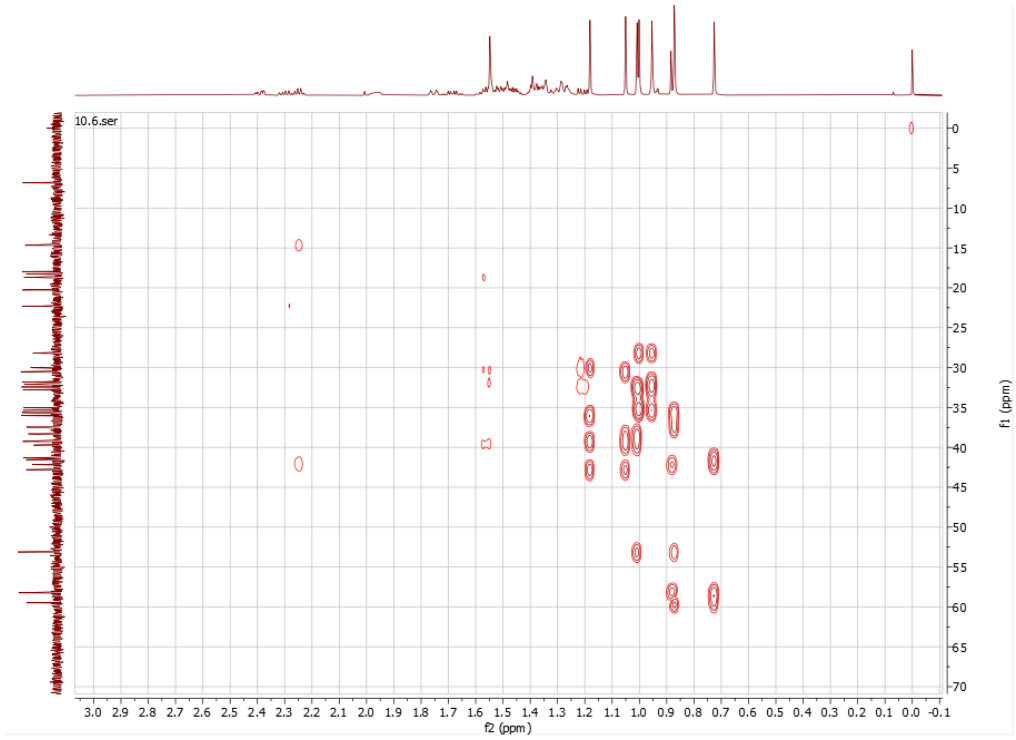

Figure A.10.5: ^{1}H-^{13}C HMBC spectrum for Sa-10, experiment performed with pulse sequence hmbcetgpl3nd and 16 scans.

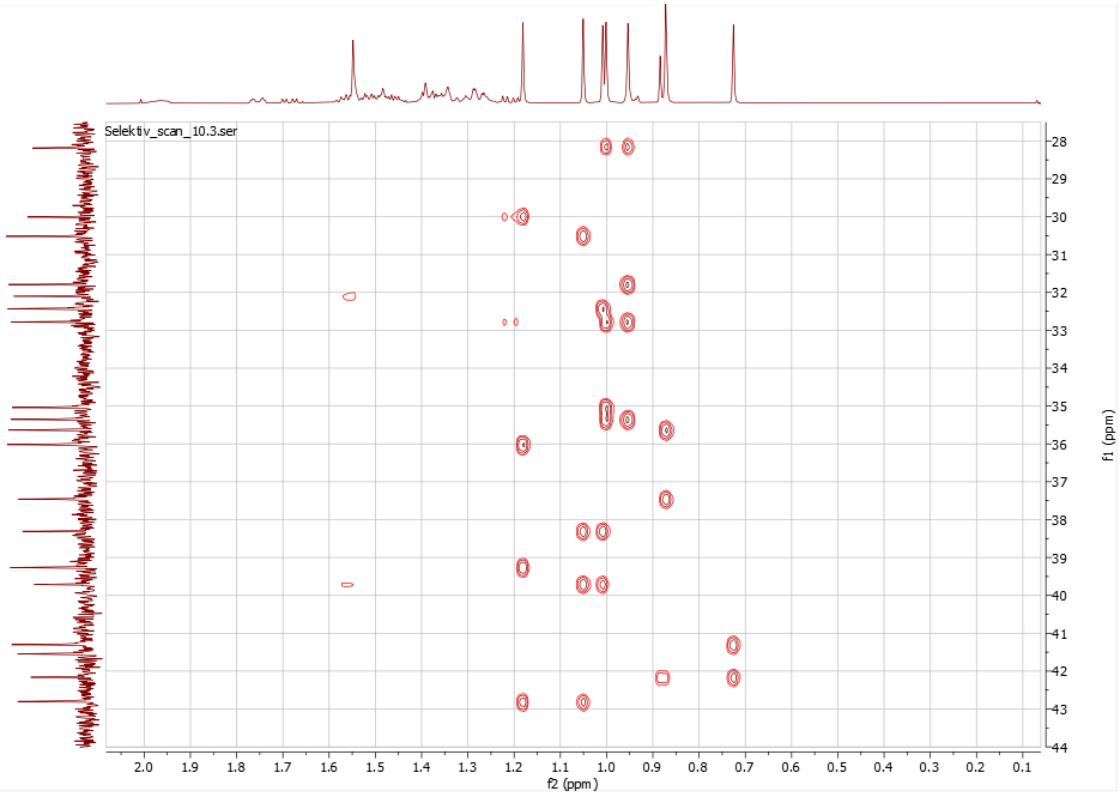

Figure A.10.6: Selective HMBC spectrum performed on the 27-46 ppm (f1 axis) on the spectrum in Figure A.10 5. The utilized pulse sequence was shmbcctetgpl2nd with 16 scans.

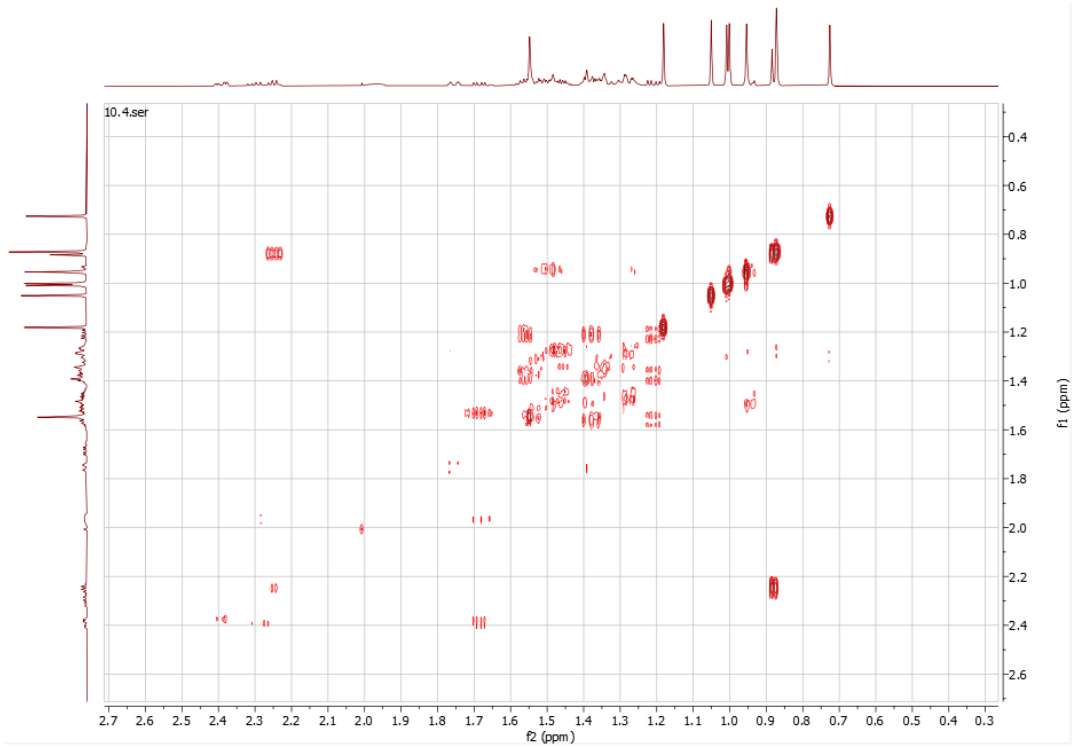

Figure A.10.7: ^{1}H-^{1}H COSY spectrum for Sa-10, utilizing pulse sequence cosygpppqf and 4 scans.

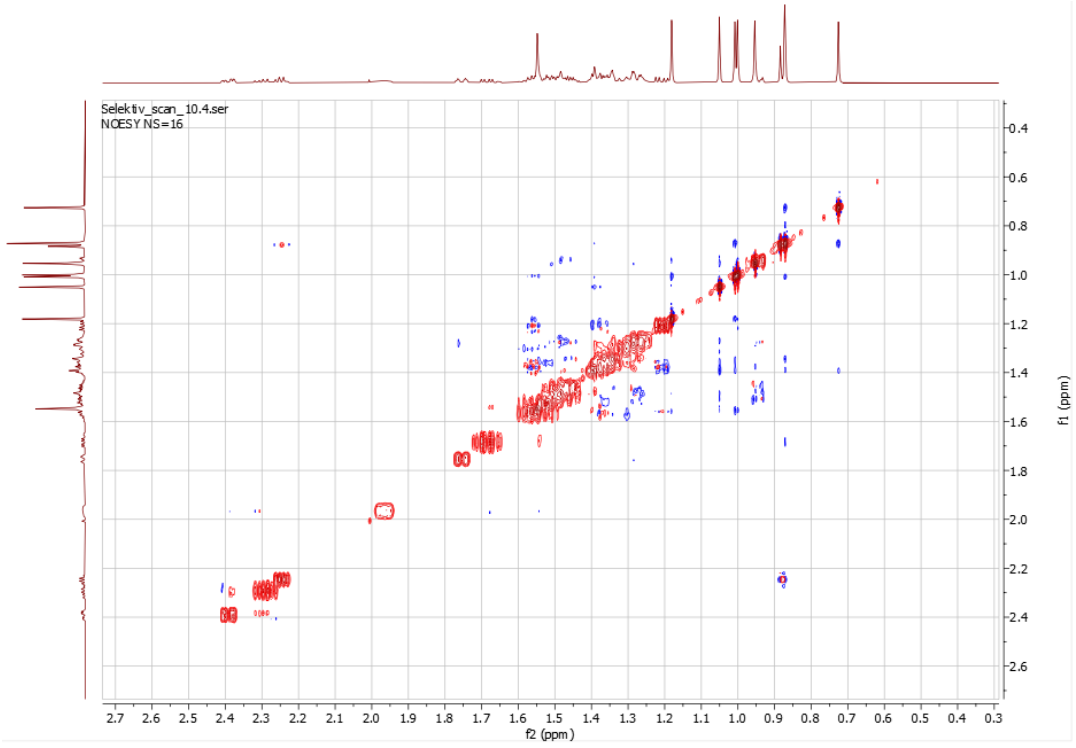

Figure A.10.8: ^{1}H-^{1}H 2D NOESY spectrum for Sa-10, performed with a noesygpphpp pulse sequence with a mixing time of 300 ms and 16 scans.

Sa-11

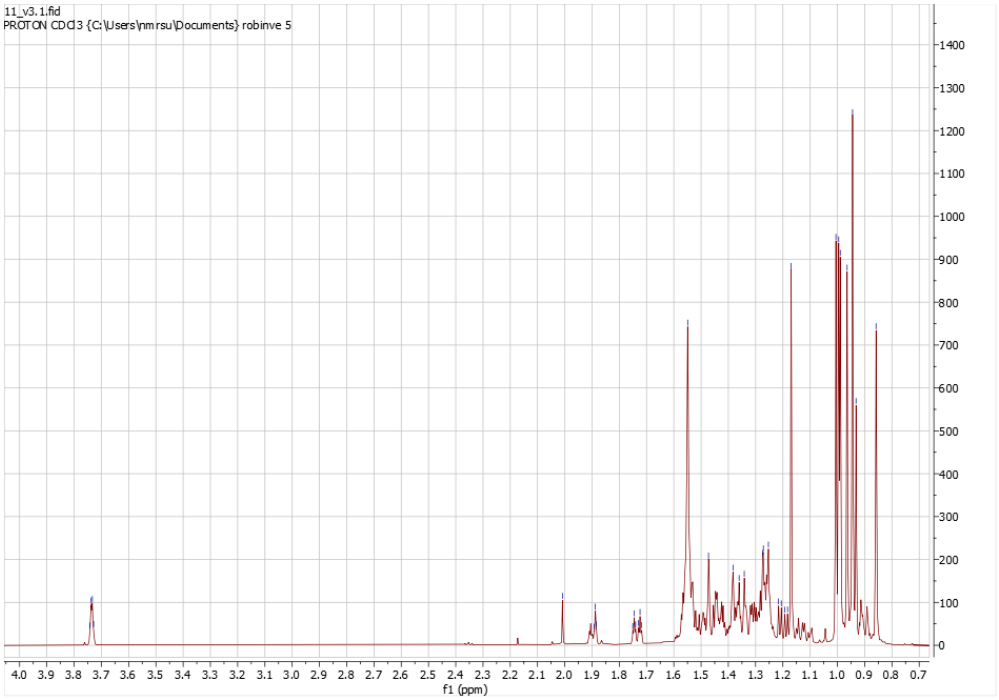

Figure A.11.1: ^{1}H spectrum for Sa-11, obtained with the zg30 pulse sequence with 128 scans.

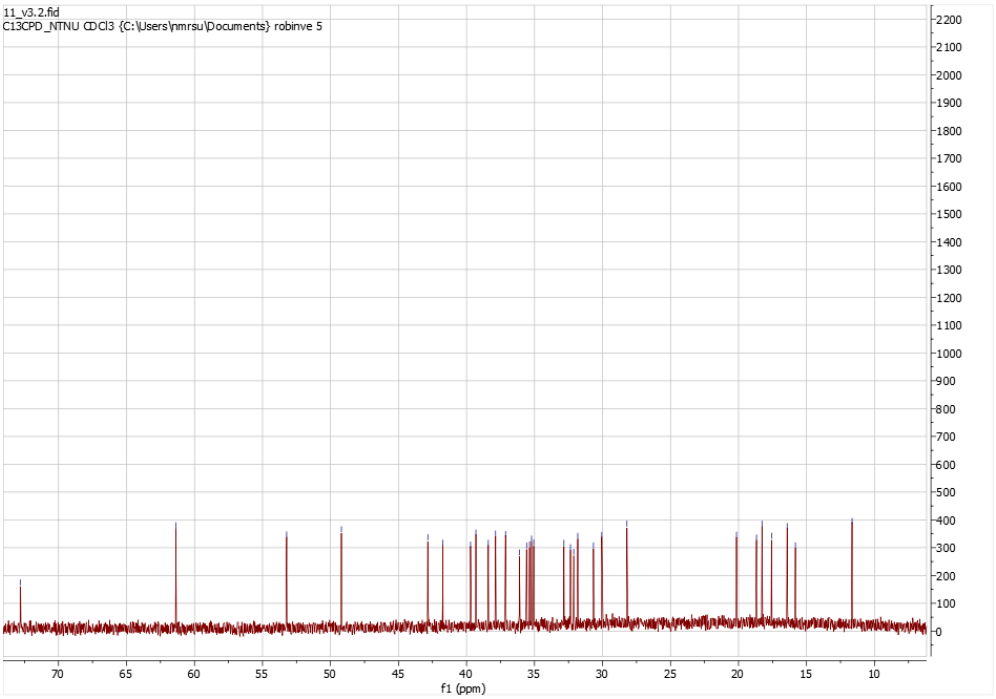

Figure A.11.2: ^{13}C spectrum for Sa-11. The utilized pulse sequence was zgpg30 with 4096 scans.

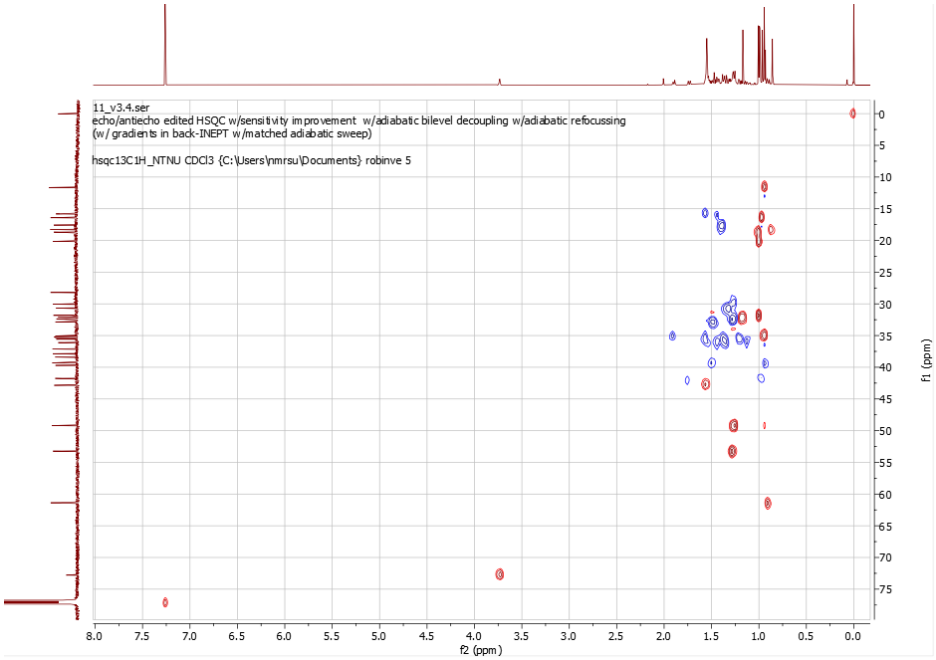

Figure A.11.3: Edited HSQC spectrum Sa-11, obtained with the hsqcedetgpsisp2.3 pulse sequence and 16 scans.

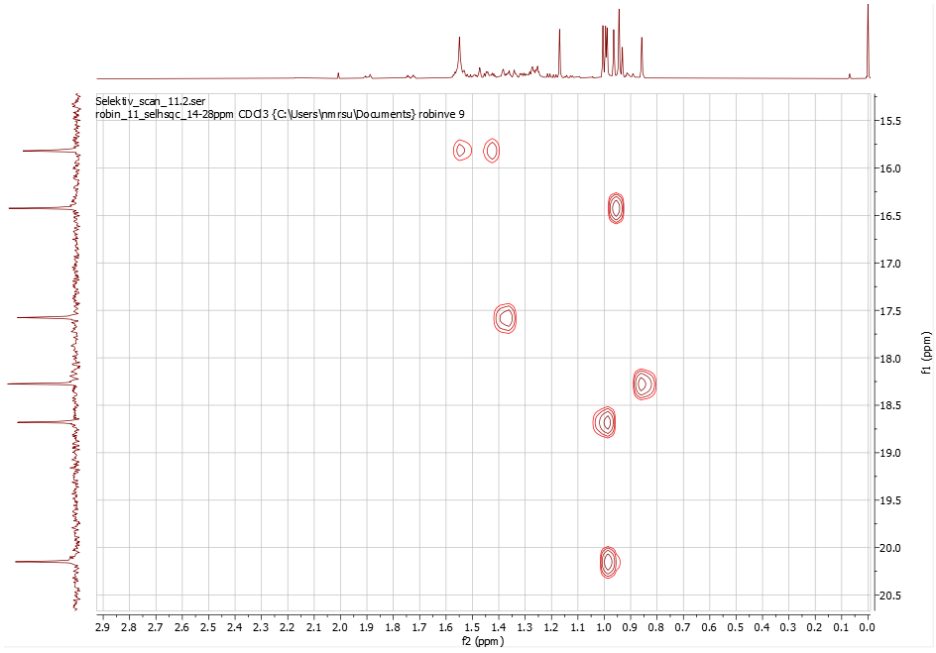

Figure A.11.4: Selective HSQC performed on the 14,0-28,0 ppm area (f1 axis) of the spectrum in Figure A.11 3. Pulse sequence shsqcedetgpsisp2.2 was used, with 16 scans.

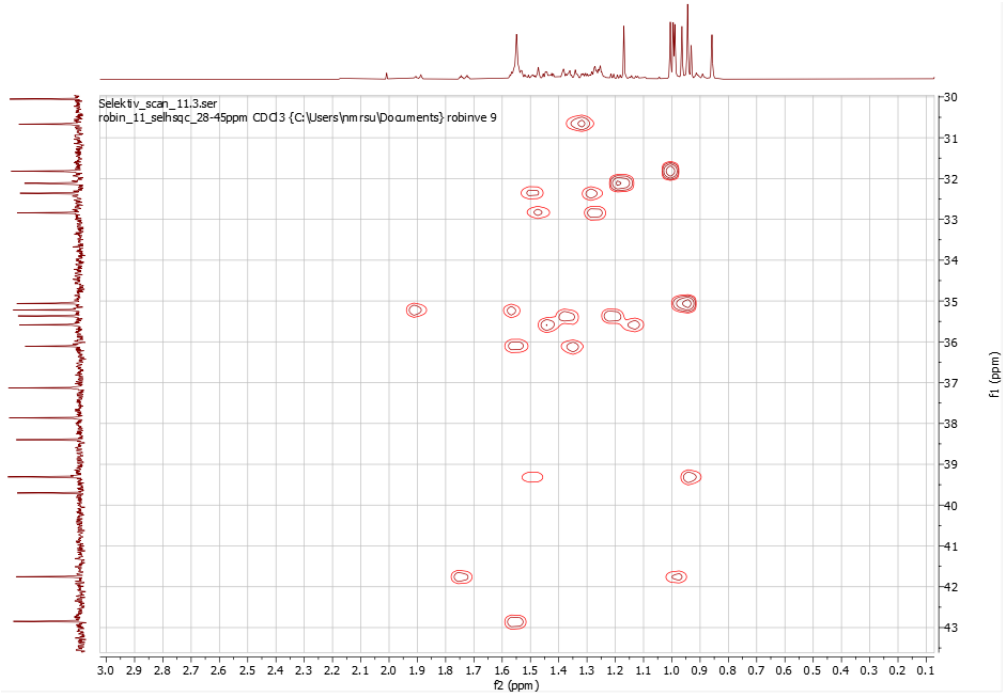

Figure A.11.5: Selective HSQC performed on the 28,0-45,0 ppm area (f1 axis) of the HSQC spectrum in Figure A.11.3. Pulse sequence shsqcedetgpsisp2.2 was used, with 16 scans.

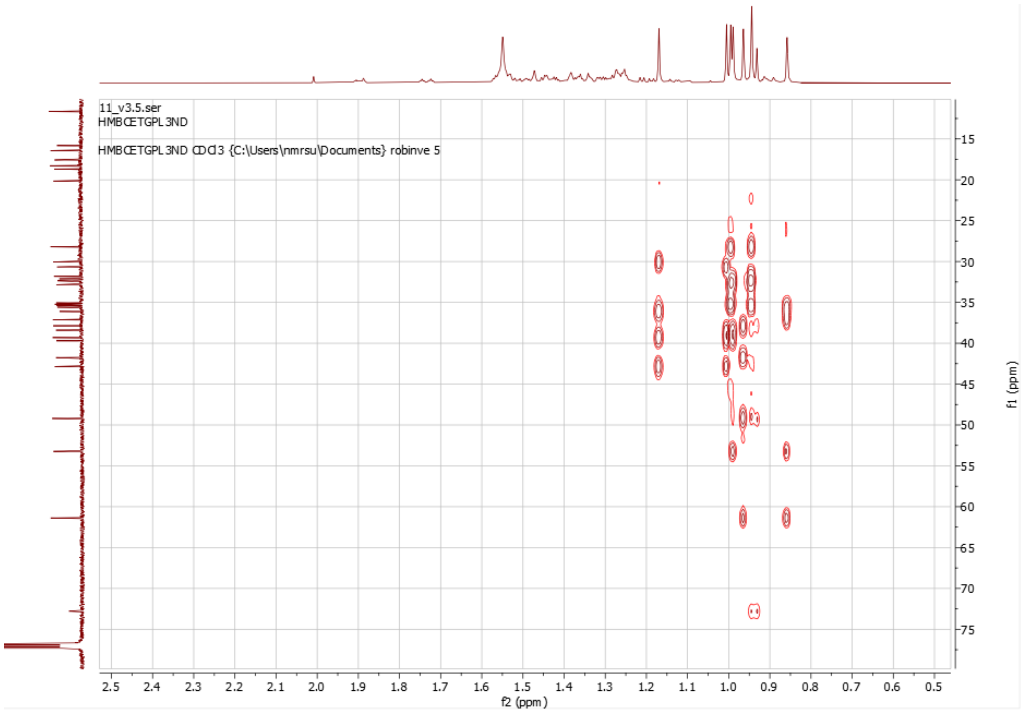

Figure A.11.6: HMBC spectrum for Sa-11, obtained with pulse sequence HMBCETGPL3ND and 16 scans.

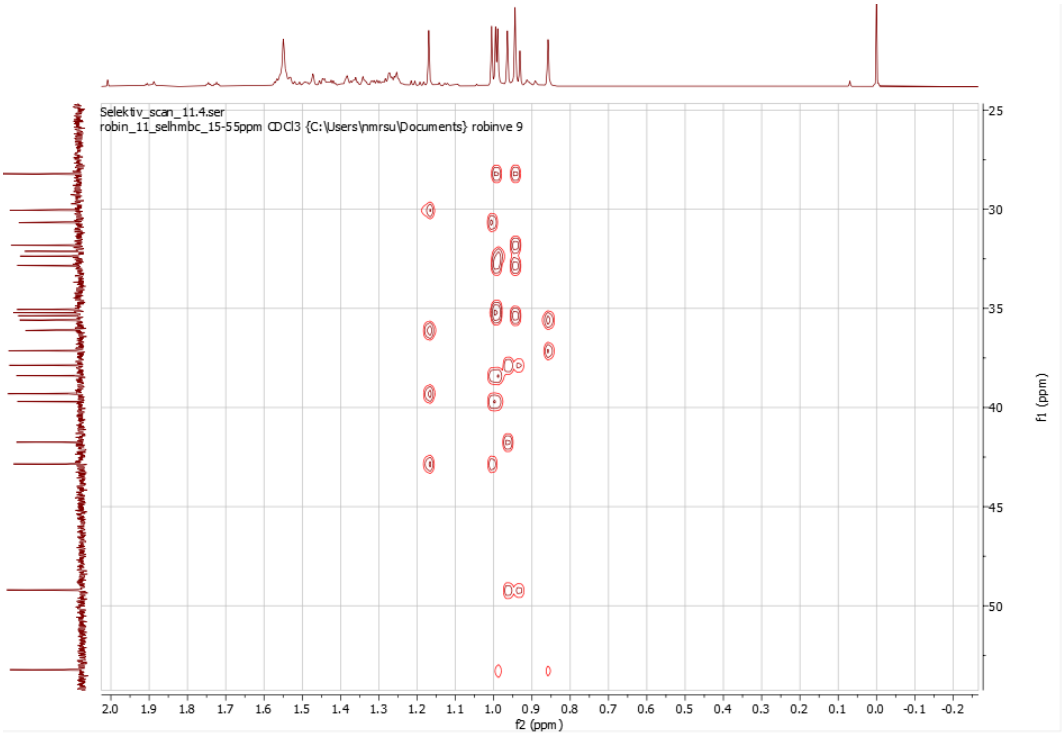

Figure A.11.7: Selective HMBC spectrum for Sa-11, in the 15,0-55,0 ppm f1 range. Acquired with pulse sequence shmbcctetgpl2nd and 16 scans.

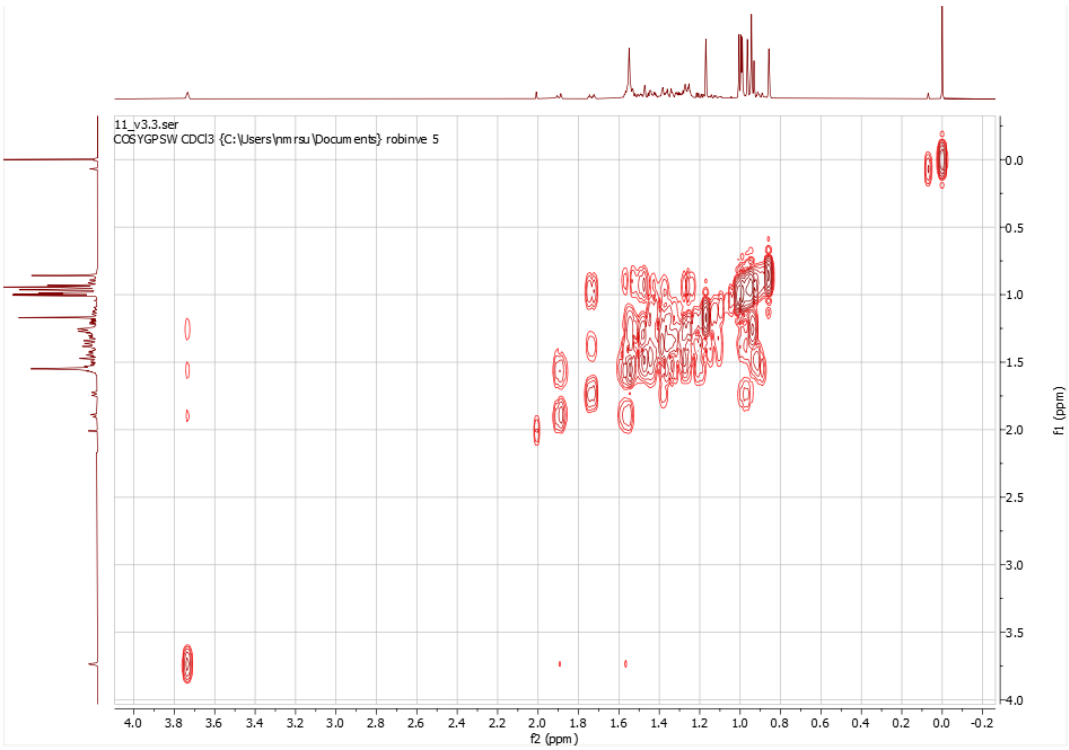

Figure A.11.8: COSY spectrum obtained for Sa-11 with pulse sequence cosygpppqf and 2 scans.

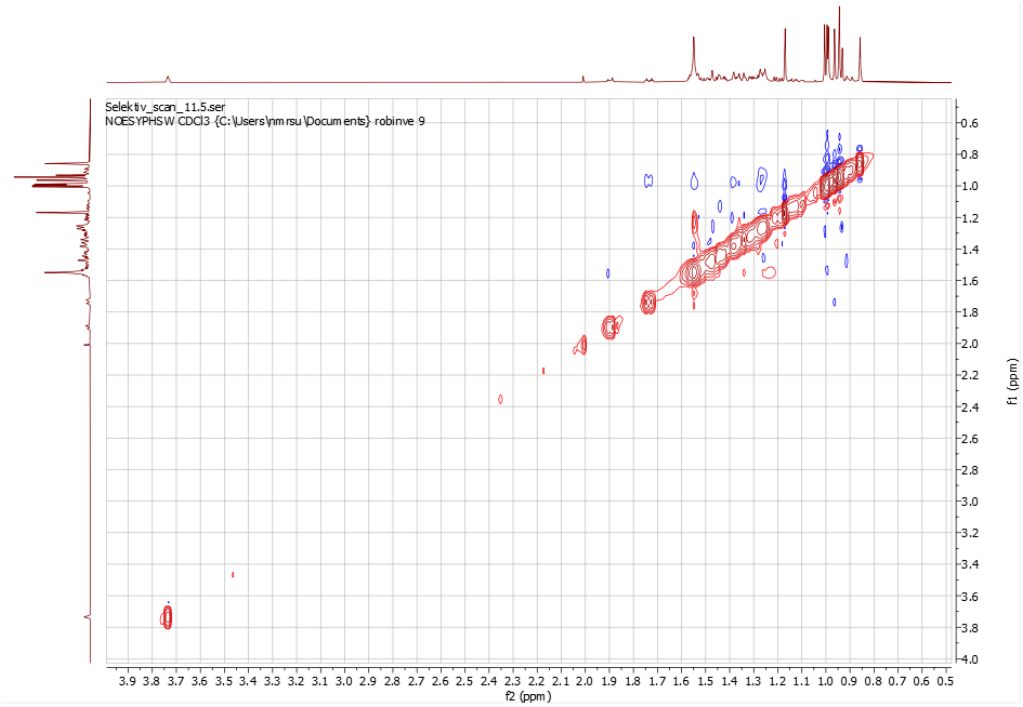

Figure A.11.9: NOESY spectrum for Sa-11 obtained with pulse sequence noesygphpp, 16 scans, and 300 ms mixing time.

Sa-12

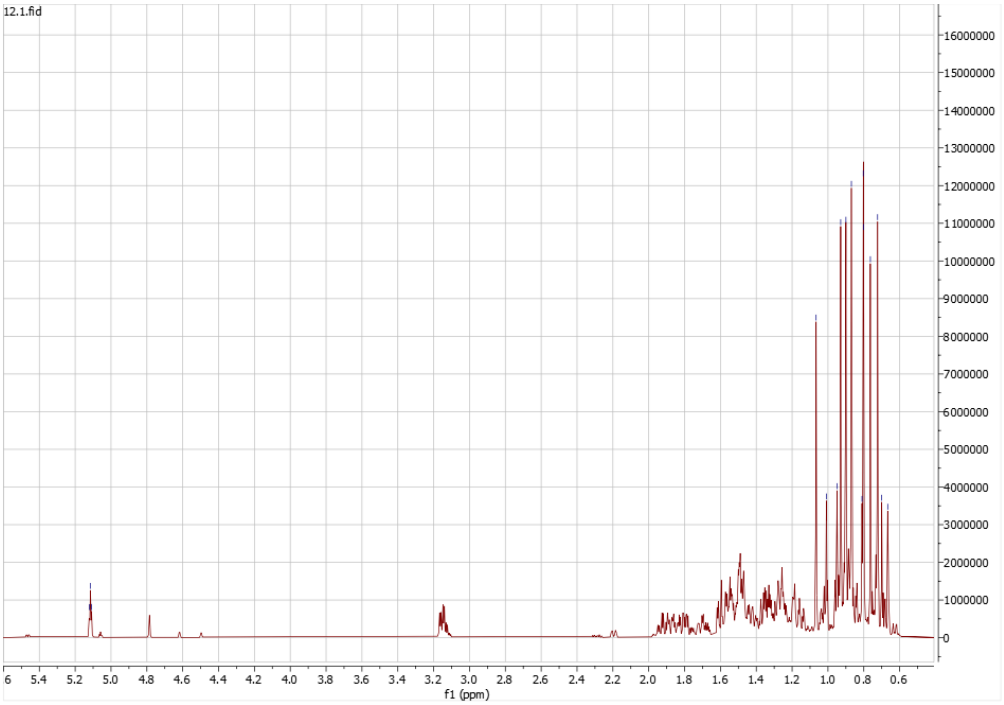

Figure A.12.1: ^{1}H spectrum of Sa-12, obtained with pulse sequence zg30 and 128 scans.

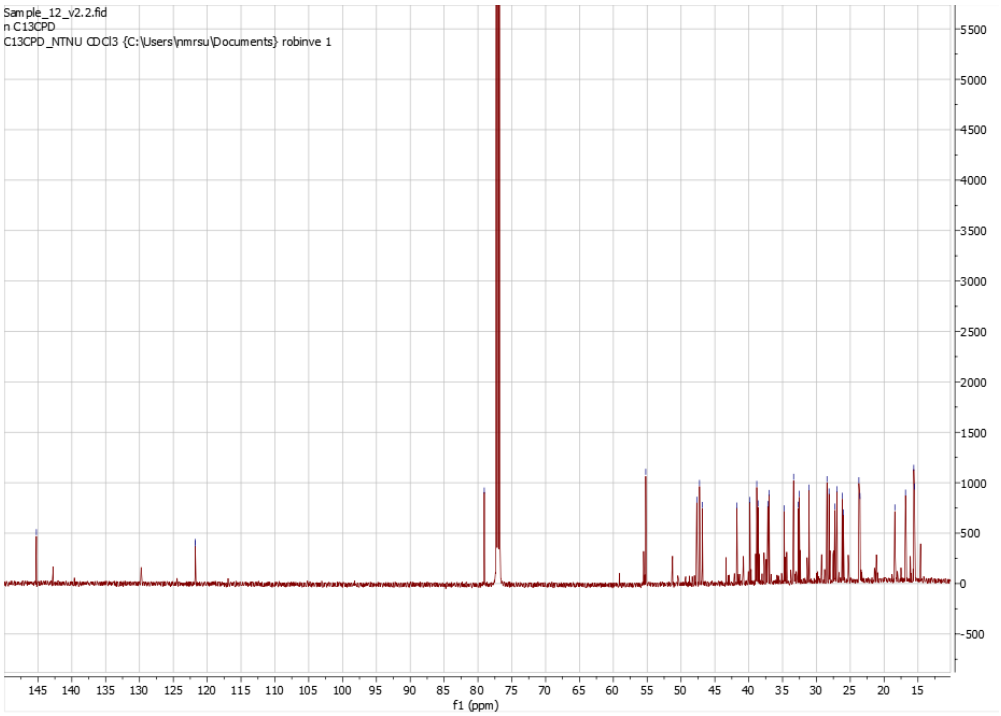

Figure A.12.2: ^{13}C spectrum of Sa-12. Pulse sequence zgpg30 was used to obtain the spectra, with 4096 scans.

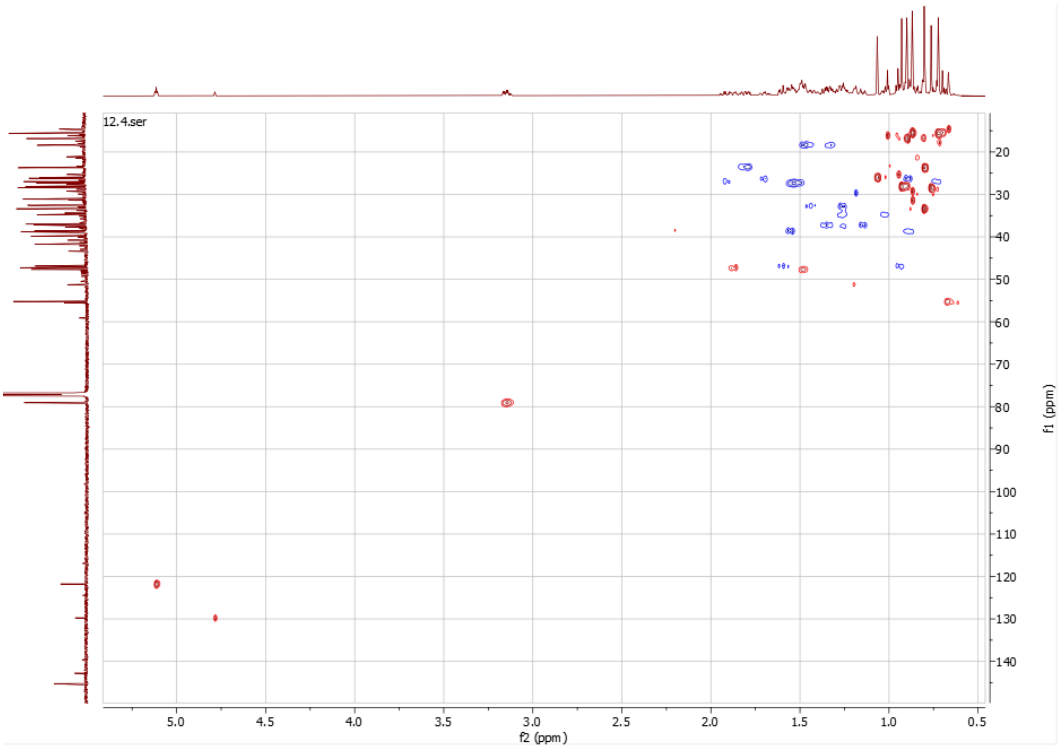

Figure A.12.3: Edited HSQC of Sa-12, obtained with pulse sequence hsqcedetgpsisp2.3 and 16 scans.

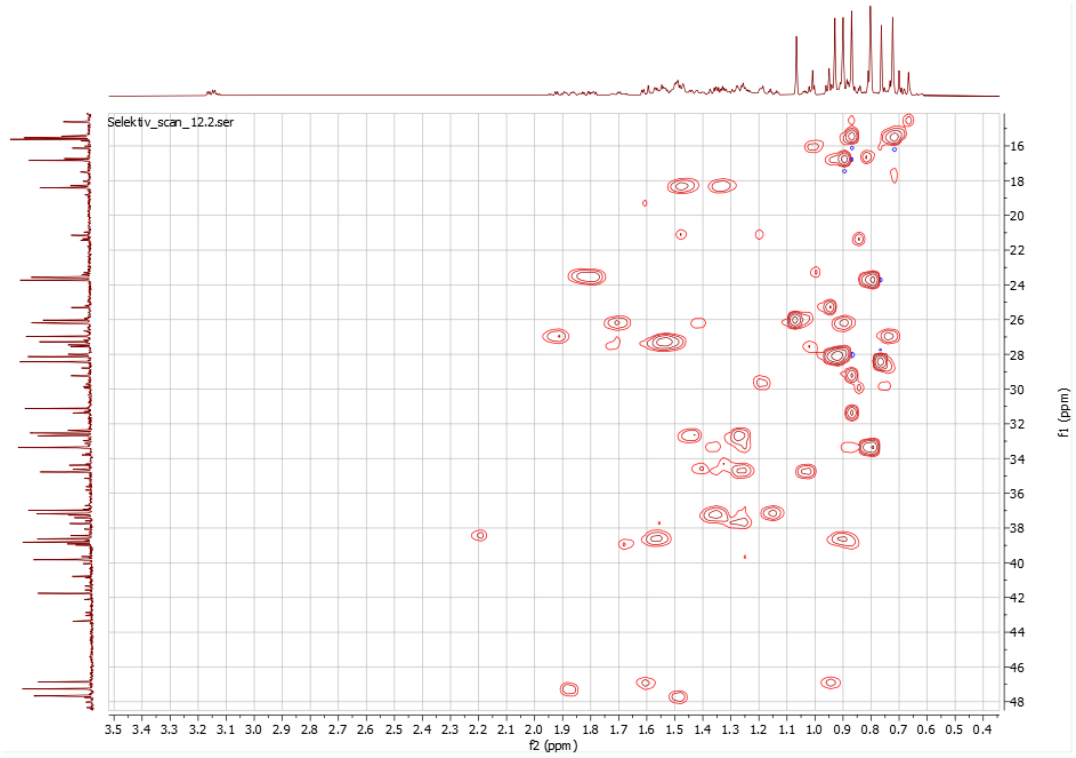

Figure A.12.4: Selective HSQC performed on the 14,0-49,0 ppm f1 range of the spectrum in Figure A.12 3. Pulse sequence shsqcedetgpsisp2.2 was used, with 16 scans.

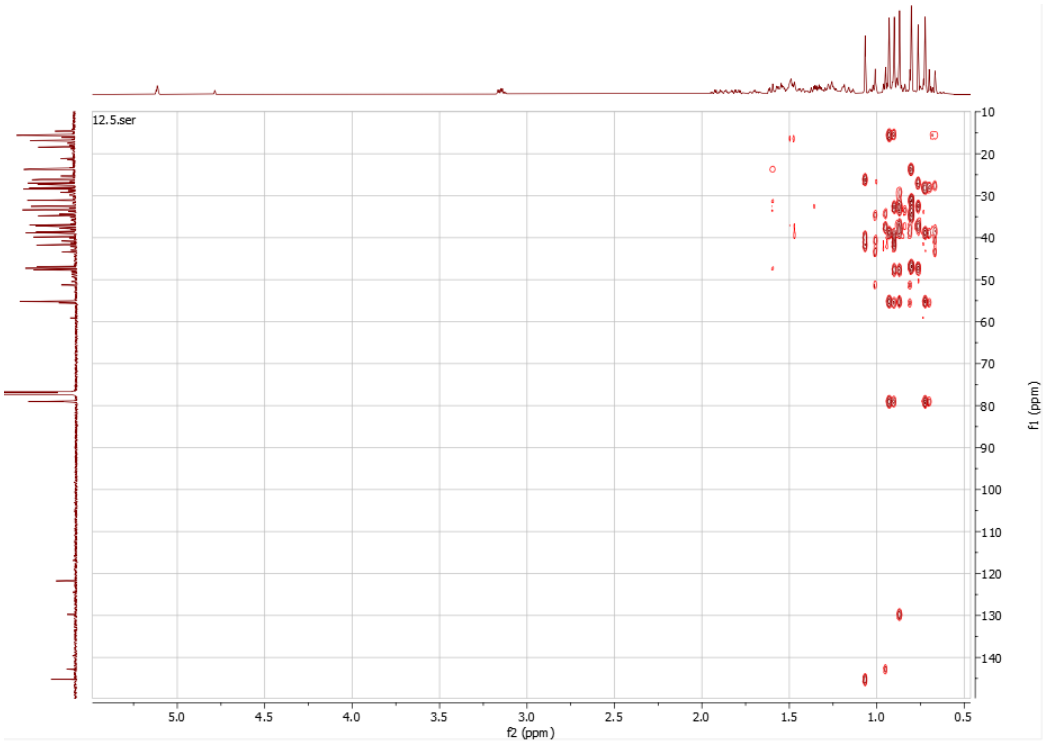

Figure A.12.5: HMBC spectrum for Sa-12, acquired with pulse sequence hmbcetgpl3nd and 16 scans.

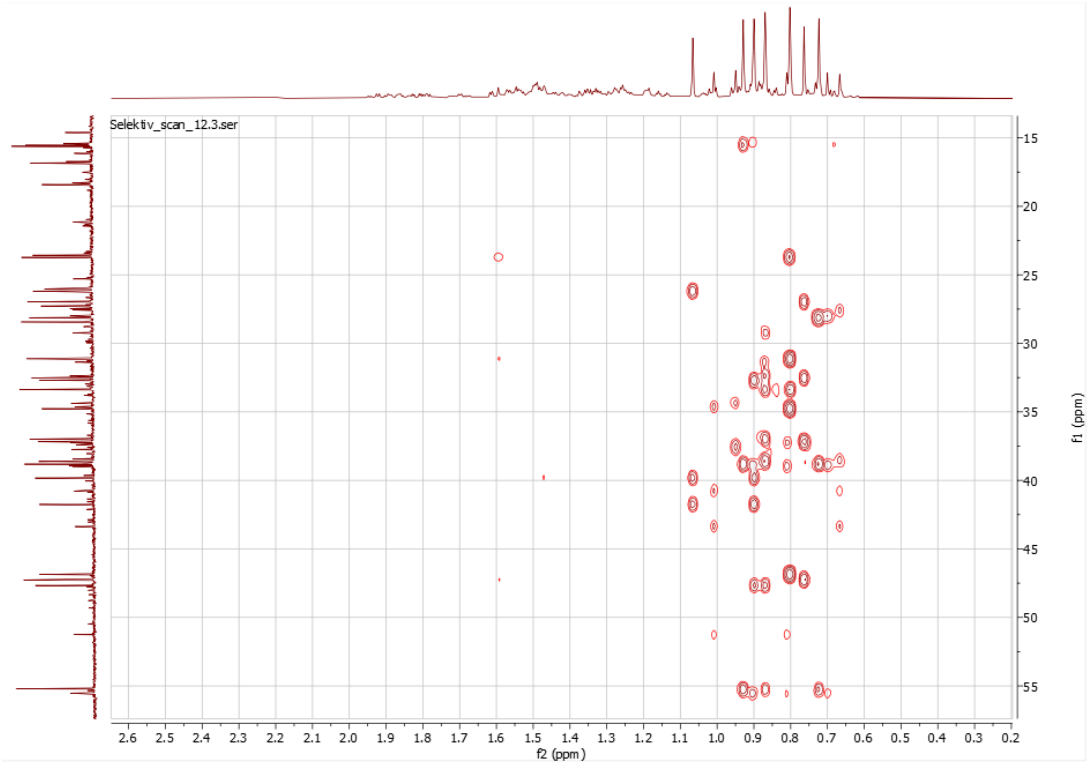

Figure A.12.6: Selective HMBC spectrum for Sa-12, in the 14,0-56,0 ppm f1 range. Acquired with pulse sequence shmbcctetgpl2nd and 16 scans.

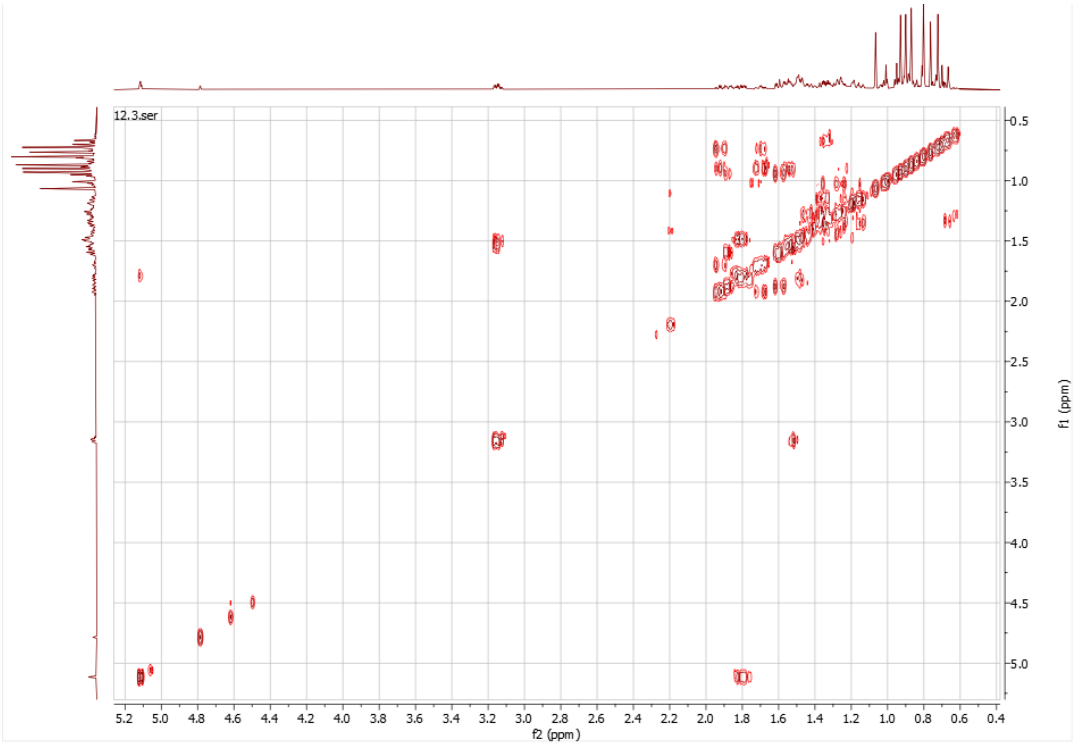

Figure A.12.7: COSY spectrum for Sa-12. The pulse sequence used was the cosygpppqf sequence with 1 scan.

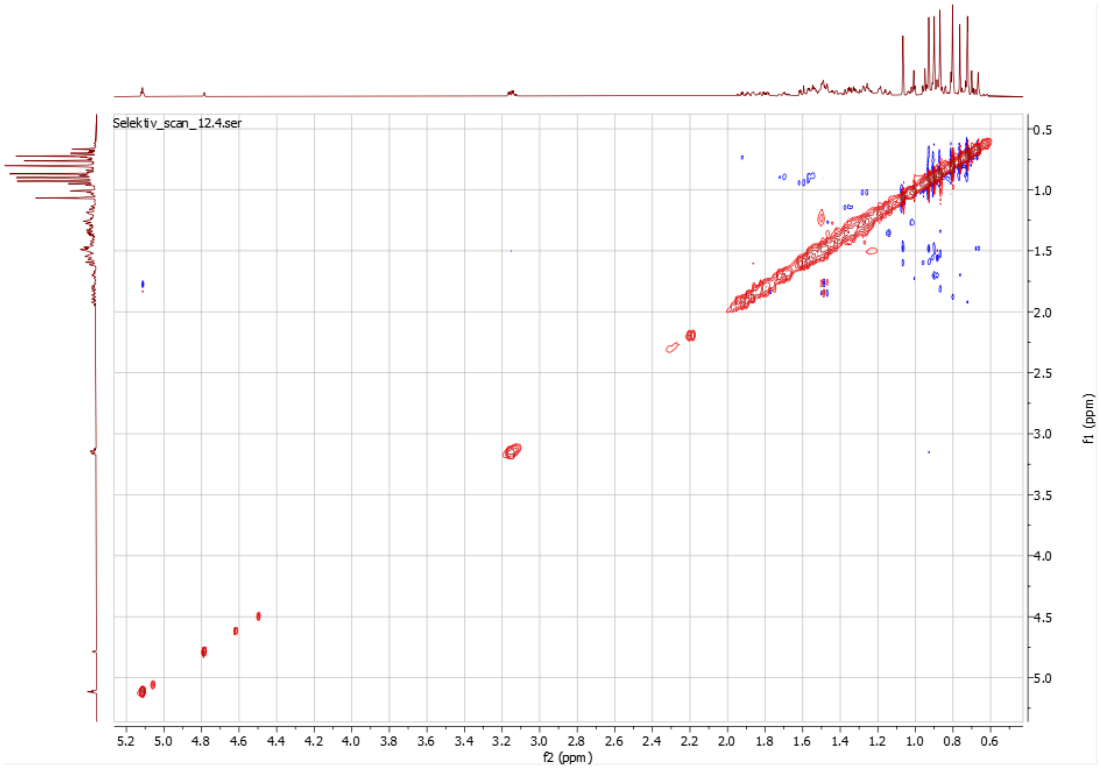

Figure A.12.8: NOESY spectrum for Sa-12, obtained with the noesygpphpp sequence with 16 scans and a mixing time of 300 ms.

Sa-13

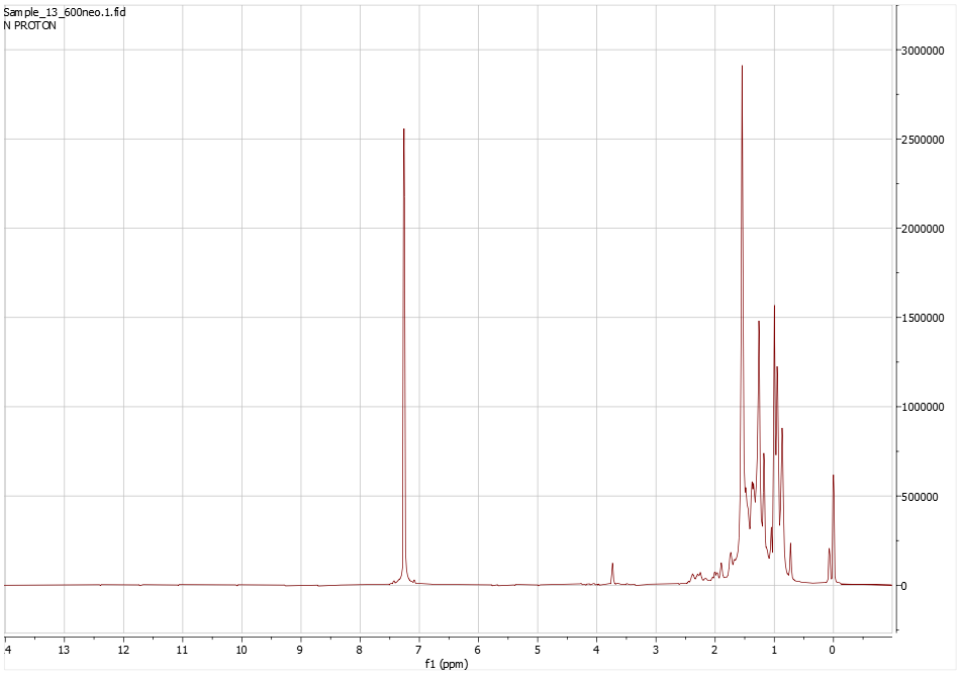

Figure A.13.1: ^{1}H spectrum for Sa-13, obtained with the zg30 pulse sequence with 256 scans

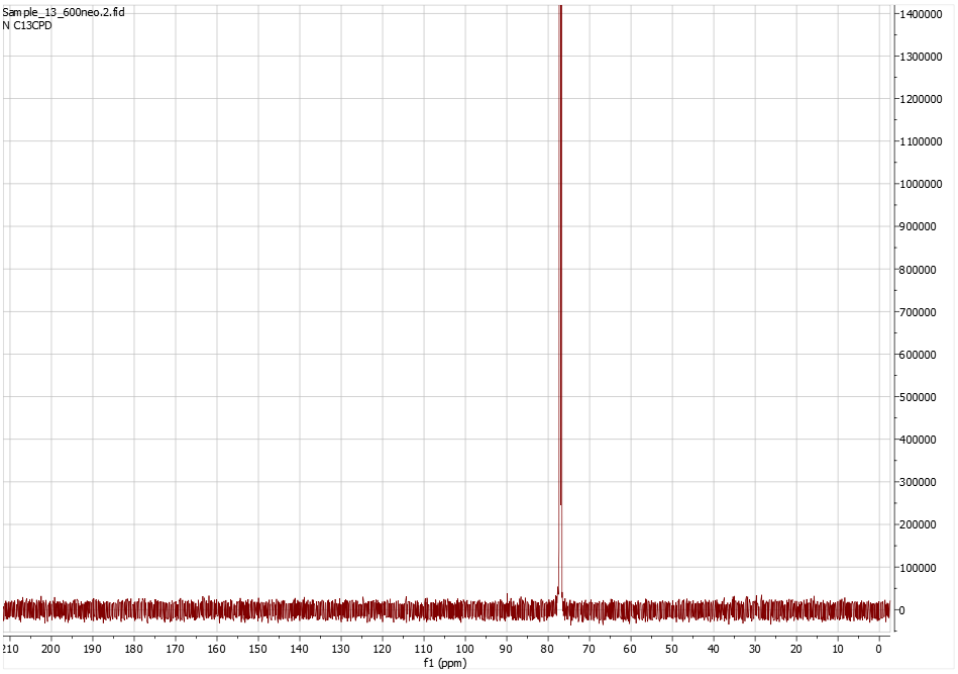

Figure A.13.2: ^{13}C spectrum for Sa-13, obtained with pulse sequence zgpg30 and 2048 scans.

Appendix B: IR spectra for assorted compounds

Sa-2

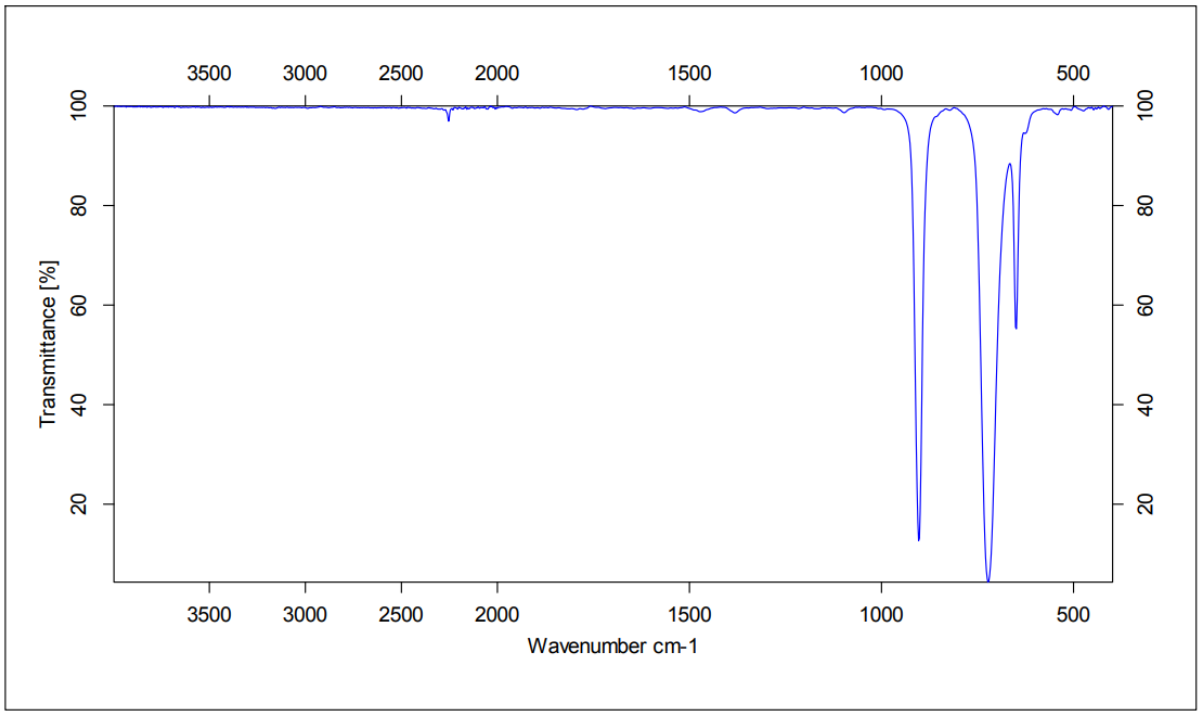

Sample : RV_SA_2	Frequency Range : 3996.98 - 398.261	Measured on : 12.05.2022	
Technique : Instrument type and	Resolution : 4	Instrument : Alpha	Sample Scans : 24
Customer : Administrator	Zerofilling : 2	Acquisition : Double Sided,Forv	

Figure B.1: IR spectrum obtained for Sa-2.

Sa-5

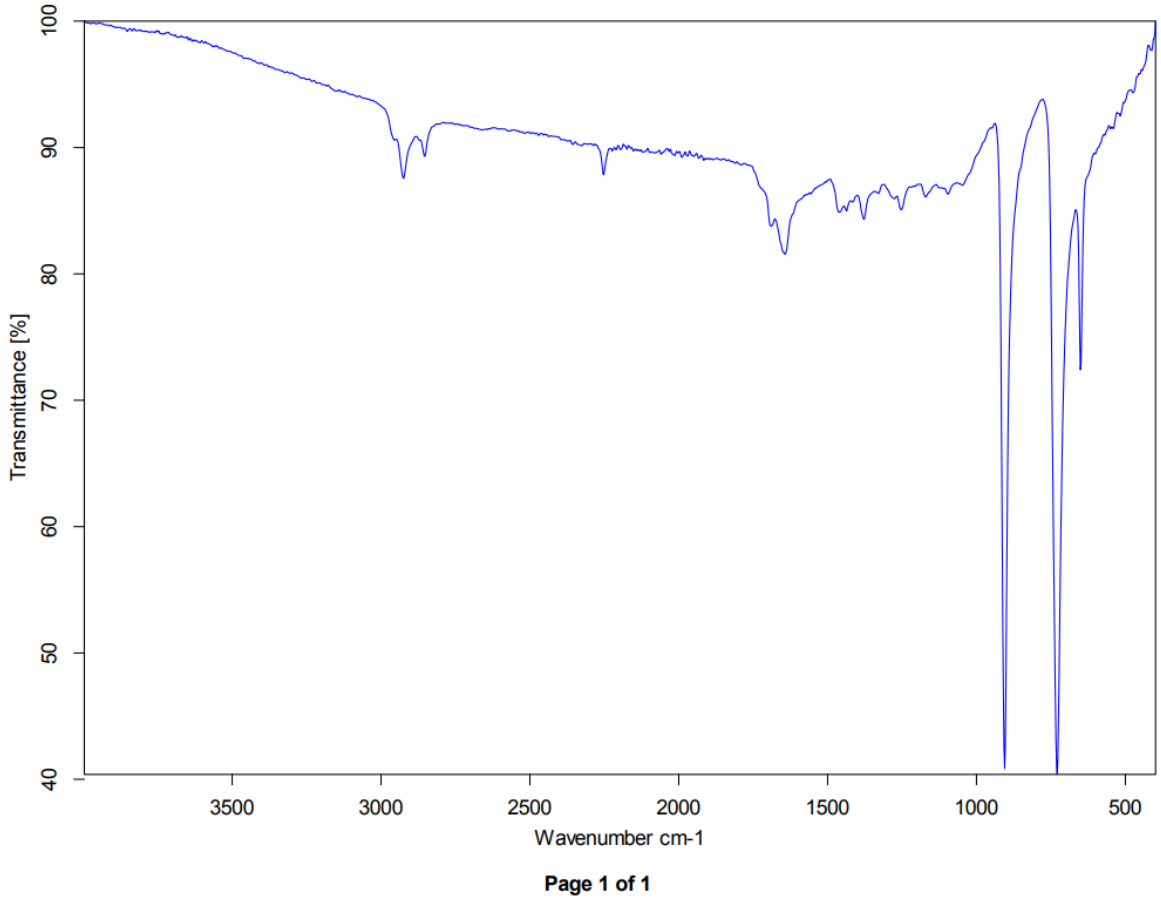

Figure B.2: IR spectrum obtained for Sa-5.

Sa-6

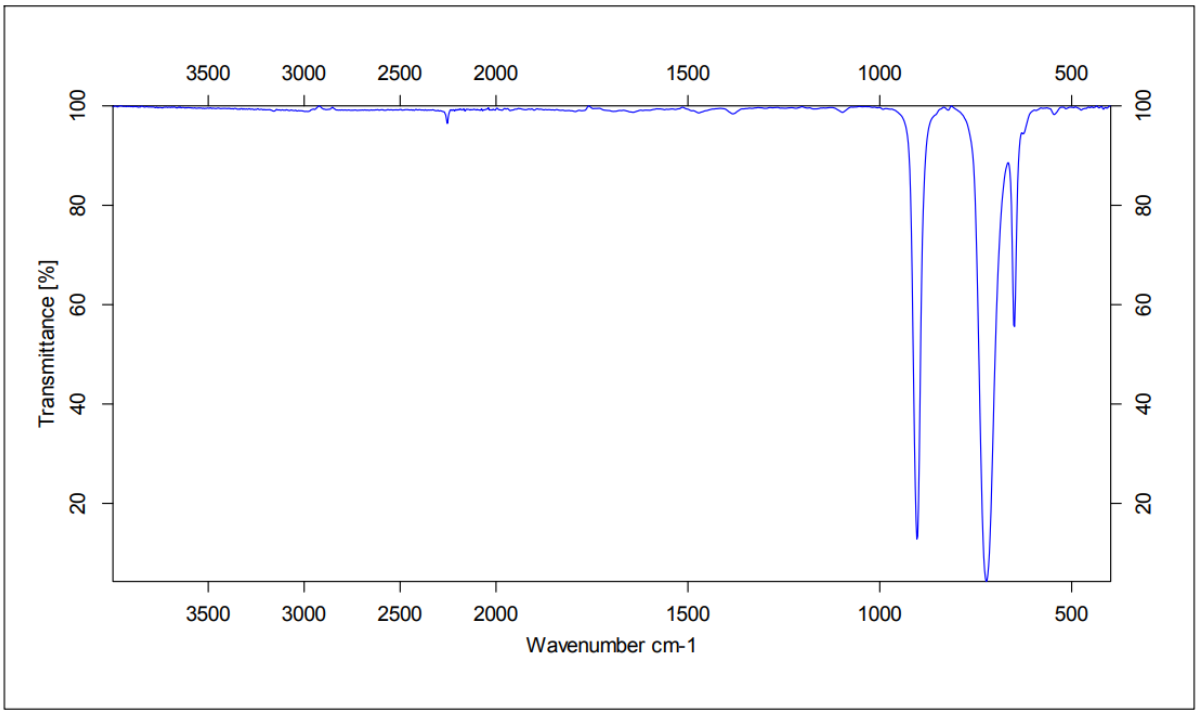

Sample : RV_SA_6	Frequency Range : 3996.98 - 398.261	Measured on : 12.05.2022	
Technique : Instrument type and	Resolution : 4	Instrument : Alpha	Sample Scans : 24
Customer : Administrator	Zerofilling : 2	Acquisition : Double Sided,Forv	

Figure B.3: IR spectrum of Sa-6.

Sa-7

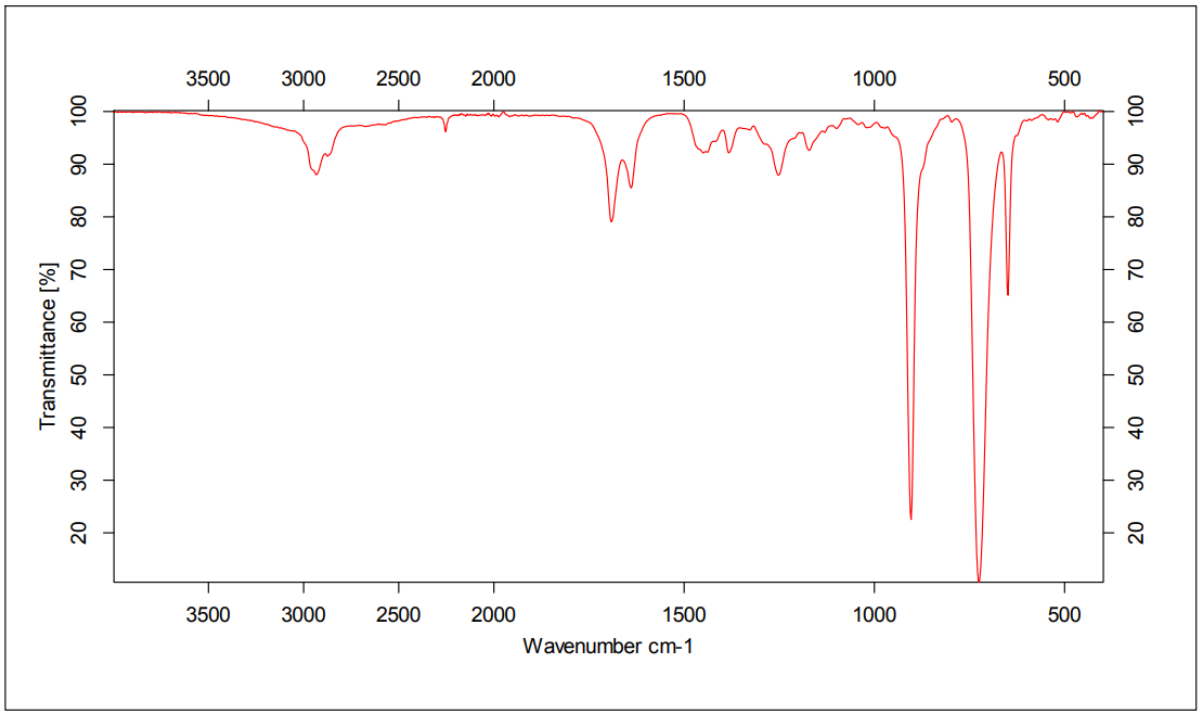

Sample : RV_SA_7	Frequency Range : 3996.98 - 398.261	Measured on : 11.05.2022	
Technique : Instrument type and	Resolution : 4	Instrument : Alpha	Sample Scans : 24
Customer : Administrator	Zerofilling : 2	Acquisition : Double Sided,For	

Figure B.4: IR spectrum obtained of Sa-7.

Sa-8

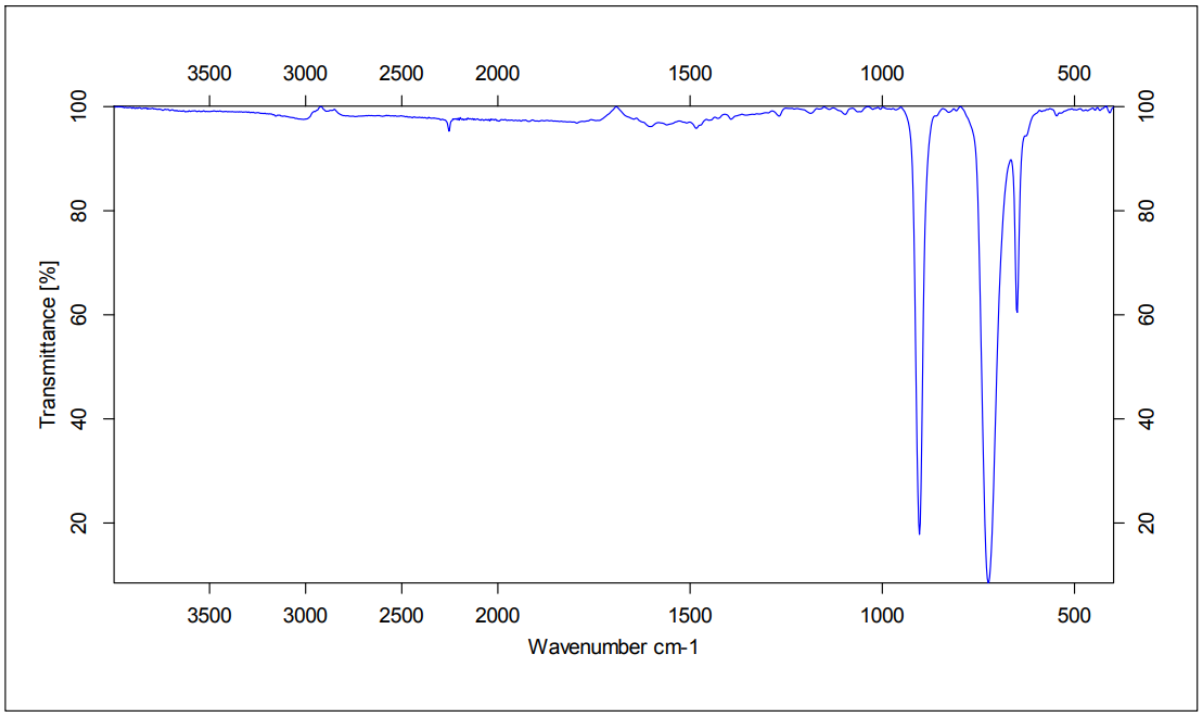

Sample : RV_SA_8	Frequency Range : 3996.98 - 398.261	Measured on : 11.05.2022	
Technique : Instrument type and	Resolution : 4	Instrument : Alpha	Sample Scans : 24
Customer : Administrator	Zerofilling : 2	Acquisition : Double Sided,Forv	

Figure B.5: IR spectrum obtained for Sa-8.

Sa-9

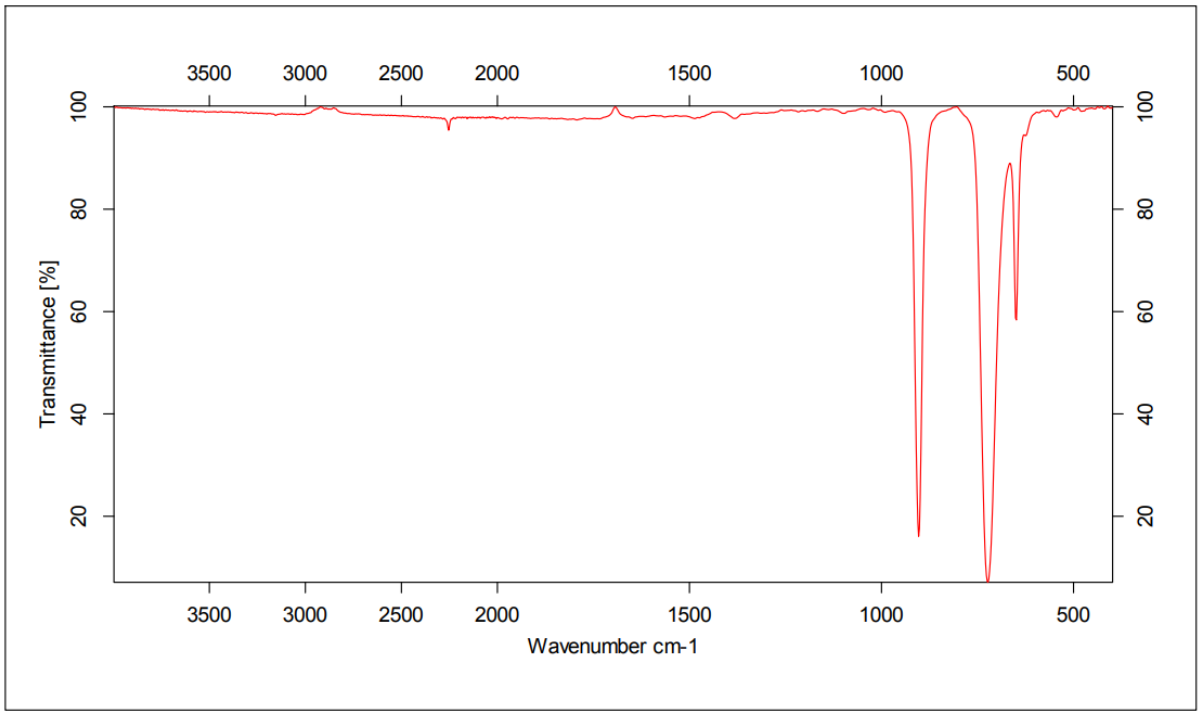

Sample : RV_SA_9	Frequency Range : 3996.98 - 398.261	Measured on : 11.05.2022	
Technique : Instrument type and	Resolution : 4	Instrument : Alpha	Sample Scans : 24
Customer : Administrator	Zerofilling : 2	Acquisition : Double Sided,For	

Figure B.6: IR spectrum obtained for Sa-9.

Sa-10

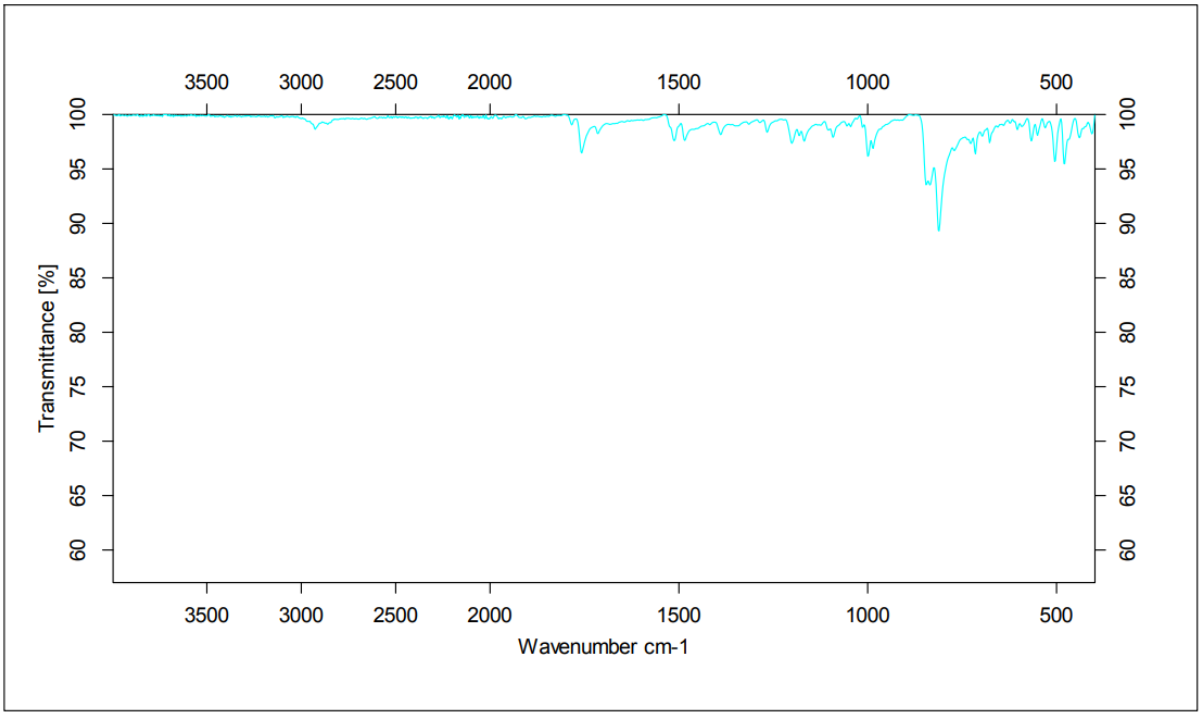

Sample : RV_SA_10	Frequency Range : 3996.98 - 398.261	Measured on : 10.05.2022	
Technique : Instrument type and	Resolution : 4	Instrument : Alpha	Sample Scans : 24
Customer : Administrator	Zerofilling : 2	Acquisition : Double Sided,Forv	

Figure B.7: IR spectrum of Sa-10.

Sa-11

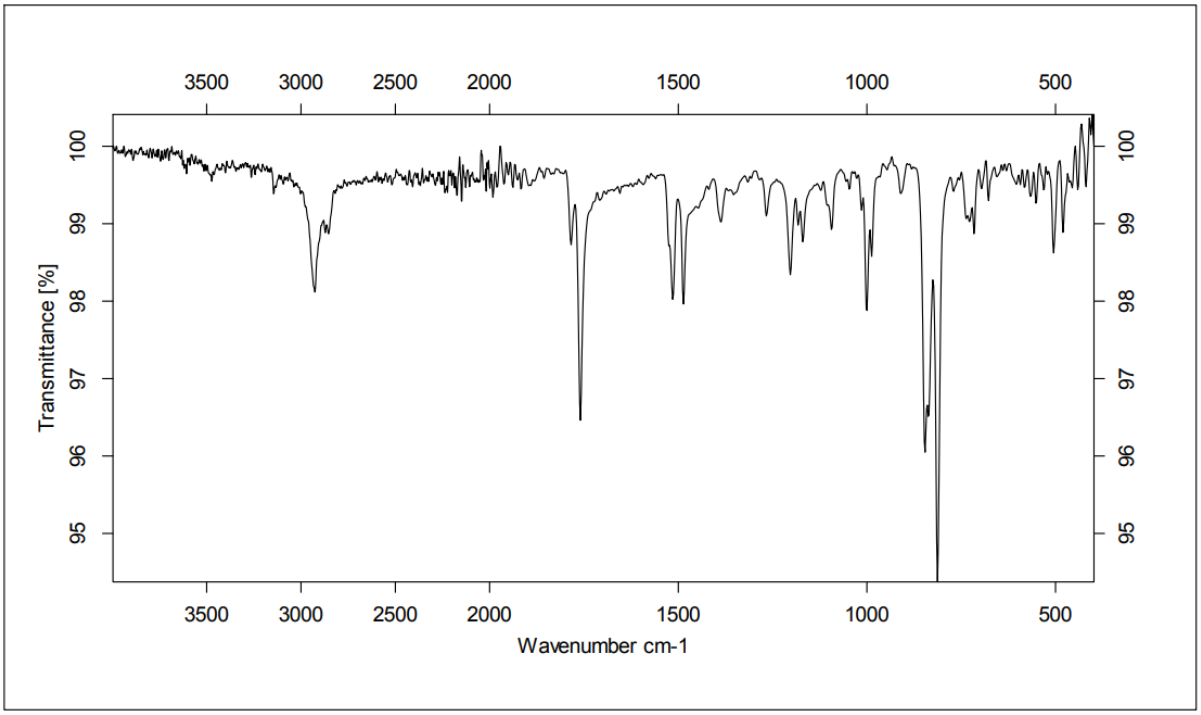

Sample : RV_SA_11	Frequency Range : 3996.98 - 398.261	Measured on : 10.05.2022	
Technique : Instrument type and	Resolution : 4	Instrument : Alpha	Sample Scans : 24
Customer : Administrator	Zerofilling : 2	Acquisition : Double Sided,For	

Figure B.8: IR spectrum obtained for Sa-11.

Sa-12

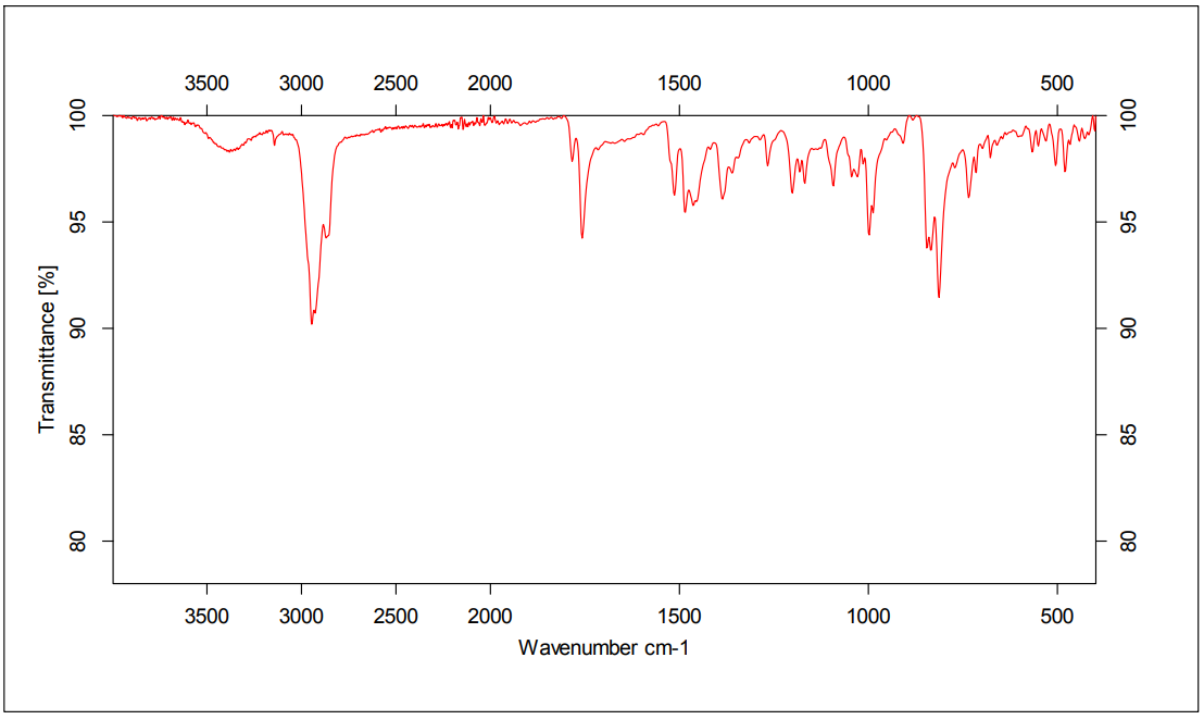

Sample : RV_SA_12	Frequency Range : 3996.98 - 398.261	Measured on : 10.05.2022	
Technique : Instrument type and	Resolution : 4	Instrument : Alpha	Sample Scans : 24
Customer : Administrator	Zerofilling : 2	Acquisition : Double Sided,Forv	

Figure B.9: IR spectrum obtained for Sa-12.

Appendix C: Exhaustive MS chromatograms for all compounds

Sa-2

Elemental Composition Report **Page 1**

Single Mass Analysis
Tolerance = 5.0 PPM / DBE: min = -1.5, max = 50.0
Element prediction: Off
Number of isotope peaks used for i-FIT = 3

Monoisotopic Mass, Even Electron Ions
933 formula(e) evaluated with 3 results within limits (up to 50 closest results for each mass)
Elements Used:
C: 0-100 H: 1-1000 N: 0-5 O: 0-5 Si: 0-1 S: 0-2
ReqID1461 90 (1.776) AM2 (Ar,35000.0,0.00,0.00); Cm (90:93)
1: TOF MS ASAP+

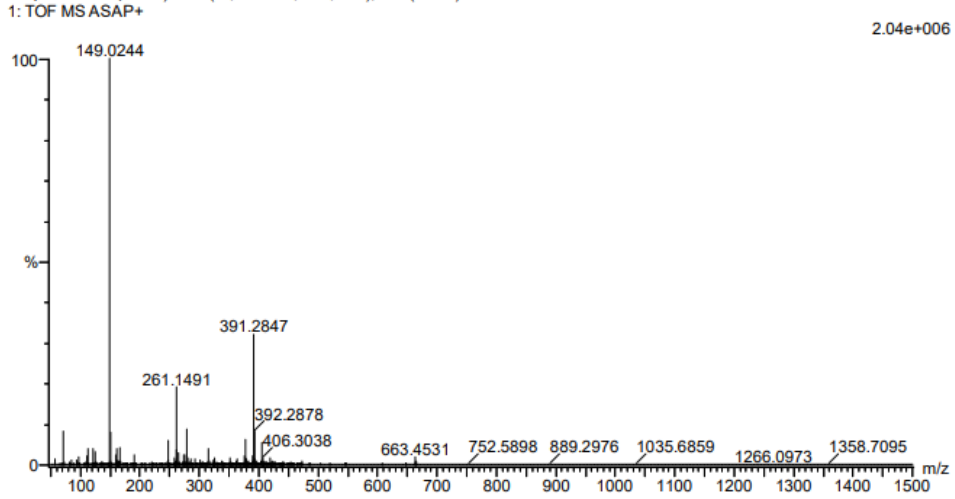

Mass	Calc. Mass	mDa	PPM	DBE	i-FIT	Norm	Conf(%)	Formula
Minimum:				-1.5				
Maximum:		5.0	5.0	50.0				
391.2847	391.2848	-0.1	-0.3	5.5	1116.1	0.005	99.52	C24 H39 O4
	391.2855	-0.8	-2.0	4.5	1134.8	18.744	0.00	C24 H43 Si S
	391.2862	-1.5	-3.8	10.5	1121.4	5.331	0.48	C25 H35 N4

Figure C.1: Elemental composition report for Sa-2.

Sa-3

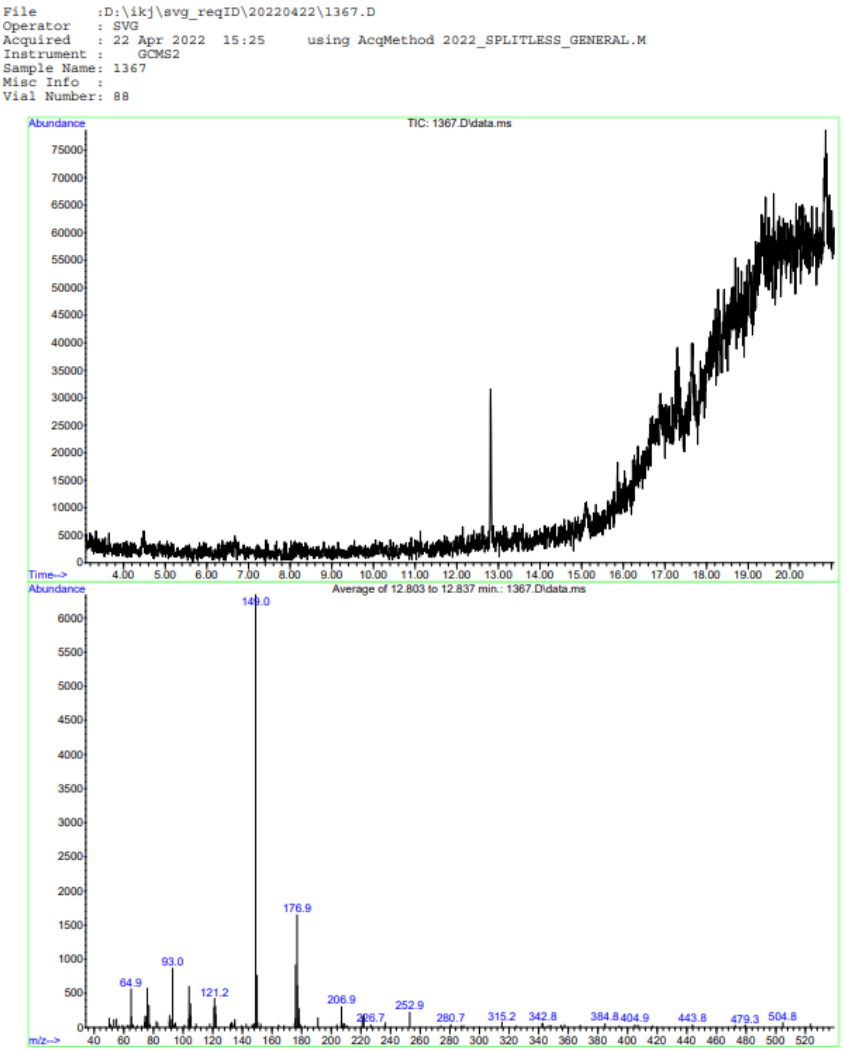

Figure C.2: Chromatogram (top) of the GCMS analysis with accompanying mass spectrum (bottom) for Sa-3.

Unknown: Average of 12.803 to 12.837 min.: 1367.D\data.ms
Compound in Library Factor = -302

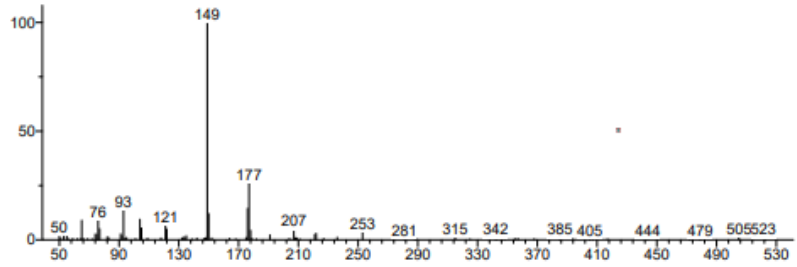

Hit 1 : Diethyl Phthalate
C12H14O4; MF: 740; RMF: 886; Prob 46.9%; CAS: 84-66-2; Lib: replib; ID: 19810.

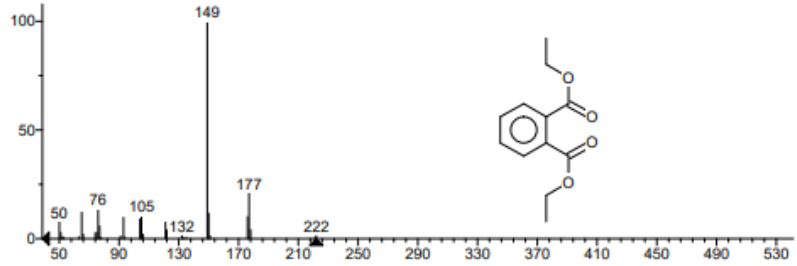

Hit 2 : Diethyl Phthalate
C12H14O4; MF: 732; RMF: 859; Prob 46.9%; CAS: 84-66-2; Lib: mainlib; ID: 96325.

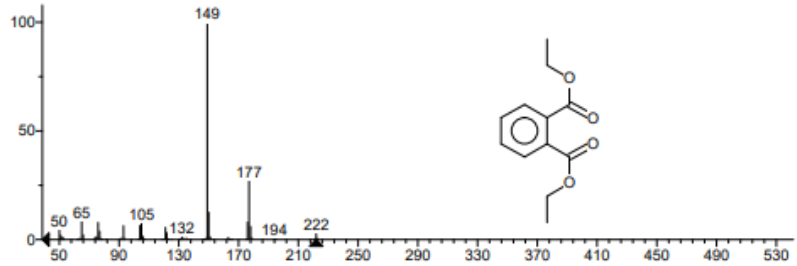

Figure C.3: The top search results of the mass spectrum for Sa-12 when run against the NIST library.

Sa-4

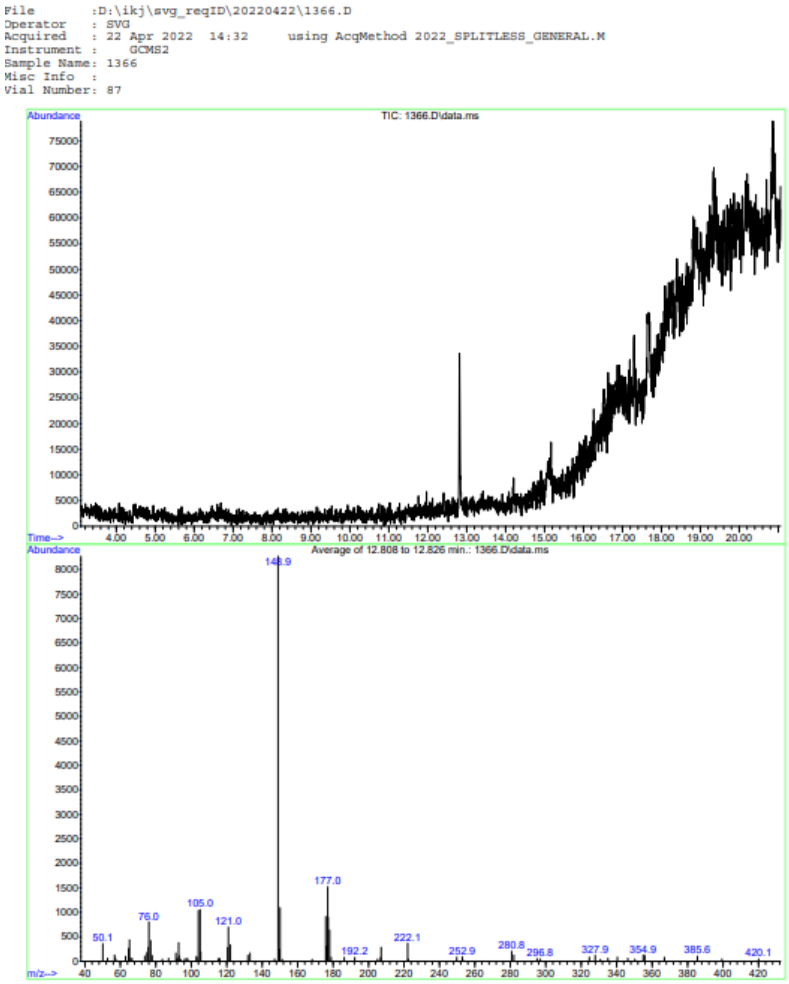

Figure C.4: Chromatogram (top) of the GCMS analysis with accompanying mass spectrum (bottom) for Sa-4. NIST library search returned the same results as displayed in Figure C.3.

Sa-5

Elemental Composition Report **Page 1**

Single Mass Analysis
Tolerance = 3.0 PPM / DBE: min = -1.5, max = 50.0
Element prediction: Off
Number of isotope peaks used for i-FIT = 3

Monoisotopic Mass, Even Electron Ions
505 formula(e) evaluated with 1 results within limits (up to 50 closest results for each mass)
Elements Used:
C: 0-100 H: 1-1000 N: 0-10 O: 0-10 I: 0-3

ReqID1329 84 (0.795) AM2 (Ar,35000.0,0.00,0.00); Cm (84:105)
1: TOF MS ES+ 7.16e+006

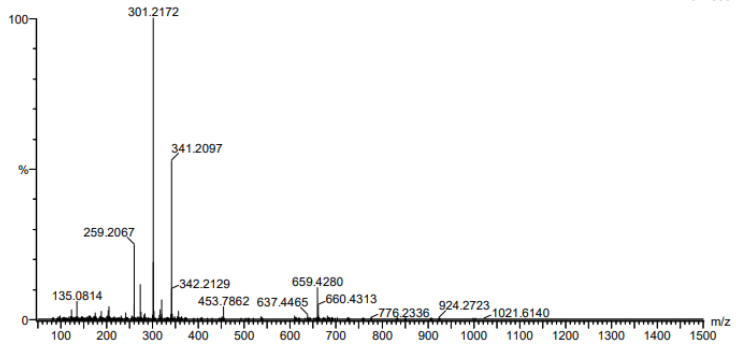

Minimum:	80.00				-1.5				
Maximum:	100.00		5.0	3.0	50.0				
Mass	RA	Calc. Mass	mDa	PPM	DBE	i-FIT	Norm	Conf(%)	Formula
301.2172	100.00	301.2168	0.4	1.3	6.5	1509.7	n/a	n/a	C20 H29 O2

Figure C.5: Elemental composition analysis of Sa-5 with respect to the 301 m/z peak.

Elemental Composition Report **Page 1**

Single Mass Analysis
Tolerance = 3.0 PPM / DBE: min = -1.5, max = 50.0
Element prediction: Off
Number of isotope peaks used for i-FIT = 3

Monoisotopic Mass, Even Electron Ions
2156 formula(e) evaluated with 3 results within limits (up to 50 closest results for each mass)
Elements Used:
C: 0-100 H: 1-1000 N: 0-10 O: 0-10 Na: 0-1 S: 0-1 I: 0-3

ReqID1329 84 (0.795) AM2 (Ar,35000.0,0.00,0.00); Cm (84:105)
1: TOF MS ES+ 7.16e+006

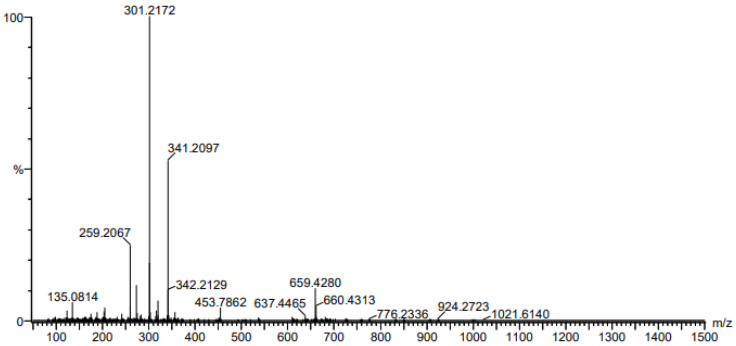

Minimum:				-1.5				
Maximum:		5.0	3.0	50.0				
Mass	Calc. Mass	mDa	PPM	DBE	i-FIT	Norm	Conf(%)	Formula
341.2097	341.2100	-0.3	-0.9	1.5	1318.0	14.094	0.00	C13 H30 N6 O Na S
	341.2093	0.4	1.2	5.5	1304.0	0.048	95.34	C20 H30 O3 Na
	341.2090	0.7	2.1	9.5	1307.0	3.066	4.66	C18 H25 N6 O

Figure C.6*:* Elemental composition analysis of Sa-5 with respect to the 341 m/z peak.

Sa-6

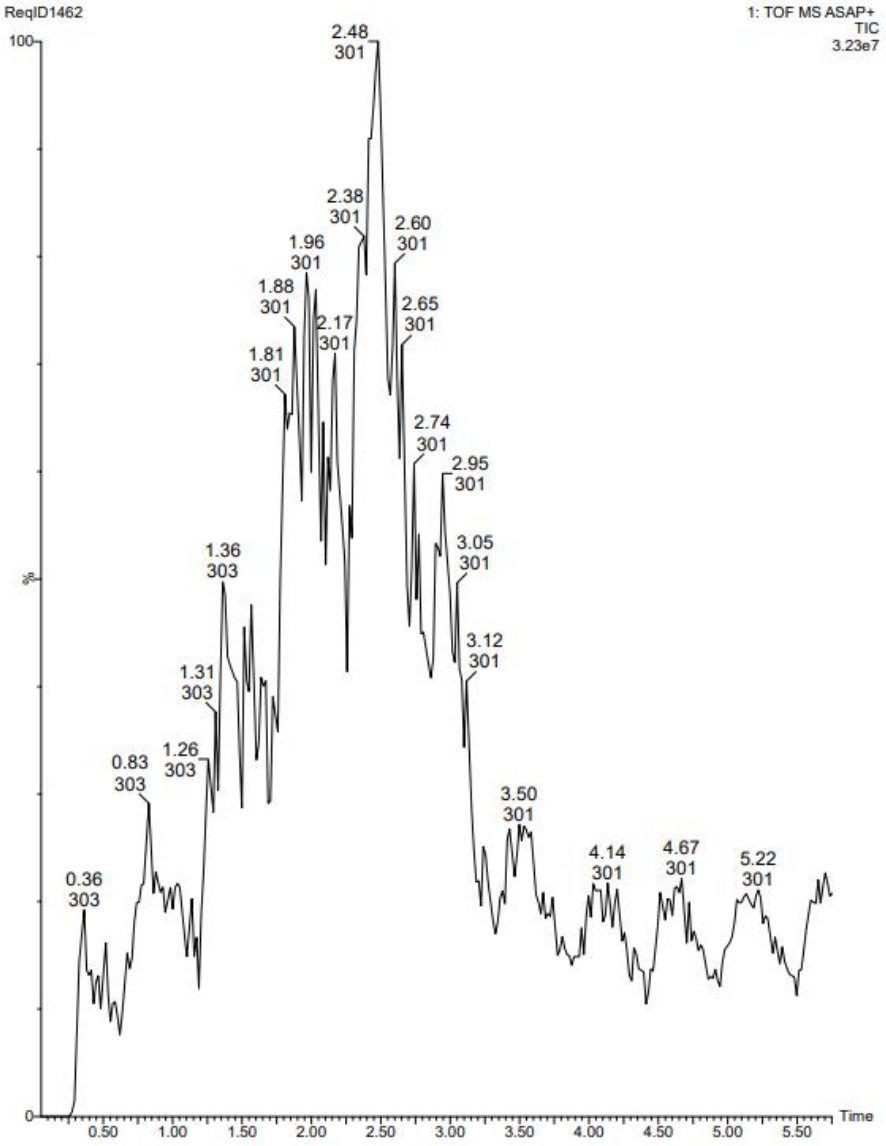

Figure C. 7: chromatogram of Sa-6, proving the presence of two separate compounds with molecular masses 301 and 303 Da.

Sa-7

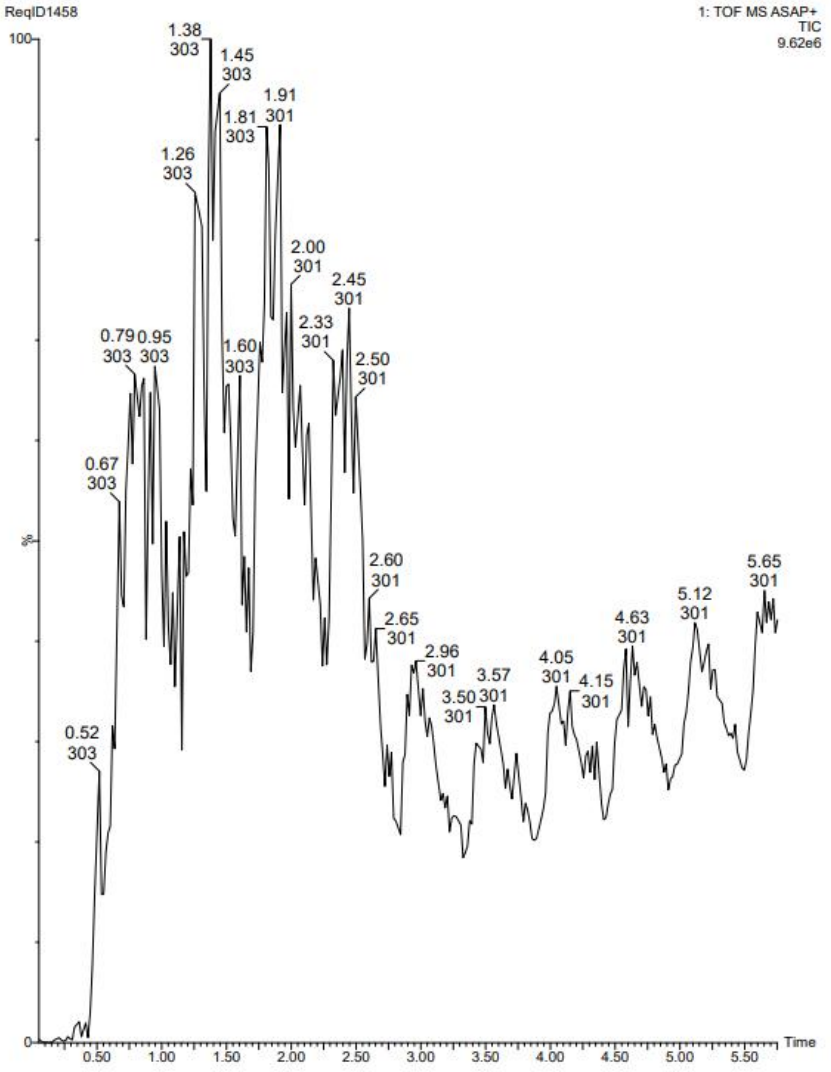

Figure C. 8: chromatogram of Sa-7, proving the presence of two separate compounds with molecular masses 301 and 303 Da like in Sa-6.

Elemental Composition Report **Page 1**

Single Mass Analysis
Tolerance = 5.0 PPM / DBE: min = -1.5, max = 50.0
Element prediction: Off
Number of isotope peaks used for i-FIT = 3

Monoisotopic Mass, Even Electron Ions
708 formula(e) evaluated with 1 results within limits (up to 50 closest results for each mass)
Elements Used:
C: 0-100 H: 1-1000 N: 0-5 O: 0-5 Si: 0-1 S: 0-2
ReqID1458 128 (2.497) AM2 (Ar,35000.0,0.00,0.00); Cm (126:130)
1: TOF MS ASAP+

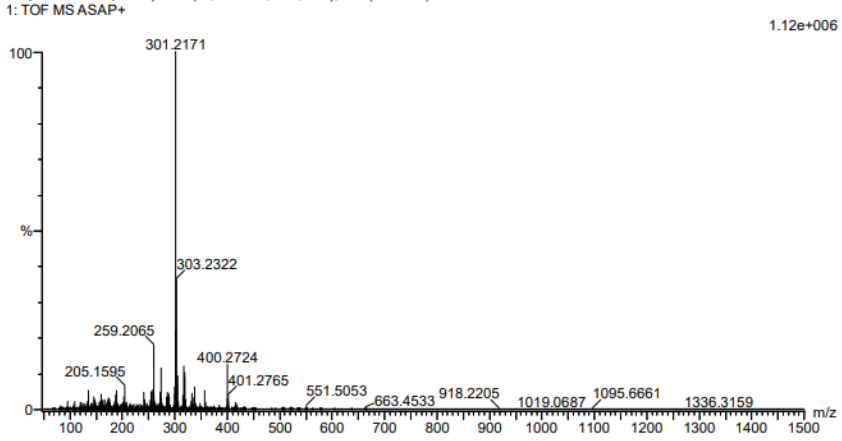

Minimum:	80.00				-1.5				
Maximum:	100.00		5.0	5.0	50.0				
Mass	RA	Calc. Mass	mDa	PPM	DBE	i-FIT	Norm	Conf(%)	Formula
301.2171	100.00	301.2168	0.3	1.0	6.5	1347.7	n/a	n/a	C20 H29 O2

Figure C.9: Elemental composition analysis of Sa-7 with respect to the 301 m/z peak.

Elemental Composition Report **Page 1**

Single Mass Analysis
Tolerance = 5.0 PPM / DBE: min = -1.5, max = 50.0
Element prediction: Off
Number of isotope peaks used for i-FIT = 3

Monoisotopic Mass, Even Electron Ions
710 formula(e) evaluated with 1 results within limits (up to 50 closest results for each mass)
Elements Used:
C: 0-100 H: 1-1000 N: 0-5 O: 0-5 Si: 0-1 S: 0-2
ReqID1458 31 (0.620) AM2 (Ar,35000.0,0.00,0.00); Cm (28:32)
1: TOF MS ASAP+

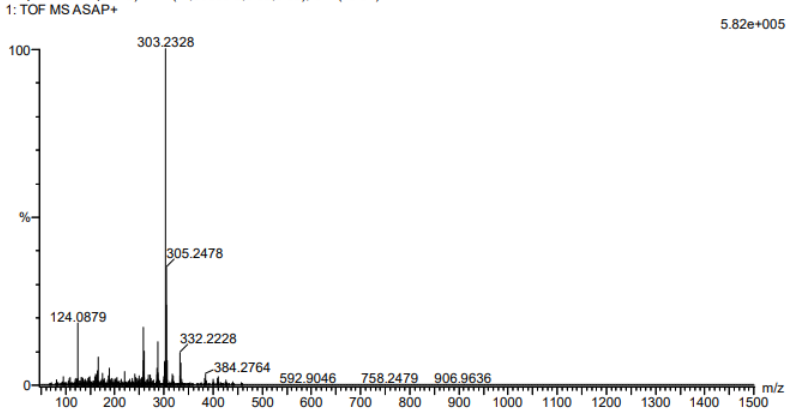

Minimum:	80.00				-1.5				
Maximum:	100.00		5.0	5.0	50.0				
Mass	RA	Calc. Mass	mDa	PPM	DBE	i-FIT	Norm	Conf(%)	Formula
303.2328	100.00	303.2324	0.4	1.3	5.5	1263.0	n/a	n/a	C20 H31 O2

Figure C.10: Elemental composition analysis of Sa-7 with respect to the 303 m/z peak.

Sa-8

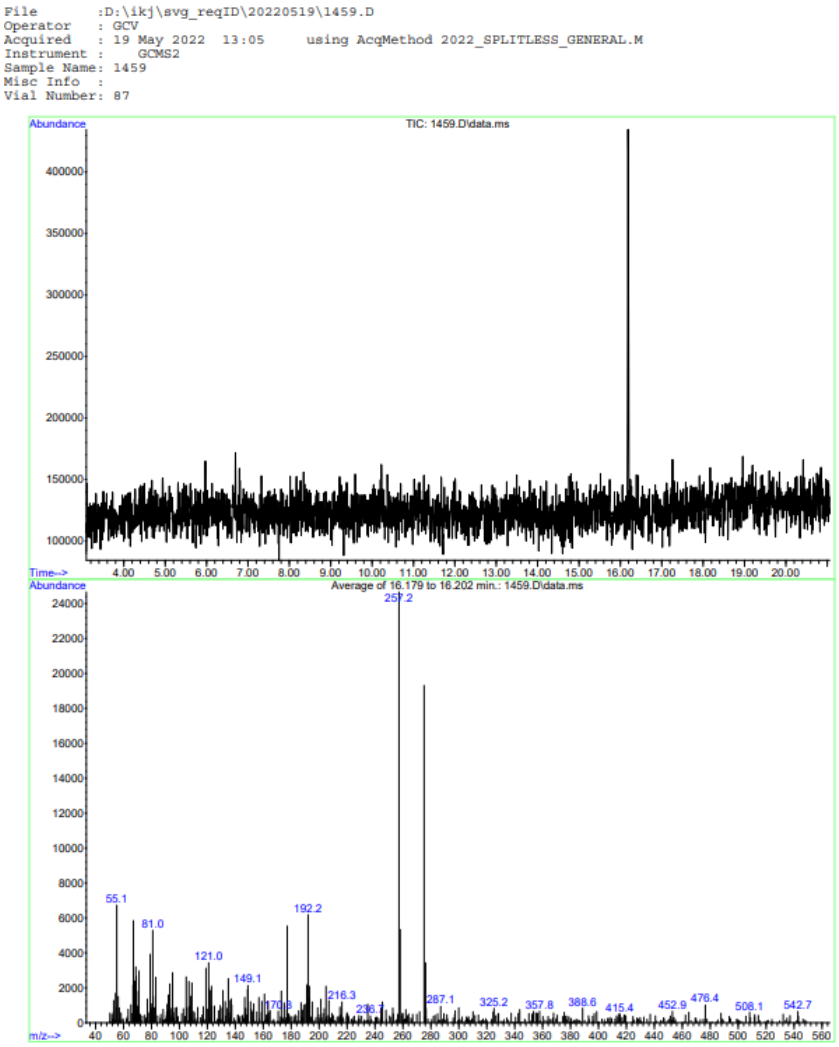

Figure C.11: Chromatogram (top) of the GCMS analysis with accompanying mass spectrum (bottom) for Sa-8.

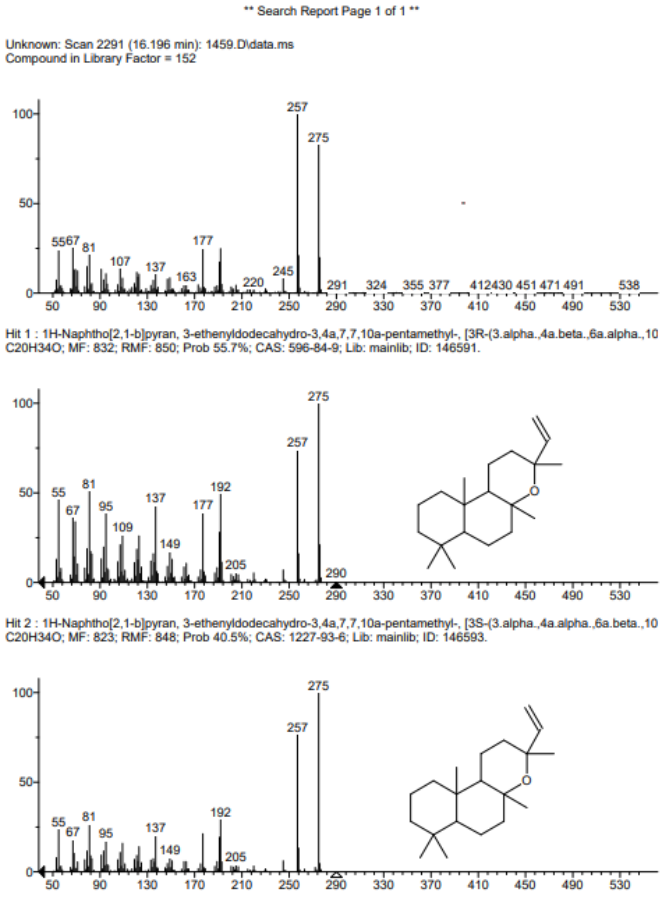

Figure C.12: The top search results of the mass spectrum for Sa-8 when run against the NIST library.

Elemental Composition Report **Page 1**

Single Mass Analysis
Tolerance = 5.0 PPM / DBE: min = -1.5, max = 50.0
Element prediction: Off
Number of isotope peaks used for i-FIT = 3

Monoisotopic Mass, Even Electron Ions
178 formula(e) evaluated with 1 results within limits (up to 50 closest results for each mass)
Elements Used:
C: 0-100 H: 1-1000 N: 0-6 O: 0-6
ReqID1459 94 (1.843) AM2 (Ar,35000.0,0.00,0.00); Cm (90:95)
1: TOF MS ASAP+

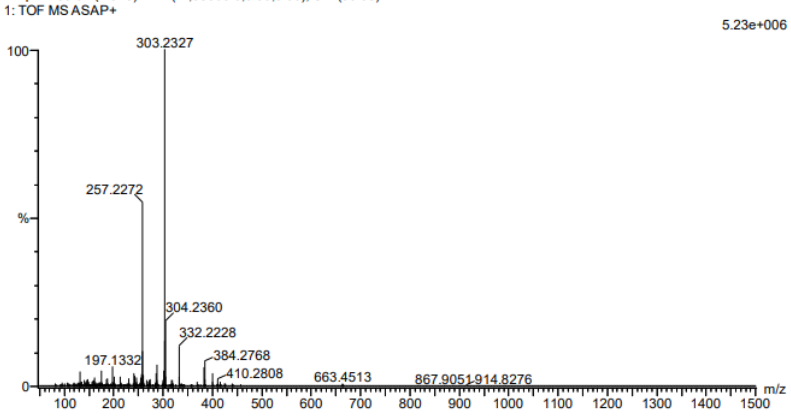

Minimum:				-1.5				
Maximum:		5.0	5.0	50.0				
Mass	Calc. Mass	mDa	PPM	DBE	i-FIT	Norm	Conf(%)	Formula
303.2327	303.2324	0.3	1.0	5.5	1459.1	n/a	n/a	C20 H31 O2

Figure C.13: Elemental composition analysis of Sa-8.

Sa-9

Elemental Composition Report **Page 1**

Single Mass Analysis
Tolerance = 5.0 PPM / DBE: min = -1.5, max = 50.0
Element prediction: Off
Number of isotope peaks used for i-FIT = 3

Monoisotopic Mass, Even Electron Ions
482 formula(e) evaluated with 1 results within limits (up to 50 closest results for each mass)
Elements Used:
C: 0-100 H: 1-1000 N: 0-5 O: 0-5 Si: 0-1 S: 0-2
ReqID1460 3 (0.087) AM2 (Ar,35000.0,0.00,0.00)
1: TOF MS ASAP+

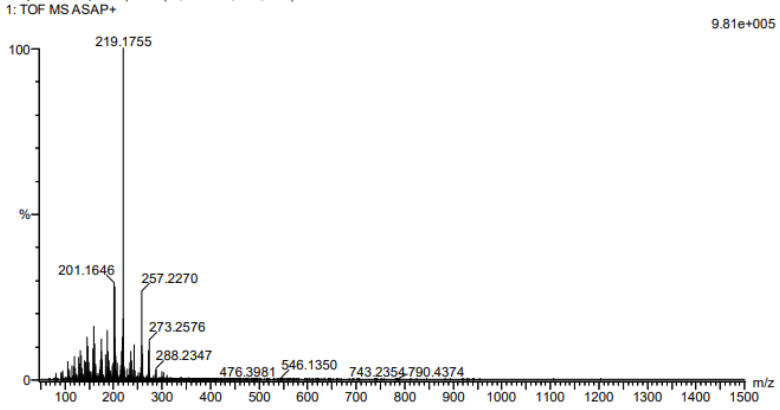

Minimum:	80.00				-1.5				
Maximum:	100.00		5.0	5.0	50.0				
Mass	RA	Calc. Mass	mDa	PPM	DBE	i-FIT	Norm	Conf(%)	Formula
219.1755	100.00	219.1749	0.6	2.7	4.5	1799.9	n/a	n/a	C15 H23 O

Figure C.14: Elemental composition analysis of Sa-9.

Sa-10

```
File       :D:\ikj\svg_reqID\20220513\TEST1454.D
Operator   :
Acquired   : 13 May 2022  13:42     using AcqMethod 2022_SPLITLESS_GENERAL.M
Instrument :
    GCMS2
Sample Name:
Misc Info  :
Vial Number: 86
```

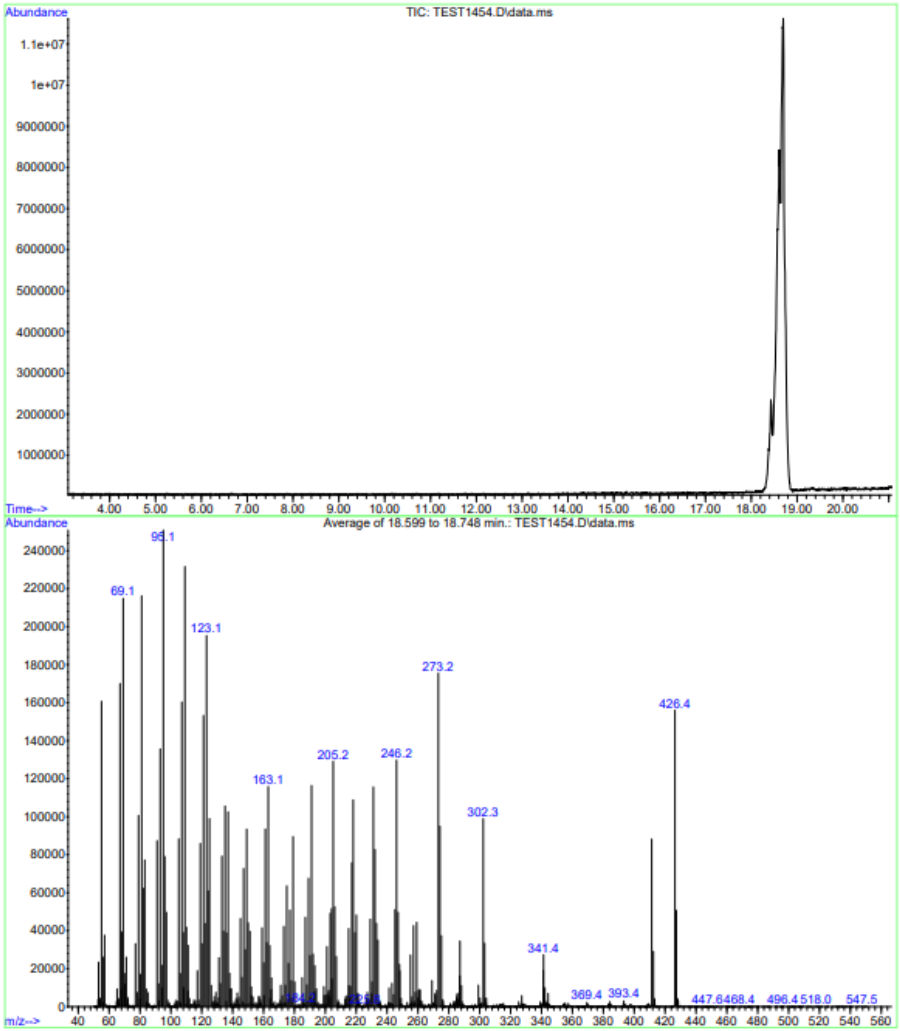

Figure C.15: Chromatogram (top) of the GCMS analysis with accompanying mass spectrum (bottom) for Sa-10.

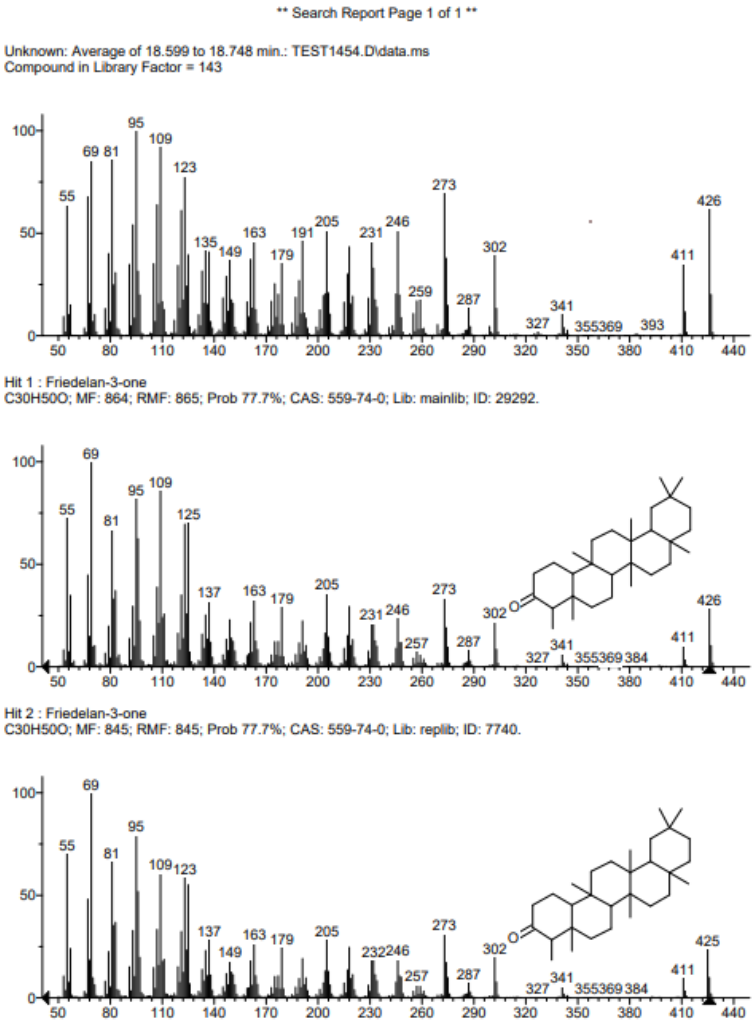

Figure C.16: The top search results of the mass spectrum for Sa-10 when run against the NIST library.

Sa-11

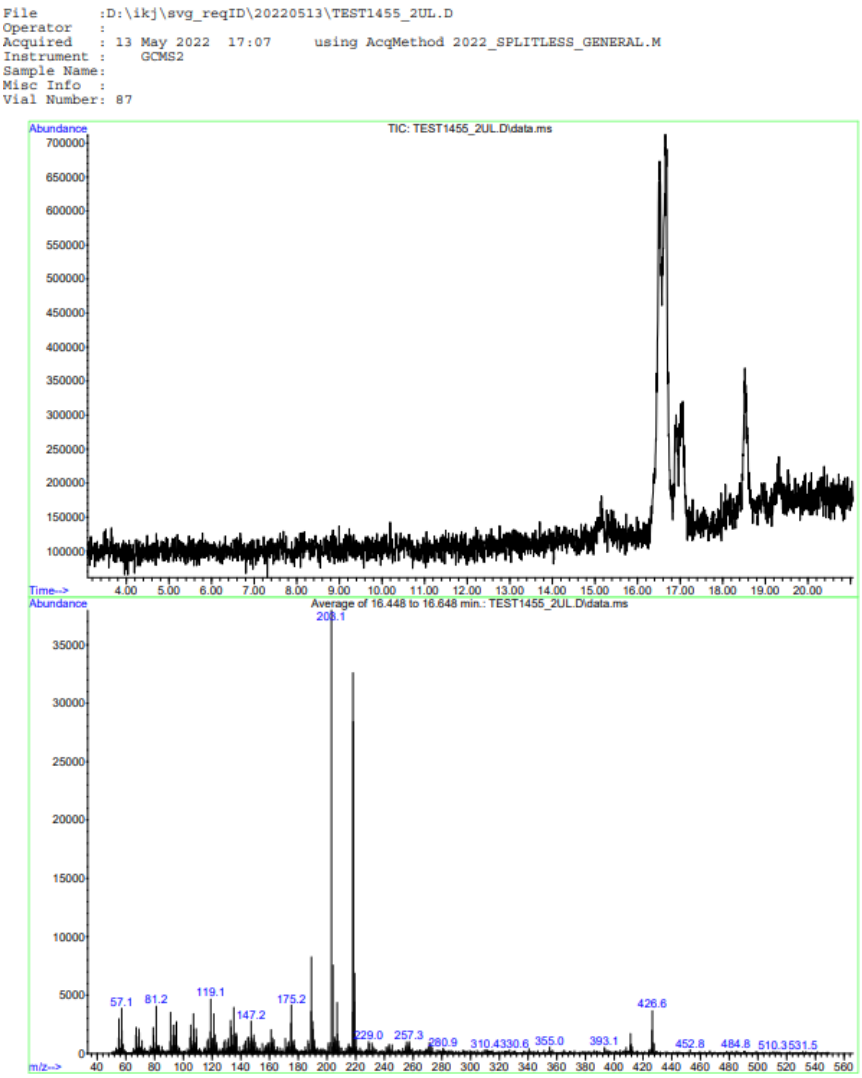

Figure C.17: Chromatogram (top) of the GCMS analysis with accompanying mass spectrum (bottom) for Sa-11.

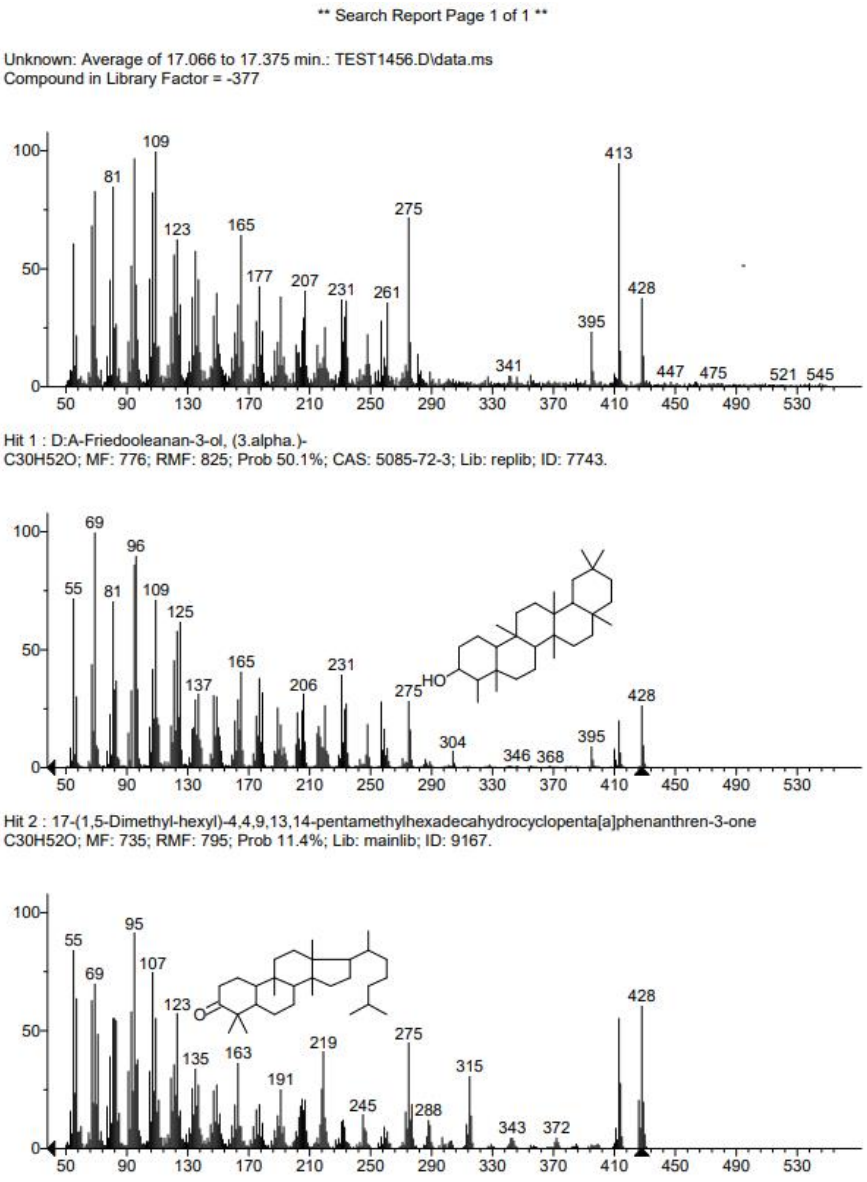

Figure C.18: The top search results of the mass spectrum for Sa-11 when run against the NIST library.

Sa-12

```
File       :D:\ikj\svg_reqID\20220513\TEST1456.D
Operator   :
Acquired   : 13 May 2022  16:38     using AcqMethod 2022_SPLITLESS_GENERAL.M
Instrument :
    GCMS2
Sample Name:
Misc Info  :
Vial Number: 88
```

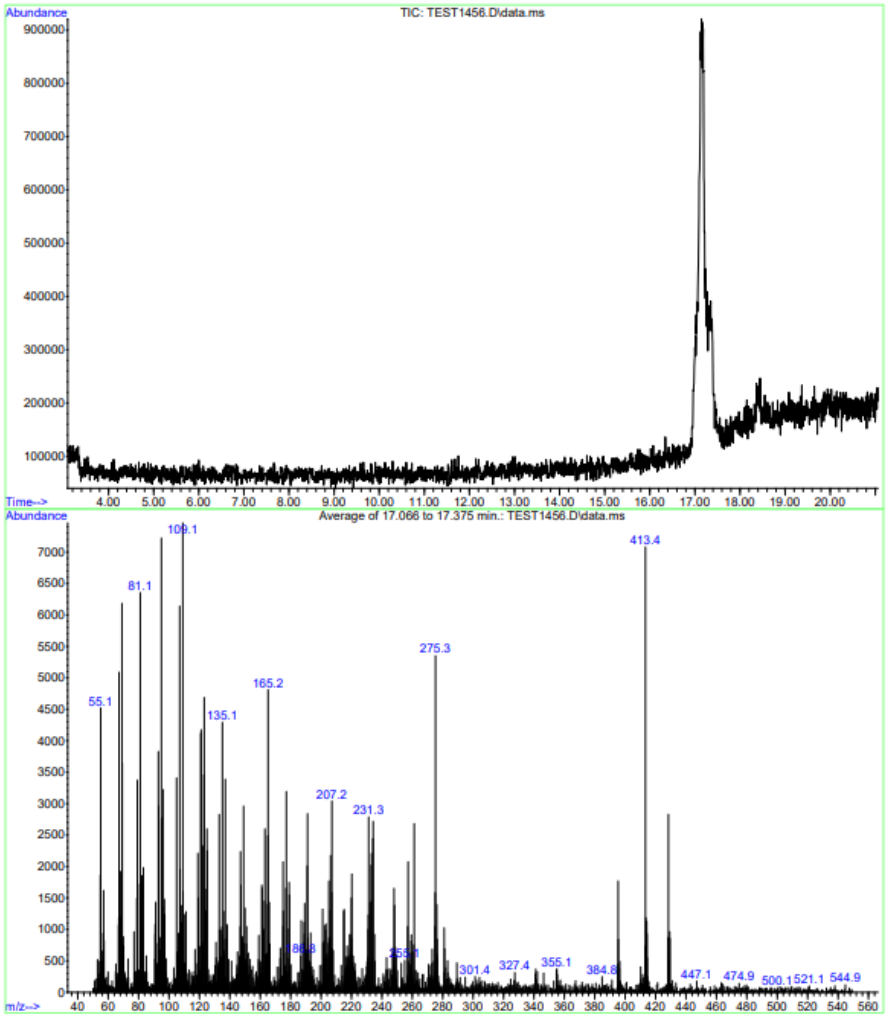

Figure C.19: Chromatogram (top) of the GCMS analysis with accompanying mass spectrum (bottom) for Sa-12.

Unknown: Average of 16.448 to 16.648 min.: TEST1455_2UL.D\data.ms
Compound in Library Factor = -623

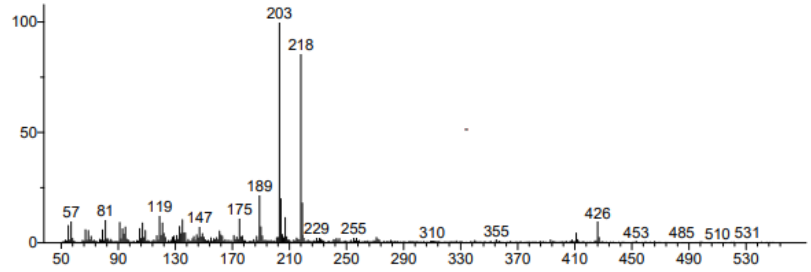

Hit 1 : .alpha.-Amyrin
C30H50O; MF: 749; RMF: 815; Prob 35.7%; CAS: 638-95-9; Lib: replib; ID: 24695.

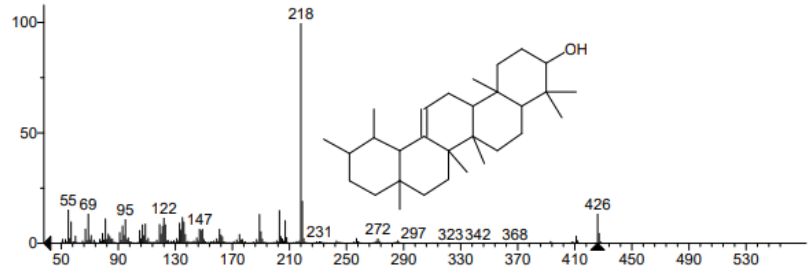

Hit 2 : .beta.-Amyrin
C30H50O; MF: 742; RMF: 836; Prob 27.3%; CAS: 559-70-6; Lib: mainlib; ID: 130764.

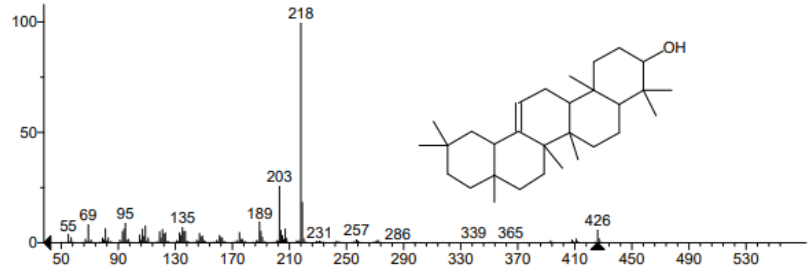

Figure C.20: The top search results of the mass spectrum for Sa-12 when run against the NIST library.

Sa-13

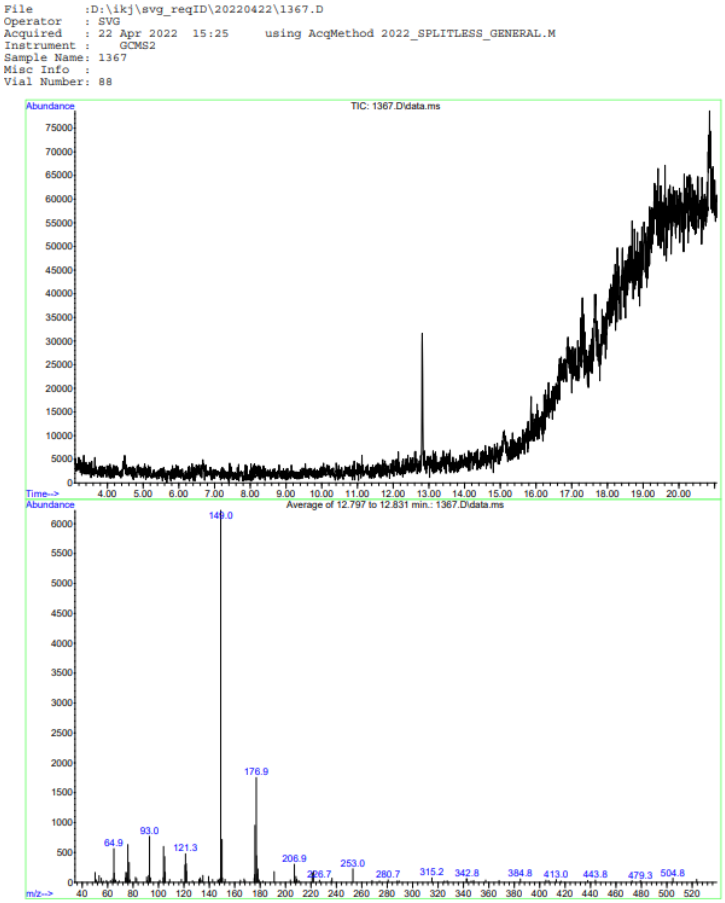

Figure C.21: Chromatogram (top) of the GCMS analysis with accompanying mass spectrum (bottom) for Sa-13. NIST library search returned similar results as Sa-3, displayed in Figure C.3.

Appendix D: Reported NMR spectra

Included here are reported spectra for the elucidated compounds. Where stereochemistry of the sample was indeterminable, reported spectra for the most occurring stereoisomer are displayed.

Sa-5

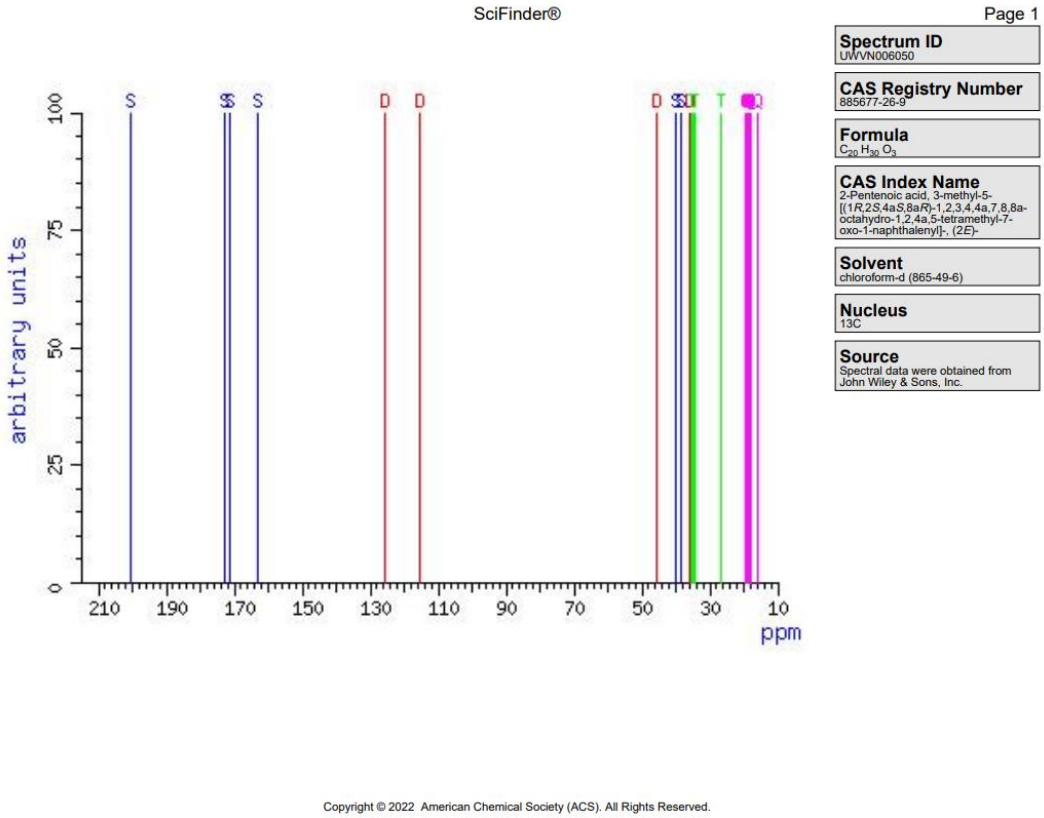

Figure D.1: ^{13}C spectrum of (E)-3-methyl-5-((1R,2S,4aS,8aR)-1,2,4a,5-tetramethyl-7-oxo-1,2,3,4,4a,7,8,8a-octahydronaphthalen-1-yl)pent-2-enoic acid, obtained from John Wiley & Sons, inc

Kaur-16-en-18-oic acid

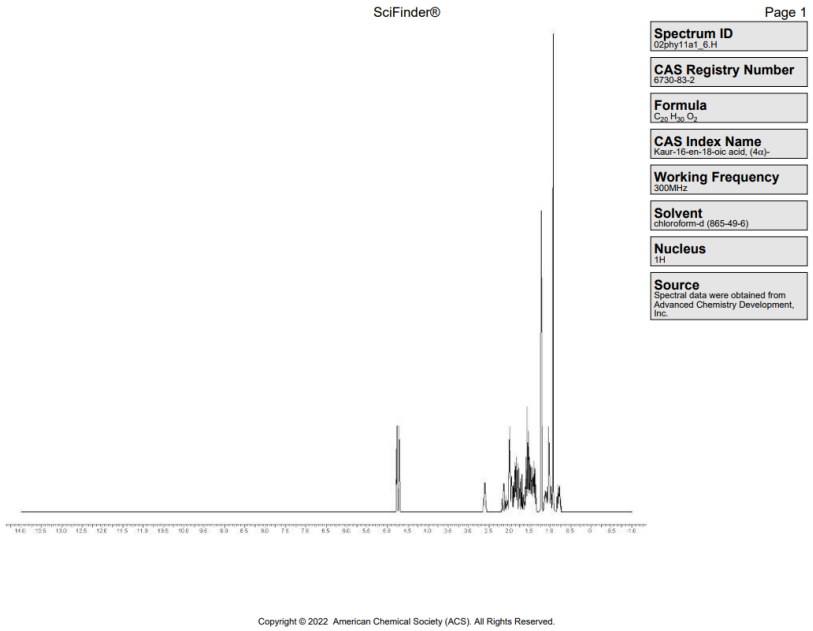

Figure D.2: ^{1}H spectrum of kaur-16-en-18-oic acid , obtained from Advanced Chemistry Development, Inc.

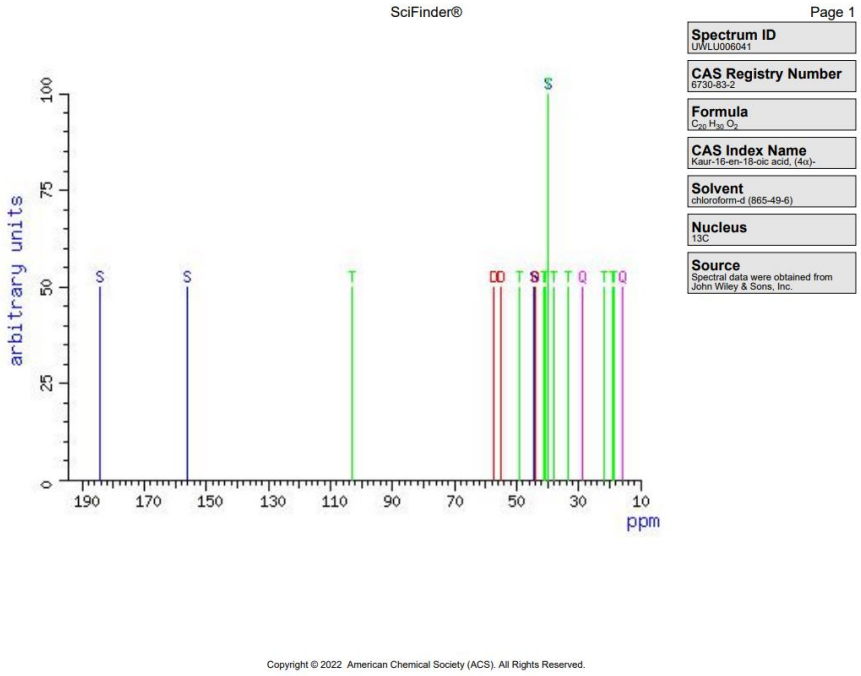

Figure D.3: ^{13}C spectrum of kaur-16-en-18-oic acid , obtained from John Wiley & Sons, Inc.

Sa-10

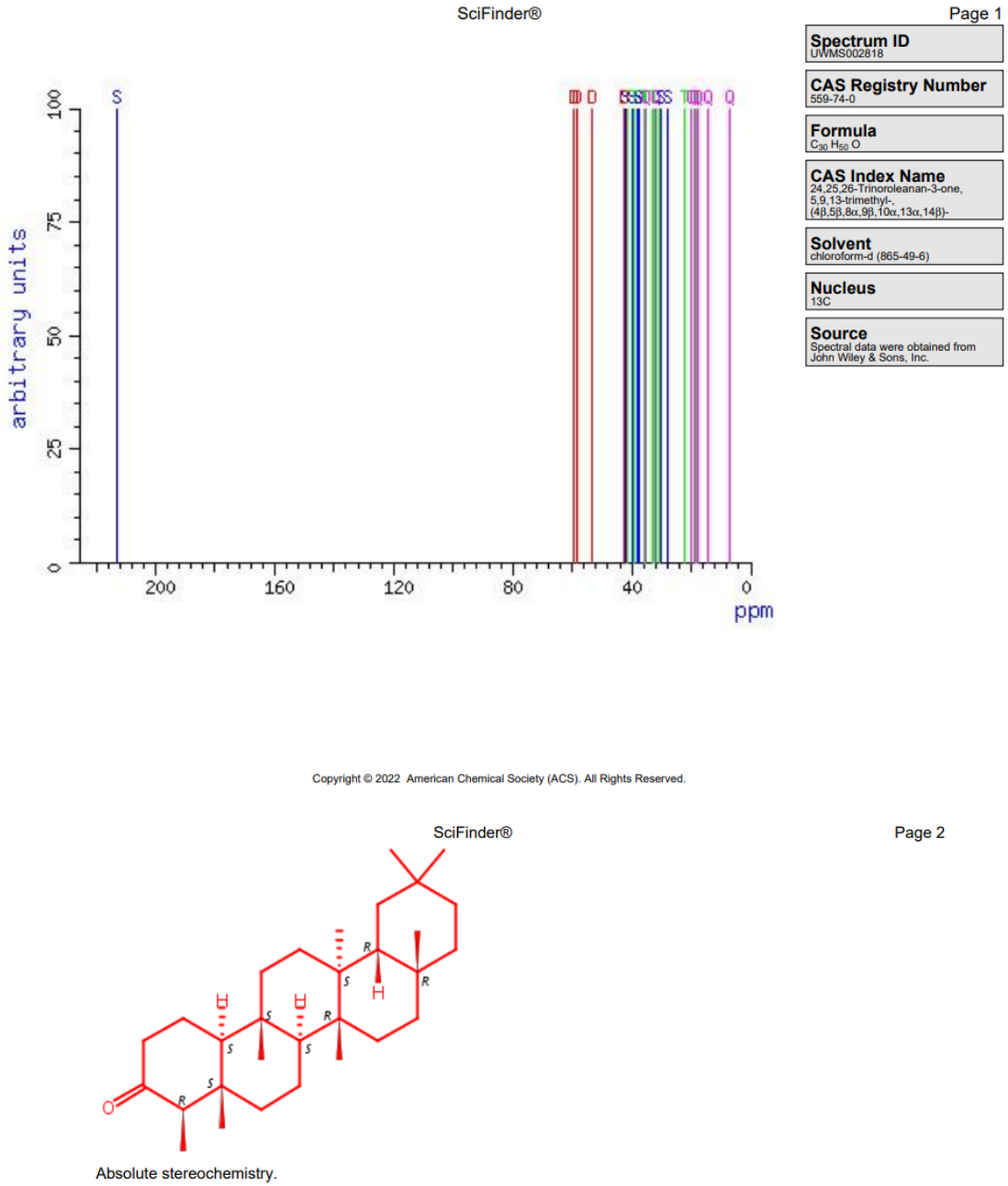

Figure D.4: Reported ^{13}C spectrum of 24,25,26-Trinoroleanan-3-one, 5,9,13-trimethyl-, (4β,5β,8α,9β,10α,13α,14β), along with molecular structure, obtained from John Wiley & Sons, Inc.

Sa-11

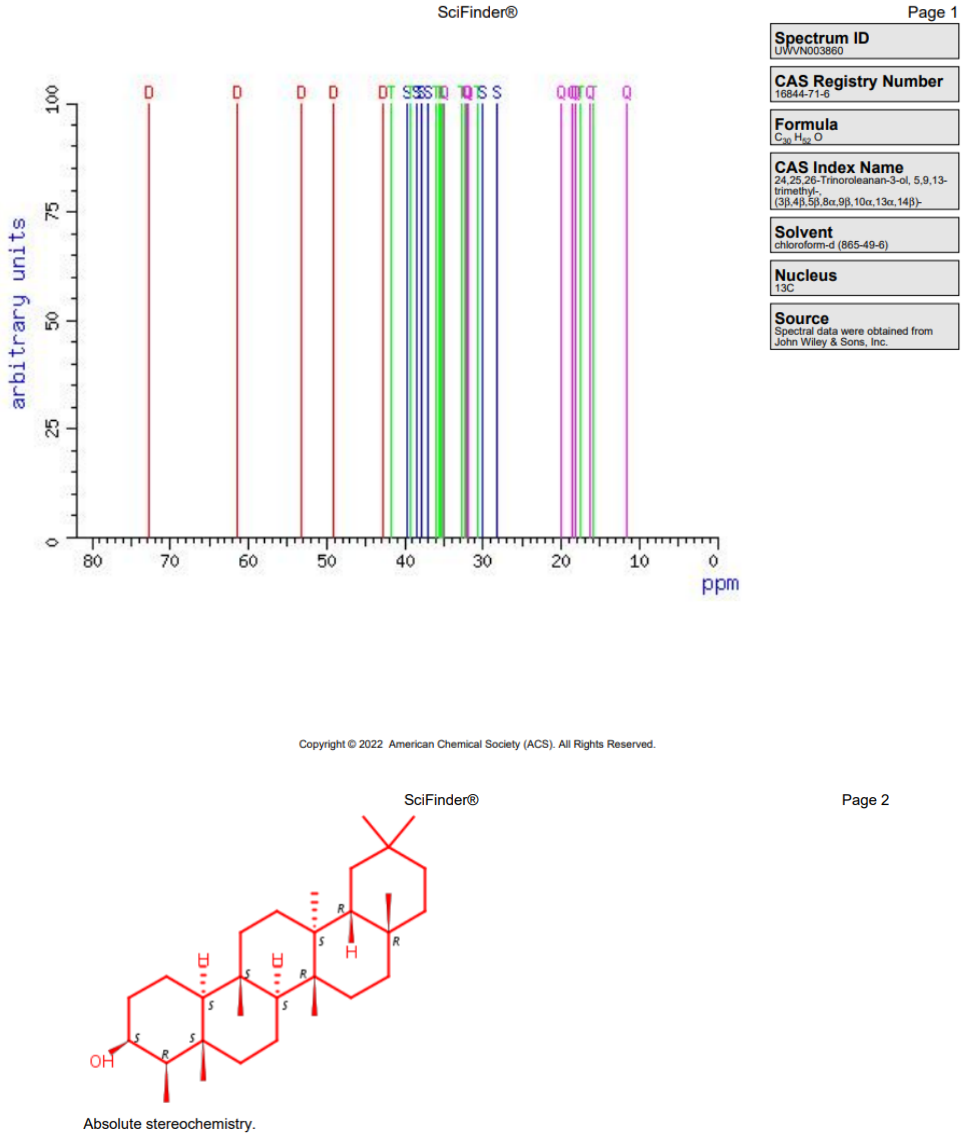

Figure D.5: Reported ^{13}C spectrum of 24,25,26-Trinoroleanan-3-ol, 5,9,13-trimethyl-, (3β,4β,5β,8α,9β,10α,13α,14β), along with molecular structure, obtained from John Wiley & Sons, Inc.

Sa-12

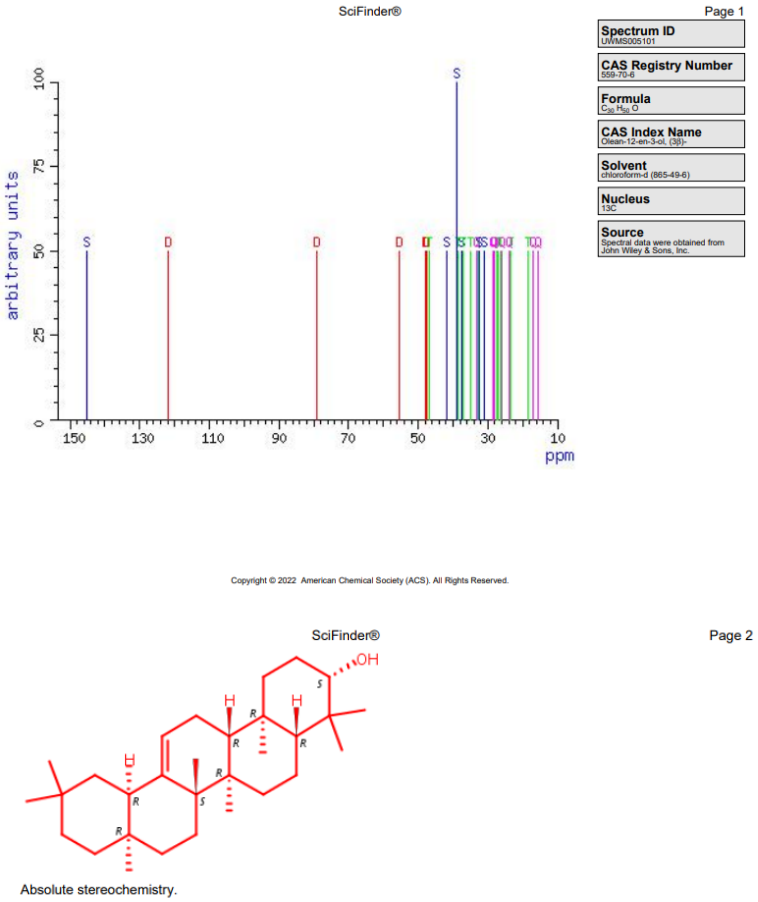

Figure D.6: Reported ^{13}C spectrum of Olean-12-en-3-ol, (3β), along with molecular structure, obtained from John Wiley & Sons, Inc.

R. Verkerk

Master's thesis

NTNU
Norwegian University of
Science and Technology